Bioreactors and process monitoring for scale-up of stem cell production

Toon LAMBRECHTS

Supervisors:
Prof. Dr. Jean-Marie Aerts (KU Leuven, Promotor)
Dr. Jan Schrooten (Antleron, Co-promotor)

Examination committee:
Prof. Dr. Bert Sels (KU Leuven, Chair)
Prof. Dr. Frank P. Luyten (KU Leuven)
Prof. Dr. Liesbet Geris (Université de Liège – KU Leuven)
Prof. Dr. Daniel Berckmans (KU Leuven)
Thierry Bovy (Promethera Biosciences)
Prof. Dr. Qasim Rafiq (Aston University)

Dissertation presented in partial fulfilment of the requirements for the degree of Doctor of Bioscience Engineering

November 2016

Doctoraatsproefschrift nr. 1384 aan de faculteit Bio-ingenieurswetenschappen van de KU Leuven.

Uitgegeven in eigen beheer, Toon Lambrechts, Division Animal and Human Health Engineering, Kasteelpark Arenberg 30, B-3001 Leuven

Preface

After almost 4 years, 6 848 200 000 cells produced in 4 different culture vessel types, 146 bottles of cell culture medium and countless hours in the lab, I am happy to present this text as the materialization of the work performed during this PhD project. Since this is the result of many fruitful collaborations and interactions with inspiring people, I would like to take the opportunity in this preface to thank everyone who somehow contributed to this work.

First and foremost I would like to thank Prof Jean-Marie Aerts and Dr. Jan Schrooten, respectively the promoter and co-promoter of this work. After graduating from a second masters I was initially not even considering to start a PhD. But with their enthusiasm Jean-Marie and Jan somehow convinced me to start this project, which turned out to be an exciting adventure. Over the past 4 years, both of you spent a huge amount of your time guiding the project, providing feedback, correcting manuscripts, and attending our monthly "Molen meetings". So Jean-Marie and Jan, for all your input and for the many opportunities you two created for me during this project a very sincere thank you! Prof. Frank Luyten, I always appreciated your no-nonsense feedback on the projects I worked on and your healthy skepticism towards bioreactors and engineers in general motivated me to always perform better. Prof. Lies Geris and Prof. Daniel Berckmans, you were always available to discuss any issue and I learned a lot from both your scientific and management insights. Thanks also to the external jury members and chair of the PhD examination committee, Prof. Qasim Rafiq, Thierry Bovy and Prof. Bert Sels, for your motivation and time to review this work.

It goes without saying that I owe a big thank you to all the Prometheus and M3-BIORES colleagues who contributed to this work, maybe directly with scientific knowledge, but for sure indirectly by providing a positive work environment. I really enjoyed working in the multicultural and

multidisciplinary context of this lab! While there are many colleagues that I should thank in person, a special shout-out to my fellow bioreactor buddies, Ioannis and Maarten, is indispensable here: for the endless analysis of bioreactors, daydreams of controlled stem cell bioprocesses, the long list of potential improvements for this work, but of course also for the enjoyable non-work related chats. I would like to extend my sincere gratitude to the often unsung heroes of the lab: to Kathleen, Jenny, Lennert, Stijn, Inge, Carla and Melanie for the many helping hands whenever needed, to Johan for the technical support and relentlessly coming up with new designs and prototypes of the 3D bioreactor and to Annemie and Inge for the administrative help. And also thank you to Richard and Veerle from imec. Brent from Terumo and the entire Octane team for their fresh 'outside KU Leuven' perspectives.

While bioreactors are good fun, it's necessary to take a break from them once in a while! Luckily I have some awesome friends to remind me of the other important things in life, such as having a beer on Friday night, cycling early Sunday mornings, playing football with moderately talented team mates (yes, I'm talking to both of you Sporting Bonifanzios and FC Heverse Vrienden),…

Of course my family, and for sure my parents, cannot be missed in this list. Thanks for the continuous support, the warm nest and for providing me with all the opportunities for personal development one could wish. A very special thanks and a big hug go to Debra, the daily witness of the ups and downs of this work, for being my greatest supporter and just for being you.

Finally, thank you for getting this far in the text and happy further reading!

Toon

November 2016, Leuven

Abstract

For almost two decades it is claimed that cell-based therapies will revolutionize the field of medicine. Albeit major scientific breakthroughs that present cells as the active ingredient of a clinical therapy are succeeding each other at increasing speed, today only few of these research successes are able to materialise their full clinical potential and develop into a widely available commercial cell-based treatment. Besides the remaining scientific challenges (e.g. mechanisms of action), costly product development, and a complex regulatory and reimbursement landscape, it is hypothesised that the lack of automated, controlled and cost-effective production strategies forms a major hurdle towards a wide-spread clinical translation of cell based therapies. The objective of this work was therefore to create enabling tools and knowledge for monitored and controlled large-scale stem cell production, with the ultimate goal of facilitating the manufacturing process of qualitative and cost-effective cell-based therapies.

Flask-based cell expansion processes are currently still the gold standard culture vessels, despite the disadvantage of their limited scale-up and automation potential. In a first phase, the translation from flask-based cell production processes to a bioreactor-based process was investigated, without adversely influencing the quality of the cells. Two commercial large-scale bioreactor types were evaluated for their ability to produce qualitative batches of cells for an autologous cell-based advanced therapy medicinal product (*ATMP*) that is being developed for the treatment of large bone defects at the Prometheus (KU Leuven) lab. The first bioreactor that was evaluated was the Xpansion® Multiplate Bioreactor System from Pall Life Sciences in combination with the Ovizio iLine S imaging system. It was shown that the growth dynamics of the cells in the bioreactor closely matched the dynamics as observed in the standard flask. Both cultures resulted in the same cell density at the time of harvest (17 500 cells/cm^2 in the 5.6 L bioreactor with a 30 600 cm^2 culture surface and 17 300 cells/cm^2 in the tissue flasks with a 175 cm^2 culture surface).

The second scale-up study evaluated the Quantum® Cell Expansion System from Terumo BCT. This hollow fibre bioreactor was able to support expansion processes starting from very low cell seeding densities, therefore resulting in a more efficient expansion process compared to the standard flask-based process (average expansion factor of 16.4 in the bioreactor compared to 3.0 for the flasks). Both bioreactors were able to yield the clinical amount of cells (around 350 million human periosteum derived cells or *hPDCs*) required for the ATMP under development at Prometheus. After the bioreactor-based cell expansion processes, the cultured cells performed similarly to the cells from a standard flask in a standard set of *in vitro* and *in vivo* characterisation assays. Additionally, an interactive tool for the objective comparison of multiple cell expansion strategies was developed, based on a visualisation of 73 different cell expansion processes in 5 types of culture vessels for 7 different types of mesenchymal stem cells.

In parallel to the bioreactor-based scale-up, this work investigated how data measured during these bioreactor processes can be utilised to non-invasively monitor critical process parameters in real-time, and then utilise this information for process control strategies that enable more informed process decisions, ultimately leading to an improved product quality. A monitoring strategy was developed for the quantification of the number of cells (as low as 1×10^5 cells) in a perfusion bioreactor based on a data-based model on oxygen data from a single sensor under dynamic perfusion conditions. Also a real-time imaging-based monitoring strategy was developed for the determination of the ideal time to inhibit the enzymatic cell harvest reaction at the end of an expansion step in 2D culture vessels.

In conclusion, this work shows that the scale-up of human periosteum derived progenitor cells for their use in a cell-based therapy is feasible by making use of automated bioreactor processes. Additionally, new methods were developed to monitor and control critical process parameters during bioreactor culture by making use of process data and data-based models.

Samenvatting

Al ruim 20 jaar wordt beweerd dat cel-gebaseerde therapieën een revolutie zullen teweegbrengen op geneeskundig gebied. Hoewel de grote wetenschappelijke doorbraken die voorstellen om cellen als actief bestanddeel van een therapie te gebruiken elkaar steeds sneller opvolgen, slagen tot op vandaag slechts enkele van deze onderzoeksuccessen er in om hun volledig klinisch potentieel waar te maken en door te groeien tot een alomtegenwoordige commerciële cel gebaseerde behandeling. Naast de overige wetenschappelijke uitdagingen (bijvoorbeeld de exacte actiemechanismen), de dure productontwikkeling en de complexe situatie inzake regelgeving en terugbetalingen van cel-gebaseerde therapieën, wordt verondersteld dat het gebrek aan geautomatiseerde, gecontroleerde en kost-effectieve productiestrategieën een belangrijke hindernis vormen voor de wijdverspreide klinische translatie van dit soort therapieën. Dit werk streeft daarom naar de ontwikkeling van tools en kennis voor het monitoren en controleren van stamcelproductie op grote schaal, met als ultieme doel het faciliteren van de vervaardiging van kwalitatieve en kost-effectieve cel-gebaseerde therapieën.

Ondanks hun beperkt opschaal- en automatisatiepotentieel is celexpansie in celcultuurflessen momenteel nog steeds de meest gangbare productietechnologie. In de eerste fase werd de translatie van een celcultuurfles gebaseerd productieproces naar een bioreactor gebaseerd proces onderzocht, zonder dat daarbij de eigenschappen van de cellen nadelig beïnvloed werden. Twee grootschalige commerciële bioreactor types werden geëvalueerd voor hun capaciteit om kwalitatieve celdosissen te produceren voor een geavanceerd autoloog cel gebaseerd medicinaal product (*ATMP*) dat momenteel ontwikkeld wordt in het Prometheus lab (KU Leuven) voor de behandeling van grote bot defecten. De eerste bioreactor die werd geëvalueerd was de Xpansion® Multiplate Bioreactor System van Pall Life Sciences in combinatie met het Ovizio iLine S beeldvormingssysteem. Het werd aangetoond dat de groeidynamiek van de cellen in de bioreactor dicht aanleunt bij de dynamiek die werd geobserveerd in de standaard celcultuurflessen. Beide culturen resulteerde op het moment van de oogst in

dezelfde celdensiteit (17 500 cellen/cm^2 in de 5.6 L bioreactor met 30 600 cm^2 cultuuroppervlak en 17 300 cellen/cm^2 in de cultuurflessen met 175 cm^2 cultuuroppervlak).

De tweede studie met betrekking tot opschaling evalueerde het Quantum® celexpansiesysteem van Terumo BCT. Deze holle vezel bioreactor was in staat om expansieprocessen te onderhouden waarbij van een zeer lage zaai densiteit gestart werd. Hierdoor werd een efficiënter expansieproces bekomen in vergelijking met het standaard proces op basis van celcultuurflessen (gemiddelde expansiefactor van 16.4 in de bioreactor vergeleken met 3.0 voor de flessen). Beide bioreactoren waren in staat om de klinische hoeveelheid cellen te producen nodig voor de ATMP die wordt ontwikkeld in het Prometheus lab (ongeveer 350 miljoen humane periostale voorlopercellen of *hPDCs*). Na de bioreactor gebaseerde expansieprocessen presteerde de cellen gelijkaardig aan de cellen uit de traditionele fles gebaseerde processen in een standaard set van *in vitro* en *in vivo* karakterisatie experimenten. Bijkomend werd een interactieve tool ontwikkeld voor de objectieve vergelijking van meerdere celexpansiestrategieën die gebaseerd is op een visualisatie van 73 verschillende celexpansieprocessen in 5 verschillende expansietechnologieën voor 7 verschillende types mesenchymale stam cellen.

In parallel met de bioreactor gebaseerde opschaling werd in dit werk ook onderzocht hoe de data van deze bioreactorprocessen gebruikt kan worden om op niet-invasieve wijze kritische procesparameters op te volgen in real-time. Van deze informatie kan daarna verder gebruik gemaakt worden door procescontrolestrategieën die beter geïnformeerde procesbeslissingen toelaten en uiteindelijk leiden tot een verbeterde productkwaliteit. Een monitoringstrategie op basis van een data-gebaseerd model en data van een enkele zuurstofsensor werd ontwikkeld voor het kwantificeren van het aantal cellen (met een ondergrens van 1 x 10^5 cellen) in een perfusiebioreactor onder dynamische perfusiecondities. Ook werd een real-time monitoringstrategie op basis van beeldvorming ontwikkeld voor het bepalen van het ideale tijdstip om de enzymatische oogstreactie aan het einde van de expansiestap te inhiberen voor 2D celcultuur opstellingen.

In conclusie, dit werk toont aan dat de opschaling van humane periostale voorlopercellen mogelijk is voor het gebruik in cel-gebaseerde therapieën door gebruik te maken van geautomatiseerde bioreactorprocessen. Bovendien werden nieuwe methodes ontwikkeld om kritische procesparameters te monitoren en controleren tijdens bioreactorprocessen door gebruik te maken van procesdata en data gebaseerde modellen.

List of Abbreviations

2D	Two dimensional
3D	Three dimensional
ADSC	Adipose derived Stem Cell
ATMP	Advanced Therapy Medicinal Product
BM MSC	Bone Marrow derived Mesenchymal Stem Cell
BMP	Bone Morphogenetic Protein
CD	Cluster of Differentiation
CE-nanoCT	Contrast Enhanced nanofocus Computed Tomography
CITD	Complex, Individual, Time varying and Dynamic
CQA	Critical Quality Attribute
DoE	Design of Experiments
EDTA	Ethylenediaminetetraaceticacid
EMA	European Medicine Agency
FBS	Fetal Bovine Serum
FDA	US Food and Drug Administration
GMP	Good Manufacturing Practice
hPDC	Human Periosteal Derived Cell
HPL	Human Platelet Lysate
ISCT	International Society for Cellular Therapy
MSC	Mesenchymal Stem Cell
PAT	Process Analytical Technology
PBS	Phosphate Buffered Saline
QbD	Quality by Design
TE	Tissue Engineering
TF	Tissue culture flask
UC MSC	Umbilical Cord derived Mesenchymal Stem Cell

Table of Contents

List of Figures

List of Tables

Chapter 1. Introduction

1.1. Cell-based therapies

Cell-based therapies aim to cure various unmet clinical conditions by utilising living cells as the active component of the treatment. While they are still in the early phase of their commercial development, cell-based therapies have the ability to reduce the burden of chronic, oncologic, neurodegenerative, genetic and age-related conditions. Especially since the discovery of the induced pluripotent stem cells (IPS) (Takahashi et al., 2007), it is generally assumed that cell-based treatments will revolutionise the medical field. While the term 'cell-based therapies' is often considered a synonym for the regenerative medicine field that aims at the regeneration of the function of defective tissues and organs (Mason and Dunnill, 2008), the scope of cell-based therapies is broader. For example, tissue engineering strategies where cells are combined with biomaterials and growth factors to replicate the anatomical and physiological nature of the original tissue are considered cell-based therapies, but also the exploitation of the immunomodulatory properties of certain cells for example in graft-versus-host treatments (Nauta and Fibbe, 2007), as well as gene editing of cells for immunotherapies (e.g. chimeric antigen receptor T cell technology) (Kalos et al., 2011) are included under the cell-based therapy umbrella. Conveniently, all the cell-based strategies are regulated under the same European legal framework (Regulation EC No 1394/2007) under the common term of Advanced Therapy Medicinal Products (*ATMPs*).

A classification of cell-based therapies can be made based on the source of the cells; *allogeneic* or *autologous* (Mason and Dunnill, 2009) (Figure 1.1). This concept has a significant repercussion on the use of the cells, the advisable production strategy and business model.

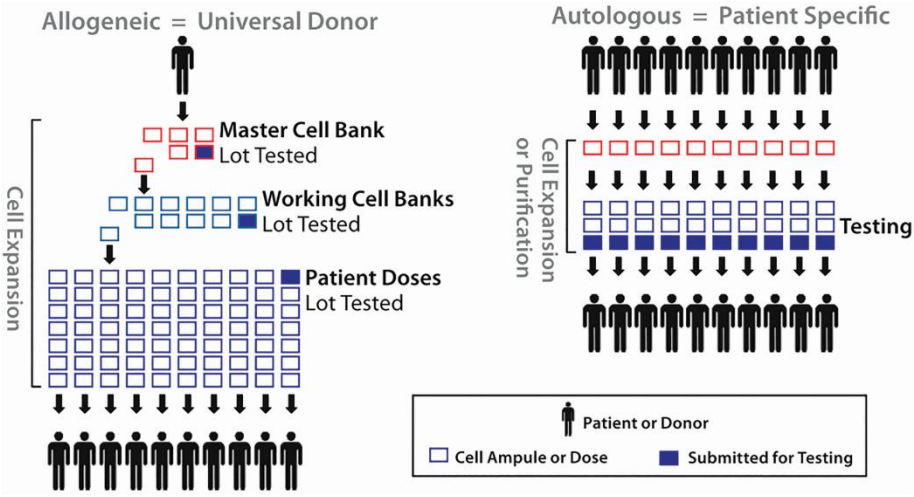

Figure 1.1: Illustration of the difference between allogeneic and autologous strategies for cell-based therapies.
For an allogeneic therapy the cells from one donor are used for many different patients and economies of scale are extremely important for the cost-effective cell processing. For an autologous therapy the donor and patient are the same person, requiring very efficient scaled-out cell processes that are able to handle donor-related variability. Figure from (Brandenberger et al., 2011)

The first option is to source the cells from a "universal donor" from which the cells are used to treat multiple patients in *allogeneic* cell-based therapies, allowing an off-the-shelf business model similar to the one of a traditional biopharmaceutical product such as monoclonal antibodies. Additionally, the allogeneic production and quality control processes benefit from economies of scale. However, the need for immunosuppression is a disadvantage for allogeneic therapies. A second strategy therefore is the *autologous* therapy, in which the donor and the patient are the same person. This approach results in a personalised therapy where product variability needs to be taken into account to a much higher degree since the biological input material for the production process changes from donor to donor. Autologous therapies have the advantage that they do not require donor matching or immunosuppression, and the production processes inherently scaled to the demand. However, the supply chain and quality controls for personalised cell-based therapies are much more complicated, and certain diseases that compromise the quality of

the donor cell material itself can likely not be cured by autologous therapies. Although not used exclusively as a cell source, *stem* cells are often of great interest for cell-based therapies since they have the ability to self-renew and can differentiate into multiple types of mature tissues.

Initial cell-based therapy ventures yielded limited but encouraging economic successes. For example the autologous *in vitro* expanded chondrocytes used by Tigenix (Belgium) in the ChondroCelect cell-based therapy for the treatment of joint surface defects in the cartilage of the knee was the first cell-based therapy approved by the European Medicine Agency (*EMA*). To date Holocar (by Chiesi Farmaceutici), an autologous *in vitro* expanded cell-based product for the treatment of physical or chemical burns of the cornea, is the first and only commercial therapy using *stem* cells that is approved by the EMA. There are multiple patients treated with stem cells in Europe under "hospital exemption" where experimental cell-based therapies are used outside the formally authorized clinical trials. In the EU member states in 2012 there were in total 60 official exemptions of the standard market authorisation track, of which 16 were granted in Belgium (European Comission, 2012). Additionally, there are multiple companies making use of cells by providing high-throughput drug screening and toxicity testing assays based on the biological response of (stem) cells on certain chemical compounds.

Although estimates differ significantly depending on the source of the study, the market value of stem cell products (taking into account both cell-based therapies and drug screening applications) was estimated in a recent report to be around $12 billion in 2014 and predicted to reach around $26.6 billion by 2020 (Mordor Intelligence, 2016). These estimates are based on the large pipeline of potential commercial cell-based therapies that are currently showing promising results in clinical trials. Heathman et al. (2015) report that in 2015 there were 1 342 active clinical trials for cell-based therapies, of which 444 used hematopoietic cells and 382 used mesenchymal stem cells. The evolution of the number of active clinical trials with mesenchymal stem cells, as illustrated in Figure 1.2, suggests that in the near future cell-based therapies will be at the forefront of modern medicine.

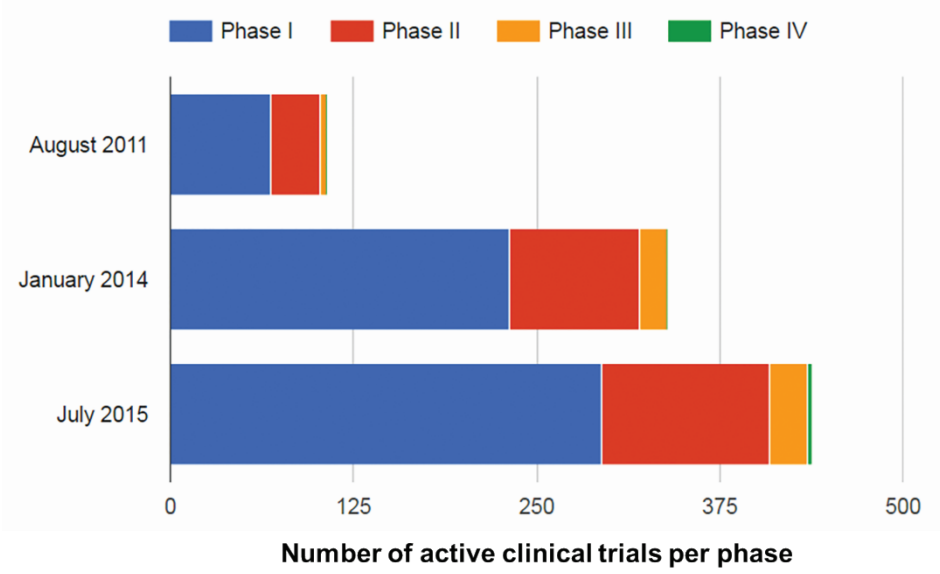

Figure 1.2: Evolution of the number of active clinical trials with mesenchymal stem cells. As reported in (Heathman et al., 2015a; Squillaro et al., 2015; Trounson et al., 2011). References were aggregated based on similarity of selection criteria and data source (ClinicalTrials.gov).

1.2. Large-scale production of cell-based therapies

One thing all cell-based therapies have in common is the need for reproducible and high quality batches of cells. As cell-based therapies are rapidly evolving beyond the laboratory scale, the demand for the production of cells at an industrial scale is rapidly increasing. Unfortunately, only a limited amount of cells can be sourced from living donors. For example, 1 mL of human bone marrow provides approximately 1 000 mesenchymal stem cells (Fennema et al., 2009), while cell-based therapies and other applications such as cell-based drug screening platforms generally require much more cells. Typically, single cell doses for cell-based therapies range between 10^7 to 10^9 cells (Jung et al., 2012; Simaria et al., 2014a). An interesting example regarding the scale and frequency of the required cell numbers is the allogeneic cell-therapy by Osiris Therapeutics, Prochymal, as a treatment against acute graft-versus-host disease. The therapy is based on *in vitro* expanded mesenchymal stem cells. Patients are treated by repeated intravenous injection of 2 x 10^6cells/kg/dose, twice a week for four weeks,

reporting 82% of the patients with positive response in phase III trials (Martin et al., 2010). Hence, it is clear that sequences of cell expansion steps are required to multiply the small number of cells taken originally from the donor biopsy to the amounts required for clinical application. Given that currently the majority of cell based-therapies remain in the early phases of the clinical trials (as seen in Figure 1.2) where only relatively small production volumes are required, it is hypothesised that the scale-up of cell-based therapy production is one of the major hurdles in translating promising cell-based therapies from the lab to an economically viable product (Davie et al., 2012).

The large-scale production of living cells is a multi-disciplinary attainment at the interface of biology and engineering. It might therefore not be a surprise that it is a daunting task to design cost-effective cell production processes that are able to robustly deliver potent cells for clinical applications. However, the biopharmaceutical industry has overcome similar challenges for the production of monoclonal antibodies and other therapeutic products by making use of cells as biological production units. The production of these 'biologics' by yeasts, and later by mammalian cells, also started off slowly with modest production titers. Now it represents a market with a value of around $ 1 425 billion per year (Marketsandmarkets, 2015). Many lessons can be learned from its evolution towards the mature industry it has become in only a couple of decades (the first monoclonal antibody was produced in 1975, the first licence for clinical use was granted in 1986 (Liu, 2014)).

Some of the current cell expansion technologies are inspired on the conventional bioprocesses for the bioreactor or fermentor-based production in the biopharmaceutical industry. However, it is clear that the production of cells for cell-based therapies requires its own distinct developments. One important difference is that for biologics the product can be purified and isolated without the need to recover the living cells, contrary to the production of the cells themselves for cell based-therapies. Additionally, in contrast to the standardised non-human cell lines used for the production of biologics (e.g. suspension cultures of Escherichia coli, Chinese hamster ovary or CHO cells), the human (stem) cells generally are sourced from many different donors with various growth characteristics, are anchorage dependent, and can potentially start to (de)differentiate during culture. Although all cell expansion processes share similar foundations, there is currently not a single process blueprint that can be applied because many different cell types and clinical applications are involved that all require fine-tuned culture conditions and protocols.

On top of the manufacturing challenges from the technical side, cell-based products for clinical applications also need to comply to stringent rules for

quality control and regulatory requirements. Since the produced cells are used eventually in clinical applications where the patient's life might be at stake, the monitoring and control of process and product characteristics is paramount. Considering that the inherent biological complexity and variability of the living product is challenging the standard regulatory framework of the traditional pharmaceutical sector, multiple directives have been written by the European Medicines agency (*EMA*) the US Food and Drug Administration (*FDA*) that guide manufacturers towards a better controlled production in order to receive market authorisation. However, in practice the implementation of these directives is challenging due to the lack of appropriate tools for monitoring and controlling bioprocesses. Preferably a continuous verification of cell potency, identity, purity and safety is required during culture and it is up to the manufacturing process to assure the presence of these critical quality attributes (*CQAs*) at the moment of the administration of the product to the patient.

As a way to implement more controlled manufacturing processes for the consistent quality of cell-based products as requested by the regulatory bodies, the use of quality assurance frameworks such as Process Analytical Technologies (*PAT*) and Quality by Design (*QbD*) are encouraged (Glassey et al., 2011; Kourti, 2006; Read et al., 2010). The main goal of QbD is to clearly define the interdependency of critical process parameters and their effect on the CQAs (by means of statistical and other data-sciences tools such as Design of Experiment or DoE) with the ultimate aim of determining a parameter space or "design space" in which the desired product quality can be guaranteed. The design space is defined by the International Council for Harmonisation of Technical Requirements for Pharmaceuticals for Human Use (ICH) as "*the multidimensional combination and interaction of input variables and process parameters that have been demonstrated to provide assurance of quality*" (ICH, 2009). In practice, this means that after the assessment and approval by the regulatory bodies of a design space, operations within this space are considered save and should result in adequate products, while operating outside of this space is not allowed without regulatory post-approval.

This implies that processes for clinical-scale cell expansion require (i) the appropriate sensors and monitoring tools to define and verify the design space and its effect on the critical quality attributes of the product, preferably in an on-line (as in close to continuously measured) and non-invasive way (discussed in section 1.4), and (ii) the appropriate hardware that allows to control the large-scale processes within the design space. This control is often found in the form of automated bioreactors that use the sensor and monitoring

tools as feedback to optimise and control the environment of the cells as discussed in the next section.

1.3. Bioreactors for cell expansion

The term ‘process intensification’ indicates efforts that, compared to the gold standard techniques used today, provide sizeable improvements in manufacturing and substantially decrease the equipment size over production capacity ratio (i.e. footprint) and resource utilisation, ultimately leading to more cost-effective technologies (Stankiewicz and Moulijn, 2000). As in any industry where process intensification is required, process engineers revert to increased automation and scale-up of processes. Since the start of the industrialisation of biology, bioreactors and industrial biotechnology have been going hand in hand for the automation and scale-up of bioprocesses. In addition, bioreactor technology is often implemented at critical process steps in order to reduce process variability and enhance process reproducibility.

Bioreactors are described as instruments that “create a biosphere that as profoundly and adequately as possible provides the ideal environment for the biological reaction” (Mandenius, 2016). Within this general definition the term ‘ideal’ is rather ill-defined and might depend on the exact application of the bioreactor. In the context of bioprocess development for cell production there are two necessary conditions before the cell environment is considered ‘ideal’ (but compared to the human body rather to be classified as ‘suitable’): (i) favourable physical conditions regarding mass balances (i.e. nutrient, waste and gas transport), energy balances (i.e. heat and shear stresses) and their evolution over time to maintain cellular function, (ii) operability in an industrial setting, i.e. providing process monitoring and control, optimising input of resources (work load, reagents, facility,..), decreasing contamination risk and facilitating regulatory approval.

Bioreactor technology historically originates from the early food processing industry (e.g. beer, wine), and evolved to other fermentation-based production processes for biochemical components (e.g. alcohols, amino acids, polymers) and the large-scale production of antibiotics (Mandenius, 2016). Since the bioreactor-based protein manufacturing (e.g. insulin, erythropoietin and monoclonal anti-bodies) the biotech industrialisation is moving up a gear and over the second half of the 20th century immense production volumes are reached for which mammalian cell suspension cultures are used to produce biopharmaceutical products (Croughan et al., 2015). Not only the bioreactor technology surged, but many process monitoring and control strategies find their origins in this industry. Since the very end of the 20th century, the efforts

of harnessing the potential of the cells themselves (and not solely their by-products) for the treatment of unmet clinical needs began. While previously the cells or their remnants were highly undesired regarding the purity of the clinical product, the use of the cells themselves in cell-based therapies preluded a paradigm shift for the design, monitoring and control of the bioreactors in which they are produced.

In the pursuit for more cost-effective cell expansion processes there are three strategies that can be followed. Generally the choice depends on the clinical application and the specific cell type. Firstly, there is *scale-out*, which means increasing the production by doing more of the same, i.e. using more culture vessels. Secondly, there is *scale-up*, or increasing the available cell culture surface by increasing the size of the vessel. In parallel there is a continuous evolution towards an *increased culture surface per volume*, i.e. increasing the available surface per vessel in order to reduce the process footprint. This is often done by replacing the gas layers in culture vessels with active oxygenation and perfusion systems and/or increasing the available surface by going from planar culture systems to bended and more 3D-like or porous surfaces. Large gains in production can be made by combining these three strategies.

The current gold standard for (anchorage dependent) cell expansion is still the planar plasma-treated polystyrene tissue culture flask. Cell culture flasks or T-flasks (Figure 1.3A) are easy to use, and relatively cheap and versatile for small-scale processes. However, there are many disadvantage associated with their use. First of all do they require extensive manual open-vessel manipulation by highly trained operators in large and expensive contamination-free environments (i.e. clean rooms and incubators compliant with Good Manufacturing Practices or *GMP*). Additionally, cultures in T-flasks will never be able to reach very high cell densities per volume due to their inherent design features with a low culture surface per total vessel volume. Cell factories or cell stacks (Figure 1.3B) are the scaled-up version of tissue flasks. Technically, by having one flask in which multiple horizontal layers of culture plastic and gas are alternated the number of open-vessel operation can be reduced. However, the increase in culture surface per volume is not significantly improved since there are still large gas layers in between the different levels in the flaks. In a more recent evolution, e.g. the hyperflask (or the larger scale hyperstack), the large gas layer above the culture medium is replaced by a very thin opening underneath the different layers of plastic that in turn is also designed to be O_2 and CO_2 permeable (Figure 1.3C). While this features saves ± 2.5 times the volume for the same amount of culture surfaces, using large numbers of any type of flask becomes impractical fairly

fast due to the clunky auxiliary peripheral devices required for filling and harvesting the flasks (Figure 1.3D).

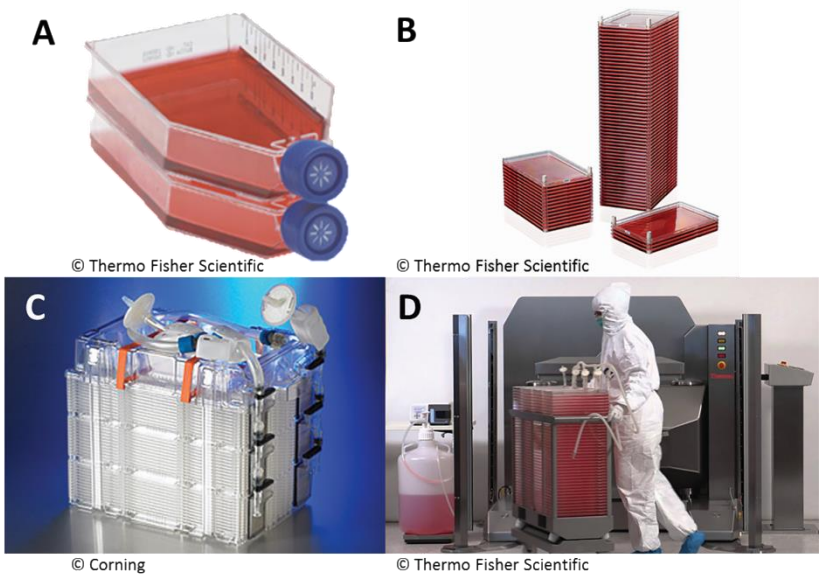

Figure 1.3: Evolution of flask-based planar culture vessels.
A) Standard T-flask. B) Cell stacks C) Hyperstack in which the gas layer above the medium is made redundant by use of a O_2 and CO_2 permeable plastic D) Peripheral instruments for filling large numbers of cell stacks.

By completely removing the gas layers in between the different polystyrene layers in a cell stack, and solving the resulting mass transfer problem with active oxygenation of the culture medium and a magnetic mixer to recirculate the oxygenated medium over all the layers of the vessel, the Xpansion bioreactor of Pall Life Sciences (Figure 1.4A, see Figure 4.3 in Chapter 4 for more details) optimises the available culture surface per volume even further. More importantly, by making use of external pumps and sterile connectors, the open processes required for flask-based cultures are avoided. Contrary to T-flasks, these bioreactor vessels are standardly equipped with temperature, pH and O_2 sensors enabling the on-line control of the process. Additionally, a peripheral holographic microscope setup allows the visual off-line monitoring of 6 to 10 plates of the bioreactor. The largest Xpansion version, with 200 layers, houses 122 400 cm^2 culture surface in 21.9L culture medium.

From here on an increase of the culture surface per volume is only possible by leaving the planar culture surfaces. For example the Terumo Quantum hollow

fibre bioreactor (Figure 1.4B, see Chapter 6 for more details) is able to culture cells in ±11 500 hollow fibres, making up 21 000 cm^2 culture surface in a volume of only 500 mL. The hollow fibre bioreactor can be perfused with fresh or recirculated medium at two independent speeds either through the hollow fibre lumen or from the outside of the fibres. Additionally, it is a benchtop bioreactor with a small footprint that with the aid of peripheral sterile welding devices is able to work without the need for biosafety cabinets and incubators. Since the configuration of the fibres does not allow to monitor the cells visually, more innovative process monitoring approaches are required (see Chapter 7 for example).

Another non-planar variation uses the surface of suspended microcarriers for cell expansion (Figure 1.4C). By growing the cells on small spherical particles (size around 200 µm) in suspension, very large culture volumes can be reached in vessels or bags with a relatively efficient culture surface per volume ratio. Additionally, monitoring tools are relatively easy to implement in these vessels or bags since they don't have to be incorporated in the tubing of the perfusion system and even cell containing culture medium samples can be taken during culture for more elaborate quality control assays. A large variety of microcarrier-based culture systems exists, both in terms of vessel types, volumes and microcarrier composition. The microcarrier-based culture was not directly the focus of this doctoral work, although it is a very promising strategy for the scale-up of allogeneic cell-based therapies due to the large batch sizes that can be reached.

A less common cell expansion strategy for human (stem) cells makes use of perfused packed beds or 3D scaffold structures from (macro)porous materials (Figure 1.4D, see Chapter 7 for more details). These 3D growth surfaces are able to significantly increase the available culture surface per volume, thereby optimising the process footprint. Since the curved surfaces of hollow fibre bioreactors or microcarriers are still having a relatively large radius compared to the cell size, these culture conditions do not differ that much from the planar culture technology. However, for the 3D surfaces that more closely resemble the natural environment of the cells, the cell behaviour is different (Braccini et al., 2005). For example the secretion of extra cellular matrix and pore bridging is often seen, making the recovery of the cells a primary concern (Sonnaert et al., 2015a). The 3D scaffold-based configuration makes these bioreactors particularly challenging for monitoring and therefore require novel monitoring approaches (see for example Chapter 7 and Sonnaert et al., 2015b).

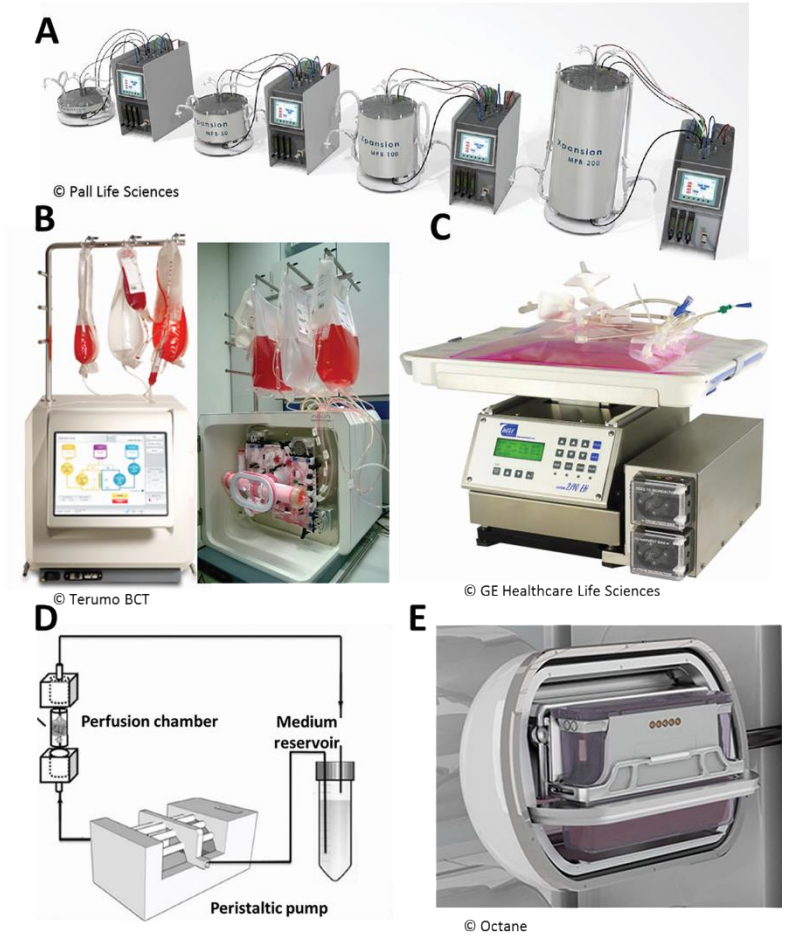

Figure 1.4: Bioreactor systems for (stem) cell expansion.
A) Pall Life Sciences Xpansion® Multiplate Bioreactor System B) Terumo® BCT Quantum Cell Expansion System, a hollow fibre bioreactor C) GE Wave® bioreactor, a microcarrier bioreactor D) Illustration of a simple perfusion bioreactor design were the cells are cultured on 3D scaffold structures E) Concept of the Octane bioreactor inside the Cocoon.

Some bioreactors take the bioprocess optimisation, and more specifically the bioprocess integration, multiple steps forward. For example the Cocoon bioreactor developed by Octane (Canada) and currently under evaluation at Lonza as a platform for personalised cell therapy manufacturing platform, aims to fully automate the cell processes from the subsequent digest of the biopsy, (stem) cell isolation, cell expansion and seeding onto a biologically active carrier materials in a benchtop bioreactor system (www.octaneco.com).

Selecting the most appropriate technology during development is not always a straightforward task since there is no 'one size fits all' solution. An overview of some of the most popular cell expansion vessels and their culture characteristics is provided in Figure 1.6. A preliminary indication for the most appropriate expansion technology can be based on the autologous or allogeneic nature of the therapy. For autologous therapies, were the cell processes are not of a massive scale and often executed close to the patient due to the lack of appropriate means for cell storage, the decentralised (scaled-out) multi-centre production model is often the most feasible strategy (Foley and Whitaker, 2012; Hourd et al., 2014). These types of production models benefit more from compact and highly automated benchtop bioreactor systems as the Terumo Quantum bioreactor that can be operated next or the patient's bedside by matter of speaking. For autologous decentralised production, process monitoring is critical in order to assure process consistency and comparability over the multiple sites and patients (Hourd et al., 2008). Allogeneic processes, where the 'economies of scale' principle applies, focus more on the production of very large uniform batches of cells. With the current technology, these large volumes can only be reached in industrial size microcarrier suspension cultures (Figure 1.5) that are inspired on the production of biopharmaceuticals such as recombinant protein, vaccines, etc.(Simaria et al., 2014b).

Figure 1.5: 12000L bioreactors for the production of recombinant protein at Celltrion. Copyright© 2016 Celltrion Inc.

As the scale of the cell production processes is increasing, the downstream processes (i.e. cell harvest, volume reduction, purification, storage and transportation) become more challenging (Hassan et al., 2015). Only recently the downstream process bottlenecks became the subject of process optimisation studies. For example Nienow et al. (2014) introduced a dynamic harvest methodology to retrieve expanded cells from microcarriers and the subsequent cryopreservation (Heathman et al., 2015d). More recently an integrated process for washing and filtration of stem cells after expansion was described (Cunha et al., 2015b; Cunha et al., 2016).

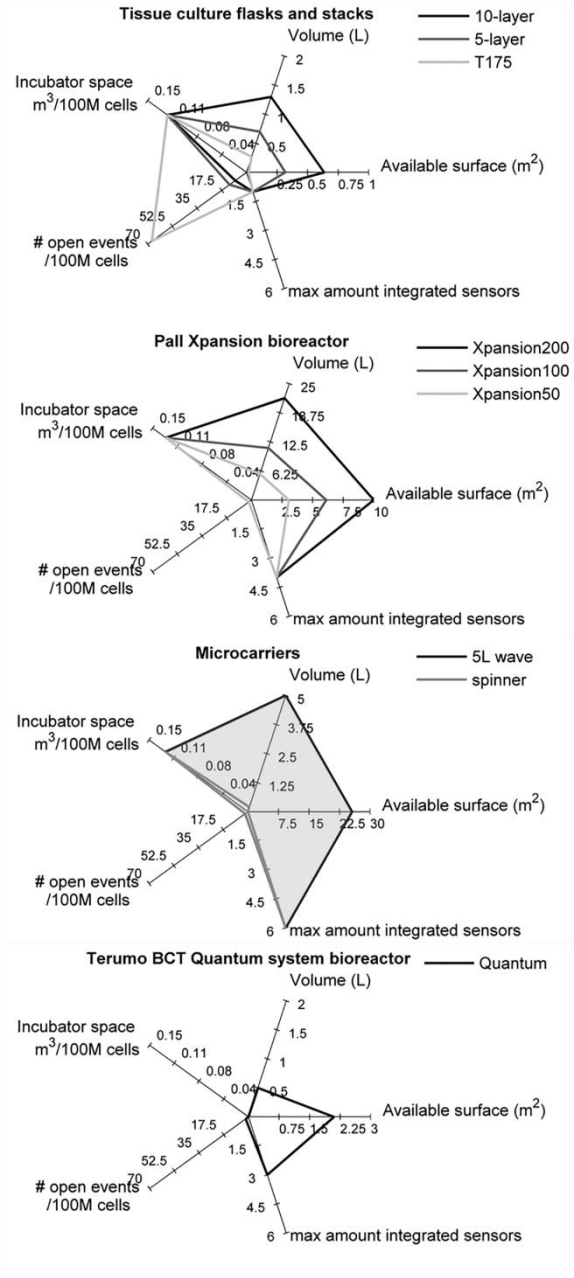

Figure 1.6: Overview of different cell expansion units and their main characteristics.
Data gathered from manufacturers' specification sheets. Data on microcarriers from (Simaria et al., 2014b).

1.4. Model-based bioprocess monitoring and control

1.4.1. Monitoring cell expansion processes

According to the European Medicines Agency's (*EMA*) guidelines, Process Validation for pharmaceutical production is defined as "documented evidence that the process, operated within established parameters, can perform effectively and reproducibly to produce a medical product meeting its predetermined specifications and quality attributes" (ICH Expert Working Group, 2000). More recently, the EMA encouraged the use of '*Continuous* Process Verification (CPV)' where process performance is continuously (or '*on-line*') monitored and the same type of performance evaluation is developed/used already during the product development phase, as this strategy facilitates scale-up, process comparability or reproducibility, and post-approval change control in later stages of the product lifecycle (EMA, 2014).

The goal of monitoring culture processes during cell therapy development and manufacturing is to assure a better replication and control of culture conditions over multiple cell-processing runs (Csaszar et al., 2013). In order for the monitoring strategy to support continuous process verification, on-line non-invasive monitoring tools are required, since these allow for up-to-date information to be obtained from the system at any time without manual interventions or time delays involved (which are typical for the more standard at-line process monitoring). Apart from the on-line or real-time nature of the measurements, the non-invasiveness (meaning that no probes or labels enter the closed culture environment) of the tool should be ensured if the process is running under GMP conditions, because otherwise the purity and sterility of the implanted cells will be more difficult to guarantee. In a second phase, on-line monitoring enables intelligent real-time control of the culture parameters, resulting in an increased robustness of the process and clinical efficacy of the therapy. On-line non-invasive process monitoring techniques for cell therapy manufacturing can be roughly divided in three major classes as described below.

Monitoring of physicochemical culture variables: Variables such as pH and dissolved O_2 or CO_2 concentration provide information on the (micro-) environment of the cultured cells. Often these variables can be non-invasively monitored in real-time (on-line) by means of fibre-optic sensors, both for 2D and 3D cultures (Sart et al., 2014). On-line monitoring of these variables is critical for the bioreactor to maintain the suitable environmental conditions for cell expansion. However, these general environmental variables are not exclusively related to the biology of the cells and therefore only

provide limited or indirect information on the critical quality attributes of the cells themselves. An strategy to use O_2 measurements to infer critical process information regarding cell growth will be discussed in more detail in Chapter 7.

Imaging technology: Image-based monitoring recapitulates the visual inspection that is currently done by a process operator. Current imaging technologies that are on-line and non-invasive (therefore excluding technologies using fluorescent labels or computed tomography) are only able to image 2D cell cultures on semi-transparent culture surfaces. The current state of the art in industrial-scale image-based bioprocess monitoring is the use of non-invasive holographic imaging (Ovizio) on large scale cell Xpansion bioreactors. This microscope is able to image and semi-automatically analyse cell features on multiple heights in a multi-stack 2D bioreactors (see Chapter 5 for details). Traditional optical microscopes use a complex assembly of lenses and focusing requires mechanical movement of these optical elements, resulting in costly and bulky systems that are difficult to integrate in on-line monitoring systems for bioreactors. Therefore Imec (Belgium) and Prometheus (KU Leuven, Belgium) work together to integrate a lens-free holographic image-based technology with a very large field of view in cell culture systems to monitor cell growth and morphological changes during culture by using coherent light (i.e. a laser) and an imager to capture the light that is diffracted off the culture surface (see Figure 1.7 for a representative example of a capture with the lens-free microscope).

Image-based monitoring provides direct feedback on the cellular phenotype and is therefore from a biological point of view an indispensable monitoring technique. However, translating images into objective quantitative process parameters is challenging and requires further development in image processing and data-based cell identification techniques. Additionally, the configuration of certain bioreactors (for example microcarrier or hollow fibre-based designs) currently do not allow image-based monitoring.

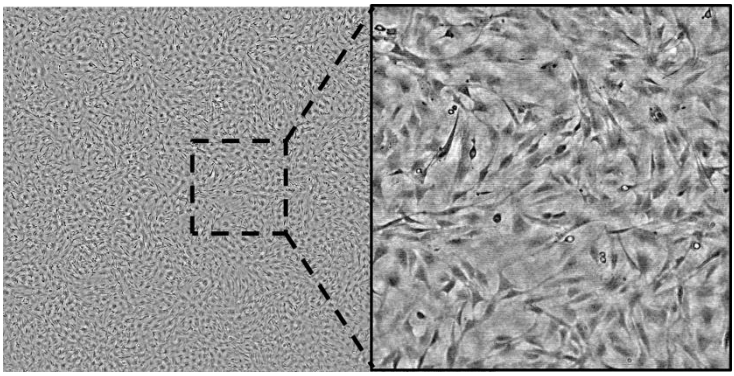

Figure 1.7: Preliminary data generated by the IMEC-Prometheus collaboration on a LFI microscope.
On the left the complete field of view is shown while on the right a more detailed zoom is provided, clearly indicating the exceptional combination of a large field of view and resolution.

Bio-sensing: By analysing the (by-)products of cell metabolism, either being taken-up from the culture medium or secreted into the medium, the biological state of the cells can be derived indirectly. These techniques generally require sterile sampling from the culture medium and can be applied to 2D and 3D cultures. An advantage here is that the read-out (often in the form of spectra) represents information from the (internal) metabolism of the cells themselves. Since the metabolism is typically governing cell fate this data has therefore a higher informative value regarding *in vivo* potency compared to the two previous types of monitoring data. However, current technologies e.g. based on immunoassays, mass spectrometry, chromatography or spectroscopy are not yet available in cost-effective on-line setups, require large efforts in sample preparation (even requiring cell samples which is certainly not non-invasive) and often lack specificity in complex culture media with a high protein background.

1.4.2. Model-based process control

While it is common that measurements of physicochemical or environmental variables (e.g. pH, O_2) are used as feedback for a controller that allows the bioreactor to maintain suitable conditions for expanding cells, it is much more challenging to obtain on-line and non-invasive information directly on the critical quality attributes (*CQAs*) of the cells themselves and use this information to directly control the features of the cultured cells, e.g. their growth characteristics, metabolic state, and ultimately *in vivo* potency. In the first place the challenge lies in developing the sensor hardware for the on-line

determination of these parameters as discussed previously. However, since more and more process data is collected, it is a promising approach to estimate the unmeasurable CQAs in real-time, based on (a combination of) indirect measurements that can be related to the CQA of interest. This is generally known as a 'soft sensor' method (de Assis and Filho, 2000; Kadlec et al., 2009), where the information of (multiple) indirect data streams is translated to interpretable process parameters. For example in Chapter 7, a method is described that exploits data from oxygen measurements and known changes in perfusion rates to derive precise on-line estimates on cell numbers in 3D scaffold-based cultures. In Chapter 6, the rate of change in lactate production of the cells is used to estimate the optimal time to start harvesting the bioreactor and in Chapter 5 the change in circularity of the cells is used as a predictor for the optimal time to stop the enzymatic harvest reaction.

The examples above are all situations where, based on process measurements and consecutive interpretation of the data by a model, real-time process monitoring tools were developed for critical process features. Ultimately this 'model-based *monitoring'* strategy, combined with a desired output trajectory can be used as the basis for 'model-based *control'* in which the measured process data and a model are used to determine or predict the most appropriate controller setting to reach the desired state of the process or the cells. Although more often used in fermentor bioreactors (Aehle et al., 2012; Kovarova-Kovar et al., 2000; Ławryńczuk, 2008; Ramaswamy et al., 2005) only limited examples of model-based control can be found in literature for stem cell bioreactors (Csaszar et al., 2012).

In between process monitoring and the actual process control, models are required for 'translating' the raw monitoring data into interpretable process parameters that can be used to make informed process control decisions. There are some important considerations regarding the models used for this translation. In general, there are two opposing ends of the modelling spectrum: on the one had there are the *data-based approaches* where the model structure is completely based on the data (inductive). On the other hand there are the *mechanistic approaches* were *a priori* knowledge on the biological system is included (deductive) (Young, 1999). Modelling techniques used for the data-driven approach range from simple transfer function models (as used in Chapter 5 and 7) to principal component analysis, and neural networks. The mechanistic models often make use of conservation equations, stoichiometry and reaction kinetics.

Mechanistic models may be superior in providing insight into the system under consideration since their parameters have a physical meaning.

However, they have a significant cost of development, are more difficult to parameterise, and are generally harder to compute in real-time which is often a requirement for process controllers. At the same time, the biological processes are often too complex to be described by mechanistic models and the experimental validation of these models quickly becomes too elaborate (for example the donor-related variability is near impossible to capture in a meaningful way without making use of data-driven methods). Data-based models on the contrary provide less insight into the system, but are more straightforward to develop and in situations where the data logging surpasses the speed of analysis they provide an ideal basis for online prediction and control (Papantoniou et al., 2014). In the cell expansion field and biotech in general, there is often abundant high quality process data available due to the GMP and quality control requirements, which is a clear advantage for data-based approaches. On the other hand, biologists, doctors and regulatory bodies might be hesitant on the 'black-box' nature of the data-based models. Additionally, results from a data-based model can often not be extrapolated to cases outside of the initial scope of the data. While this PhD project focused on data-driven approaches, both modelling strategies can contribute to a more effective translation of cell-based therapies to the clinic. In addition, hybrid strategies exist, resulting data-based mechanistic models that are able in some cases to combine best of both worlds (von Stosch et al., 2014).

1.5. Challenges for widespread clinical use of cell-based therapies

To summarise this introductory chapter, two main challenges for the widespread clinical use of cell-based therapies were identified. First, while there is an abundance of culture technology, there is a need for more integrated bioprocess designs that are able to produce cells for therapeutic products in a cost-effective and robust way. Secondly, there are not many sensors that are able to provide real-time feedback on the quality of the cells in the bioreactor. Therefore, novel monitoring strategies are required that allow on-line control of critical quality attributes of the cells in order to reduce process variability and improve *in vivo* potential of the cells.

To date, the gold standard cell production strategy consists of a series of expansions steps in tissue culture flasks (see Figure 1.8 A). Human operators are required to perform the numerous manual manipulations to monitor and control the process, and generally there is only sparse feedback on the process (e.g. off-line manual verification of confluence level and morphology). The manual interventions and the lack of continuous feedback leads to high costs and variable process outcomes. Therefore, in this work it is hypothesised that

by translating the flask-based process to an integrated and controlled bioreactor-based process, in which online monitoring of critical process parameters allows continuous process control, will increase the robustness of the cell-based product (see Figure 1.8B). Since to date no monitoring systems exist that are able to directly measure the critical quality attributes of the cells, a model will be used to link process read-outs to critical quality attributes and subsequently derive the appropriate process inputs for a controlled process.

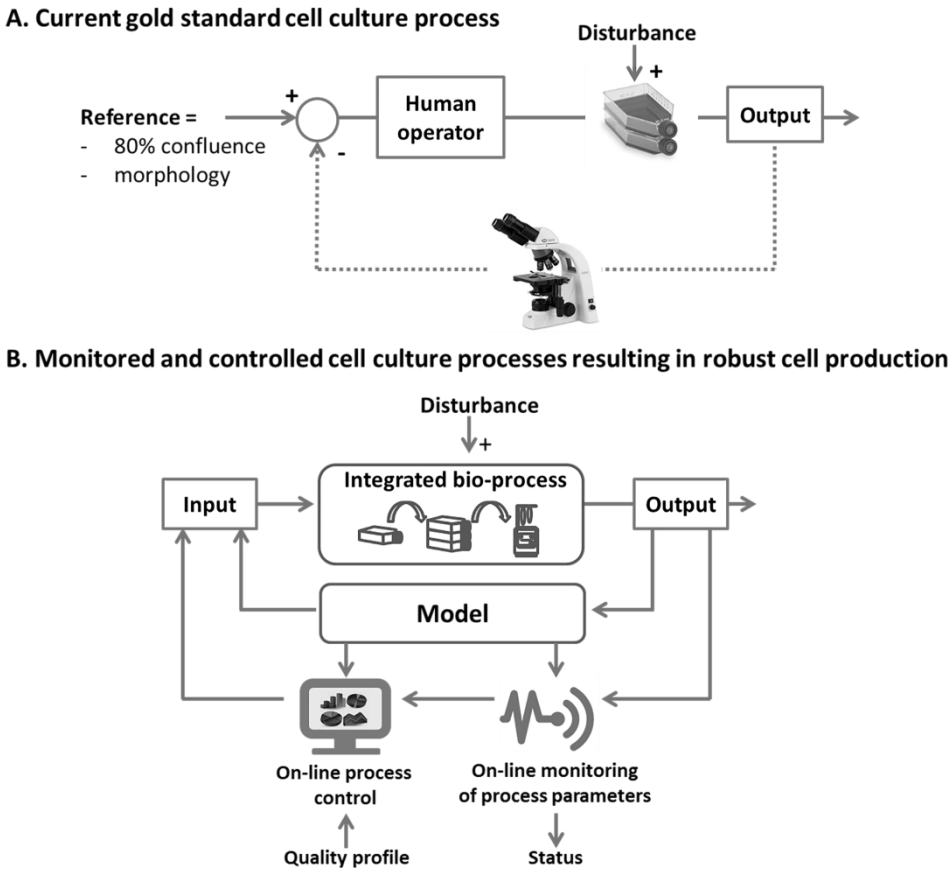

Figure 1.8: A) Current gold standard cell culture process that makes use of tissue culture flasks and human operators. B) Concept of on-line monitored and controlled cell culture process.

Chapter 2. Thesis objectives and research approach

The previous chapter attempts to familiarise the reader with the most important concepts, the state of the art and the challenges involved in large-scale (stem) cell expansion for cell-based therapies. This chapter positions the work that was done during the doctoral research in this larger framework and addresses the thesis objectives.

The common thread throughout this work is the need for a monitored and controlled expansion of progenitor cells suited for an autologous cell-based advanced therapy medicinal product (ATMP) that is currently being developed at Prometheus, the division of Skeletal Tissue Engineering of the KU Leuven. This ATMP makes use of *ex vivo* expanded human periosteal derived progenitor cells (hPDCs) for the clinical treatment of non-healing long bone defects (Lammens et al., 2012; Roberts et al., 2014). For the production of this cell-based product a small periost biopsy is taken from the patient, whereafter the stem/progenitor cells are enzymatically released and cultured *in vitro* for several weeks (10 to 12 population doublings). Ultimately, around 300 million cells are needed for implantation at the site of the bone defect, seeded on a calcium-phosphate based carrier in combination with a bioactive growth factor (BMP). Promising results were obtained in a series of large-scale pre-clinical experiments in which clinically relevant amounts of bone were formed in an orthotopic critical-size long bone defect in a large animal model (i.e. sheep).

In parallel with the scale-up of the hPDC production, data-based approaches were investigated that would allow to on-line monitor and control critical process parameters during these up-scaled expansion processes. The process monitoring and control approach was inspired on the data-based approach from the M3-BIORES (Measure, Model & Manage Bioresponses) lab. The main focus at M3-BIORES is to develop real-time model-based monitoring and control algorithms for biological processes taking into account the complex, individual, time varying and dynamic (CITD) nature of biological responses to the bioprocess environment. This approach is framed within the standard model-based control scheme as can be seen in Figure 2.1 (Brosilow and Joseph, 2002; Camacho and Bordons, 2007). The practical implementation of the control scheme varies widely, but in general it consists of a (biological) process, e.g. the cell expansion vessel in this case, and a model that is able to translate time-variant process data into interpretable information that is either used to report on the process status through a monitor, or that can be used to make informed process control decisions.

With the clinical translation of the Prometheus ATMP in mind, this work focuses on two major hurdles for the development and widespread clinical translation of cell-based therapies in general: scale-up of cell expansion processes, and process monitoring and control under inherent biological variability. Pursuing the process scale-up and at the same time developing monitoring and control strategies leads to synergistic effects. While the additional data from the monitoring and control tools can be used to validate the process comparability, working in the large-scale clinical-grade bioreactors provides an instant reality check on the clinical applicability of the monitoring tool. The structure of this work reflects this interaction. Each bioreactor scale-up chapter (Chapter 4 and 6) is followed by a chapter on a data-based monitoring tool for this specific type of bioreactor (Chapter 5 and 7).

Objective 1: **Provide a framework for benchmarking of cell expansion processes.**

Before the results of different cell expansion processes are compared in later chapters of this work, it is required to define how meaningful comparisons can be made. Especially since there are a large number of process parameters that contribute to the efficiency and cost-effectiveness of a cell expansion process (e.g. cell seeding densities, medium composition, culture vessels, medium volumes, etc.), in combination with multiple cell expansion strategies (scale-up vs scale-out, centralised production vs decentralised production), benchmarking of these processes is a challenging task. In Chapter 3 we

hypothesise that based on a selection of objective metrics (such as expansion factor, final cell yield, cell density at harvest, concentration of protein supplement ,etc.) it is possible to provide a framework for the comparison of cell expansion processes that is able to improve the general understanding of the critical process parameters that define a cell culture process, and in the future allow a more rational and integrated design of the cell expansion bioprocesses.

Objective 2: Translate the standard flask-based expansion process for the autologous Prometheus ATMP to an automated and controlled bioreactor-based process.

More and more technological developments (bioreactors, centrifuges, etc.) are becoming available for the large-scale production of stem cells, but the translation from the standard small-scale flask-based cell expansion to the large-scale bioreactor-based cell expansion is not straightforward. Challenges arise for example in how to retain the critical quality attributes of the cells during the process, matching the best available technology to a specific process strategy, and the effect of scale-up on the production cost and downstream processes. In other words, an integrated bioprocess design that takes into account cell quality, the required scale, up- and downstream workload and production costs is required. For the (pre-)clinical work that is undertaken in the Prometheus lab for the healing of long bone defects, it was hypothesised that the manual expansion of the human periosteum derived cells (hPDCs) can be translated to an automated bioreactor-based process without compromising the *in-vivo* bone healing potential of the cultured cells. Since the comparability between the bioreactor and flask-based process is critical (see Objective 3), a strong focus on evaluating the potency of the resulting cell quality is required, based on a quantitative *in vivo* bone-forming potency assay. Additional questions that were addressed are how the bioreactor-based expansion compares to the standard methods in terms of ease of use, cost of goods and scalability of production, thereby trying to connect the type of bioreactor to possible strategies for commercial cell processing.

Objective 3: Incorporate cost-effective data-based monitoring and control strategies in the large-scale production processes in order to deliver cells with a more robust quality profile and assure process comparability.

Cell expansion processes are still often operated as a ‘black box’, and thus in most cases result in sub-optimal and variable process outcomes. Functional

bioprocess control in cell expansion vessels, enabling direct control over the critical quality attributes of the cells such as proliferation rate, differentiation stage, etc., remains challenging due to inadequate on-line non-invasive monitoring tools. In addition, the living nature of the cell-based product introduces fluctuations in manufacturing outcomes while regulatory authorities desire a tight control of process performance. It is hypothesised that by skilfully utilising data that is generated by common process read-outs such as microscope images (Chapter 5) and oxygen sensors (Chapter 7), critical process parameters such as the level of confluence or the incubation time during cell harvest can be better monitored and controlled, while at the same time the inherent donor-related variability that is found in cell expansion processes can be taken into account (Chapter 6). The improved monitoring and control will ultimately lead to cells with a more robust quality profile.

Additionally, the need for process comparability is, amongst others, critical for post-approval changes to the production processes of ATMPs, translation of processes to Contract Research Manufacturers or even just to verify the results of a scaled-up process as described in Objective 2. Especially for autologous therapies where decentralised manufacturing is a common strategy and donor-dependent variation is ubiquitous, comparability is key (Hourd et al., 2008). It is hypothesised that the data-based process monitoring tools can also be applied to facilitate the demonstration of comparability between different production methods, production batches or production sites, and even the comparability between different donors.

In Figure 2.1 the core elements of the following chapters are situated in a general control scheme. At the beginning of every chapter this general control scheme will also be used to position the specific chapter within the framework of this PhD work. While Chapter 3 interactively summarises a large amount of expansion processes and introduces the framework for cell expansion process comparability, Chapter 4 and Chapter 6 both focus on the translation of a flask-based process to a large-scale bioreactor system. Chapter 5 and 7 describe for each of the bioreactor types of the previous chapter an example of the use of data-based models. The models, in combination with process data, are utilised to monitor critical quality attributes of the process, based on which informed process control decisions can be made.

Figure 2.1: Standard model-based control scheme as applied throughout the project.

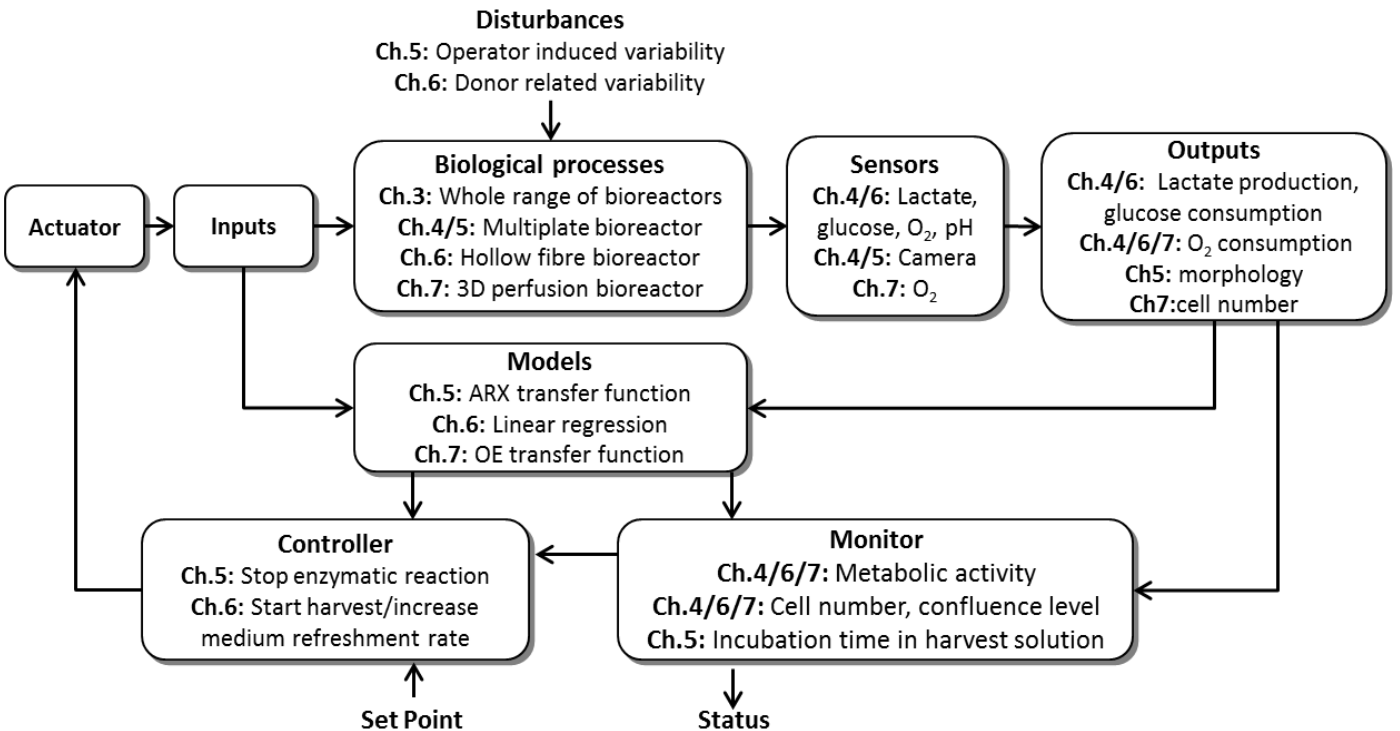

Chapter 3. Large-scale mesenchymal stem/stromal cell expansion: a visualisation tool for bioprocess comparison

Adapted from: T. Lambrechts, M. Sonnaert, J. Schrooten, F. P. Luyten, J.-M. Aerts, I. Papantoniou. Tissue Engineering Part B: Reviews (2016) doi:10.1089/ten.TEB.2016.0111, [Epub ahead of print].

3.1. Positioning within the context of the PhD project

In Objective 1, as introduced in Chapter 2, it was stated that a framework for benchmarking cell expansion processes would improve the general understanding of the critical process parameters that define a cell culture process, and ultimately facilitate a more rational and integrated design of the cell expansion bioprocesses.

This chapter therefore focuses specifically on the 'process' block of the general control scheme by analysing different strategies as described in literature for the large-scale expansion of mesenchymal stem cells. Processes using standard tissue culture flasks are included, as well as specialised bioreactor systems. An objective way of comparing the different processes, based on their input, output and process performance is introduced.

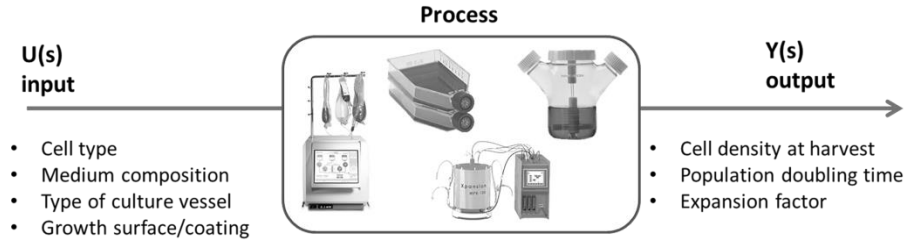

Figure 3.1: Position of Chapter 3 in the general control scheme and the larger context of this work.

3.2. Abstract

Large-scale and cost-effective cell expansion processes are a prerequisite for the clinical and commercial translation of cell-based therapies. A large variety of cell expansion processes are described in literature, utilising different cell types, culture vessels and medium formulations. Consequently there are no straightforward means for the comparison or benchmarking of these processes in terms of efficiency, scale or costs. The purpose of this study was to systematically review the available mesenchymal stromal cell (MSC) expansion literature and develop an interactive visualisation tool for comparing the expansion processes. By using this computational tool, process data could be concentrated, standardized and analysed in order to facilitate a more general understanding of the parameters that define a cell culture

process, and in the future allow rational selection or design of these bioprocesses. Additionally a set of bioprocess metrics were defined that assured the comparability between different processes. Currently the literature-based data repository holds 73 individual cell expansion processes on 7 different types of human mesenchymal stromal cells (MSC) in 5 different types of culture vessels. The visualisation tool allowed benchmarking of these processes against each other, serving as a reference point for cell expansion process efficiency.

3.3. Introduction

The number of clinical trials for cell-based therapies has been constantly increasing over the last years. Approximately 400 of these trials use human mesenchymal stromal cells (MSCs) as a therapeutic cell source, and many other (stem) cell types are considered for clinical translation (Heathman et al., 2015d; Trounson and McDonald, 2015). At the same time, the potential benefits that can be brought by cell-based therapy also seems to be recognised by industry since more and more cell-based companies arise (Culme-Seymour et al., 2013). It is expected that most cell therapy applications will require between 10^6 and 10^9 MSCs for a single dose (Jung et al., 2012; Simaria et al., 2014a). Although the relatively low number of Phase III clinical trials and limited commercialisation has been partially attributed to manufacturing challenges associated with manual flask-based cell culture, the flask-based method is still the gold standard. Manual flask-based cell culture is labour intensive, requires sequential "open events" that are prone to contamination, and does not allow online monitoring and control of the microenvironment of the cells. At the same time the flask-based strategy is limiting the attainable cell density levels and the scale of operation due to the inherent design of the flasks with a low volume to culture surface ratio.

The translation of clinically promising cell therapies to commercially successful products will require the conversion from manual cell culture processes to controlled bioprocesses that are able to guarantee the production of cell-based therapies with manageable cost of goods (COGs) and robust *in vivo* performance (Galipeau, 2013; Hourd et al., 2014; Kaiser et al., 2015; Salmikangas et al., 2015). Bioreactors have been shown to provide an improved cell culture environment by controlling nutrient refreshment and waste removal rates (Csaszar et al., 2013) while reducing complexity involved in bioprocessing (Leijten et al., 2015). From the translational perspective, bioreactors have been employed in order to provide efficiency in terms of cost, yield and scale. A growing body of literature examines the use of bioreactor systems with various designs for the expansion of human MSCs

and reflects on the concerns regarding large-scale MSC production, indicated by an increasing number of recent review papers (Cierpka et al., 2013; Kumar and Starly, 2015; Dos Santos et al., 2013).

Existing literature and regulatory perspectives (Mendicino et al., 2014) discuss a very broad number of parameters that all affect bioprocess variability and efficiency at the same time. Their effects should therefore be taken into account when analysing and designing bioprocesses for the expansion of MSCs. These parameters can be classified as follows:

Cell type and donor: There is a large variation of sources of adult progenitor cells, with the most common being bone marrow (Bianco et al., 2008), umbilical cord (Harris and Rogers, 2007), adipose (Ogura et al., 2014), synovium (De Bari et al., 2001b), periosteum (De Bari et al., 2001a). In addition, interdonor variability within the same cell type is also a factor that will affect translation to large-scale (Heathman et al., 2015b). Even from the very beginning of the process, the number of MSCs obtained from a biopsy is variable. For example, 1 mL of human bone marrow provides approximately 1 000 MSCs (Fennema et al., 2009). While for adipose derived MSCs for 0.5–2.0×10^6 cells per gram of adipose tissue the percentages of MSCs range from 1 to 10% (Oedayrajsingh-Varma et al., 2006). Again here there is a large interdonor variability regarding cell yields from biopsies that affects translation, especially for autologous cell therapies.

Type of culture vessel: Not only in the (multilayered) flask-based expansion, where the brand of culture plastic itself might already induce variability in cell yields (Sotiropoulou et al., 2006), also the large diversity of culture systems that has been reported to support MSC expansion contributes to the variety in bioprocess efficiency and variability. For instance microcarrier-based stirred tank reactors (Dos Santos et al., 2014), hollow fibre (Nold et al., 2013), wave bags (Timmins et al., 2009) and multiplate bioreactors (Lambrechts et al., 2016a) have been successfully employed to generate large-scale batches of MSCs.

Raw materials and reagents: There is a broad variety of media formulations for cell expansion that differ for example in protein source or glucose concentration. Since non-defined sources of protein such as Foetal Bovine Serum (FBS) and Human Platelet Lysate (HPL) introduce batch-dependent process variability and present a non-negligible risk for pathogen transmission, considerable effort goes to the development of defined xeno-free medium formulations that support more efficient and less variable cell

growth (Heathman et al., 2015d; Tan et al., 2015). For a review on serum free media formulations see (Gottipamula et al., 2013).

Process parameters: The operating conditions, for instance initial cell seeding density, media refreshment strategy, vessel geometry, type of impeller, mixing intensity and stress exposure, perfusion rates and dissolved oxygen tension vary for almost every process (Sart et al., 2013). The impact of the microenvironment in light of large scale MSC expansion is reviewed in (Ma et al., 2015).

To add to this complex landscape, inconsistent metrics have been used to define bioprocess efficiency making comparison across research studies a rather challenging task. Therefore, there is need for a critical and systematic analysis of existing information in order to allow comparability, process benchmarking and improved understanding of bioprocess efficiency, to ultimately allow a more rational design of these bioprocesses.

The first aim of this work was to analyse the performance of different expansion processes for MSCs. An exhaustive literature study was performed, currently resulting in a database of 73 individual cell expansion processes in 5 different types of culture vessels (tissue culture flasks, hollow fibre bioreactors, microcarrier-based bioreactors, multiplate bioreactor and fixed bed bioreactors), 7 different types of MSCs and a wide range of media compositions. The scale of the processes in terms of final cell numbers ranged between $7.5x10^6$ and $1.1x10^{10}$ cells. Interactive visual process performance maps were created where the scale, expansion efficiency, cell type, culture method, load on downstream processing, medium formulation and population doubling time could be explored. Finally, based on scale-up studies carried out in our research group we provide a cross-system cost comparison using a specific adult progenitor cell type namely, human periosteum-derived cells (hPDCs, an MSC-like cell type that holds promise for skeletal regeneration and repair strategies) reaching yields of $3.5*10^8$ cells per run.

3.4. Methods

3.4.1. Database construction:

A database of individual cell expansion processes was assembled based on a literature search for articles that have a detailed description of one or multiple cell culture processes. This database therefore not necessarily represents the current situation in industry. If multiple processes were described in one article, for example comparing different microcarrier densities or protein

sources, all described processes were included. The first criterion for a process to be included was that the article described processes for human mesenchymal stem cells (MSCs), as claimed by the authors. The second criterion was that the scale-up of the process was taken into consideration during data collection, with the aim of only including fairly optimised processes. However, scale-up was not necessarily the main goal of the article. Thirdly, precise information on critical process parameters, i.e. cell type, starting cell number at seeding, culture time, final cell yield, culture surface or microcarrier concentration, medium composition and exact type of culture vessel had to be included in the manuscript, either in text format, table or clear graphs. Unfortunately certain MSC expansion articles that were found failed to mention some of these critical parameters and were therefore not included. Finally, a cell quality read-out was required, either in terms of the International Society for Cellular Therapy (ISCT) criteria or a potency assay (Dominici et al., 2006), as long as it evaluated the influence of the process on relevant quality attributes of the specific cells. Although extremely important, (parts of the) processes that described "passage 0" (P0) results were excluded as the precise number of MSCs initially present within the biopsy is unknown. Most processes were situated between passage 1 and passage 6 (on the use of passage number as a metric, see below). Additional parameters that were collected in the database for their potential effect on the therapeutic effectiveness of the cells or indirect relation to the efficiency or cost of production, but that are therefore not explicitly used further in this work, are: brand of culture vessel, specific culture surface and coating, working volumes and refreshment rates, oxygen concentrations, maintenance of cell function or potency (yes/no) and bead-to-bead transfers in microcarrier culture (yes/no).

3.4.2. Metrics for process comparison

In order to allow a fair comparison between all the different processes in different culture vessels, specific metrics were calculated from the collected data of which the authors believe that they can provide objective comparison over multiple systems and cell types. For example, passage number is still often used to define the extent of cell growth. However, in contrast to the number of population doublings, this metric does not describe the proliferative precedent of the cultured cells. Similarly, in 2D culture the seeding and harvesting densities are generally stated as cells per cm^2 of available culture surface. As the exact culture surface is generally less easy to quantify for different microcarrier types this metric cannot be used for comparing all different culture vessels. One metric that was therefore used often in this work is Expansion Factor or Expansion fold (EF) as this allowed

us to estimate how efficient the generation of cells during a certain process step was, irrespective of the available culture surface or the vessel volume.

$$Expansion\ factor\ or\ expansion\ fold\ (EF) = \frac{number\ of\ cells \text{ in vessel at harvest } * downstream\ process\ efficiency}{number\ of\ cells\ seeded\ * seeding\ efficiency} \approx \frac{final\ cell\ yield}{number\ of\ cells\ seeded}$$

As the downstream process efficiency (e.g. taking into account the amount of cells lost during harvest or volume reduction processes, before the actual count of the cell yield) is generally not separately quantified in literature, the enumerator was simplified to the reported final cell yield. Estimates for seeding efficiency are more often mentioned for microcarrier processes, but are generally not available for flask-based or hollow fibre processes. Therefore also the seeding efficiency was not taken into account for the expansion factor calculation in this work. If an expansion factor was provided in the article that took seeding efficiency into account, it was recalculated in order to not include the cells lost at seeding, therefore resulting in a simple "cells out" over "cells in" ratio. When using the expansion factor metric as a measure for expansion efficiency, starting from the total initial number of cells seeded is more accurate from a process efficiency point of view compared to using the number of cells that are effectively seeded. Taking into account the exponential growth of cells, losing even small amounts during seeding quickly becomes expensive as these lost cells do not contribute to the final yield.

Reversely, to calculate the effective population doublings (PDs) and population doubling times (PDT) it is necessary to quantify and take into account the seeding efficiency as otherwise the apparent PDT seems longer than the effective PDT. Note that here the apparent PDT was calculated based on the initial and final cell number (as seeding efficiency and downstream process efficiency is generally not quantified in all articles) and therefore also includes lag phase and possible stationary phase at the end of the culture time:

$$Number\ of\ population\ doublings\ per\ passage\ = PD = log_2(EF)$$

$$Population\ doubling\ time = PDT = \frac{culture\ time}{PD}$$

The final volumetric cell density was calculated as the total number of cells harvested divided by the total medium volume (working volume) in the culture vessel. This metric was taken as a proxy for the load on downstream processes as it was considered that in relative terms larger cell numbers in smaller volumes are less cumbersome during volume reduction and possible purification steps.

For the classification in low and high supplemented protein concentrations an arbitrary cut-off point at 5% was chosen. A medium composition with more than 5% Foetal Bovine Serum (FBS) or human Platelet Lysate was considered to be “high FBS” and “high HPL” respectively. Medium compositions with concentrations equal or lower than 5% FBS or HPL were considered to be “low FBS” and “low HPL” respectively.

3.4.3. Cost calculations

Cost calculations were based on the cell expansion processes required for large pre-clinical studies performed in the host lab (Prometheus, KUL) for the treatment of large bone defects with hPDCs. The calculated cost included labour costs for the operators at KU Leuven, disposable costs at list price and reagent cost at list price for the expansion of 20 million hPDCs to 350 million hPDCs. Other costs such as lab space, depreciation costs and utilities were not included. All processes were performed in DMEM high glucose supplemented with 10% irradiated FBS. The hollow fibres of the Terumo BCT bioreactor were coated with human fibronectin, while no fibronectin was used in the other culture vessels.

3.4.4. Visualisations

The visualisation tool was created with JavaScript and Google Charts and the visuals are generated automatically from the database that is hosted online. In this way the tool can be easily updated with new processes when new publications become available. The process performance maps shown in this article are static representations of the interactive visualisation tool. In the online version, the viewer is able to select processes per vessel type or per cell type. The authors would like to encourage the reader to open the following link (mtm.kuleuven.be/prometheus/processmap) in their browser in order to experience the interactive dataset visualisation.

3.5. Results and Discussion

Based on data acquired through a literature search and subsequent data extraction, 73 individual bioprocesses were included in the visualisation tool.

The database included 7 different MSC types (Figure 3.2A), 5 different types of culture vessel (Figure 3.2B) and many different medium compositions that are roughly categorised based on protein source in Figure 3.2C. Although this data is based on research articles, the distribution of cell types used is comparable to the cell types used in recent clinical trials (e.g. 62% BM MSC and 15.4% ADSC as collected in (Heathman et al., 2015a), and 56% BM MSC and 12% ADSC as collected in (Sharma et al., 2014)).

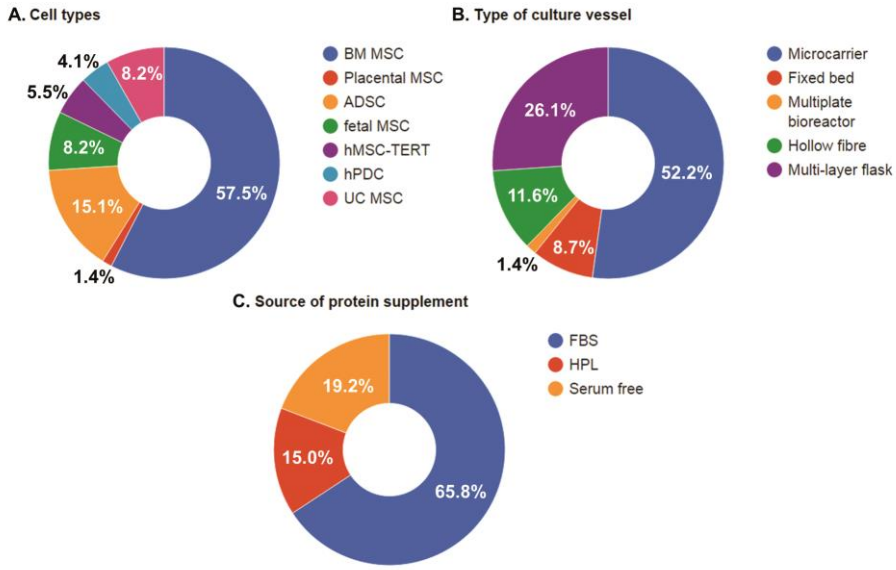

Figure 3.2: Overview of (A) cell types, (B) types of culture vessel, and (C) general source of protein supplement used for MSC expansion that are included in the database.
MSC = Mesenchymal Stromal Cell, BM = Bone Marrow, ADSC = Adipose Derived Stem Cell, hPDC = human Periost Derived Cell, UC=Umbilical Cord, FBS = Fetal Bovine Serum, HPL = Human Platelet Lysate.

3.5.1. Visualising process performance

In order to present a complete overview of all the processes, an interactive tool was created where process performance maps can be plotted allowing a visual analysis of MSC culture expansion across studies. The interactive version of the visualisation tool can be accessed online at the following link (mtm.kuleuven.be/prometheus/processmap). For all process performance maps presented in this work the Y-axis represents the expansion factor for a single passage as an approximation of the expansion efficiency. The scale of each process is reflected by the X-axis that is indicating the final cell yield of

the passage. Figures 3, 4 and 5 provide additional information regarding cell density (cells/ml) at harvest represented by the size of the circles, while different colours are indicative of the specific MSC type.

An interesting observation is that there seems to be a barrier on the process scale around a batch size greater than $1x10^9$ cells that is not often exceeded in the scientific MSC expansion literature. This could indicate a technological barrier (i.e. size of bioreactor or load on downstream processes), or a current lack of market demand. For certain cell types and medium combinations this might also imply a biological barrier as certain MSC types undergo senescence after an extensive amount of population doublings (Larson et al., 2010).

With the interactive visualisation tool it is possible to categorize the process performance maps, for example based on the type of culture vessel. In the case of microcarrier based suspension culture (Figure 3.4) a "linear" correlation on the log-log plot (therefore actually an $y=ax^b$ correlation) between the final cell yield and the expansion efficiency can be witnessed. This is surprising considering the wide range of process parameters that could affect the expansion factor and final yield in a microcarrier-based process, e.g. the type of microcarrier, microcarrier concentrations, energy dissipation rate. Contrary, in the case of multi-layered tissue flasks where there are much less process parameters that need to be optimised, a more scattered picture is observed in Figure 3.5. The multilayer flask-based processes seem to show both some of the most efficient processes as well as some of the least efficient processes for a certain scale, however average values are close to those observed in the microcarrier case. In recent work (Nienow et al., 2016) the relative performance of MSCs from different donors was reported to be the same for cell culture flasks and during experiments with the same cells on microcarriers.

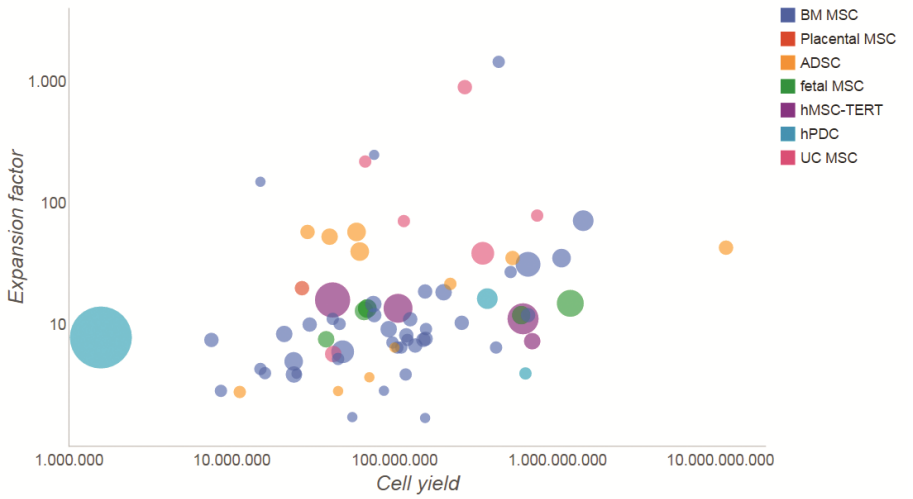

Figure 3.3: Capture of an interactive process performance map on 73 different cell expansion processes.
The y-scale indicates the expansion factor, the x-scale indicates the total cell yield, the colour of the dots indicates the specific MSC type. The size of the circle indicates final cell density (cells/mL) prior to the cell harvest step.

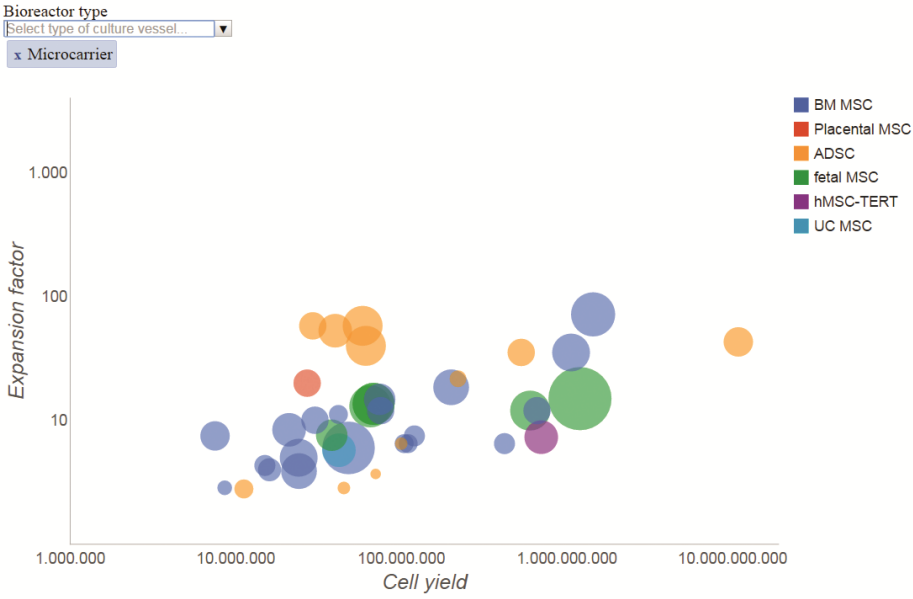

Figure 3.4: Selection of the microcarrier-based MSC expansion processes present in the database.

The y-scale indicates the expansion factor, the x-scale indicates the total cell yield, the colour of the dots indicates the specific MSC type. The size of the circle indicates final cell density (cells/mL) prior to the cell harvest step.

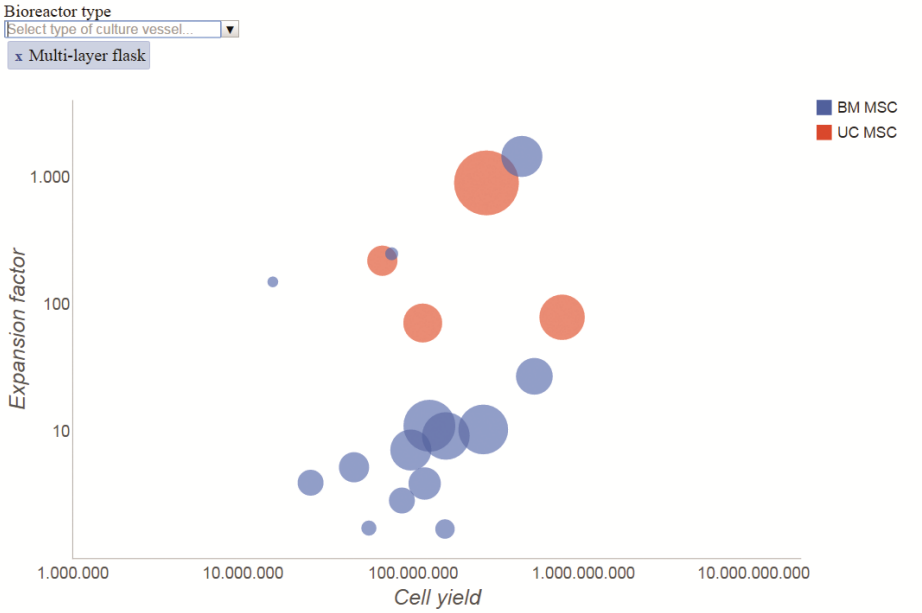

Figure 3.5: Selection of the multilayer flask-based MSC expansion processes present in the database.
The y-scale indicates the expansion factor, the x-scale indicates the total cell yield, the colour of the dots indicates the specific MSC type. The size of the circle indicates final cell density (cells/mL) prior to the cell harvest step.

In an alternative visualisation of the process performance map (Figure 3.6) it was chosen to use the same axis for scale and expansion efficiency (x and y respectively), but while the first version fousses on the technical side of the process by providing information on the type of bioreactor and load on downstream processes, here it was chosen to show more the biological side of the process. Therefore in this case, the color of the circle represents the amount and source of protein supplemented to the medium (i.e HPL, FBS or serum free medium) and the size of the circle represents the apparent population doubling time of the cells. The interactive format allows to sort the processes per cell type. It can be seen that the size of the circles was generally larger at the bottom of the map, indicating a longer population doubling time and therefore suggesting that the lower expansion factor of these processes could be attributed to a slower growth rate of the cells. Interestingly, both high and low protein content medium supplements were able to support very

efficient cell growth. HPL supplemented media result in relatively small circles, indicating fast population doubling times, and were therefore generally located at an average or higher expansion factor for a certain process scale. This indicates a more efficient cell growth in HPL supplemented medium which is often concluded from comparative studies between FBS and HPL containing media (Tan et al., 2015). Notwithstanding the clear benefits of serum-free cultures, from a process efficiency point of view certain serum-free processes reach an average expansion factor for a certain scale, while most of them currenlty resulted in a less efficient expansion process and therefore seemingly required further developments in order to accommodate every cell type – culture vessel combination (Tan et al., 2016).

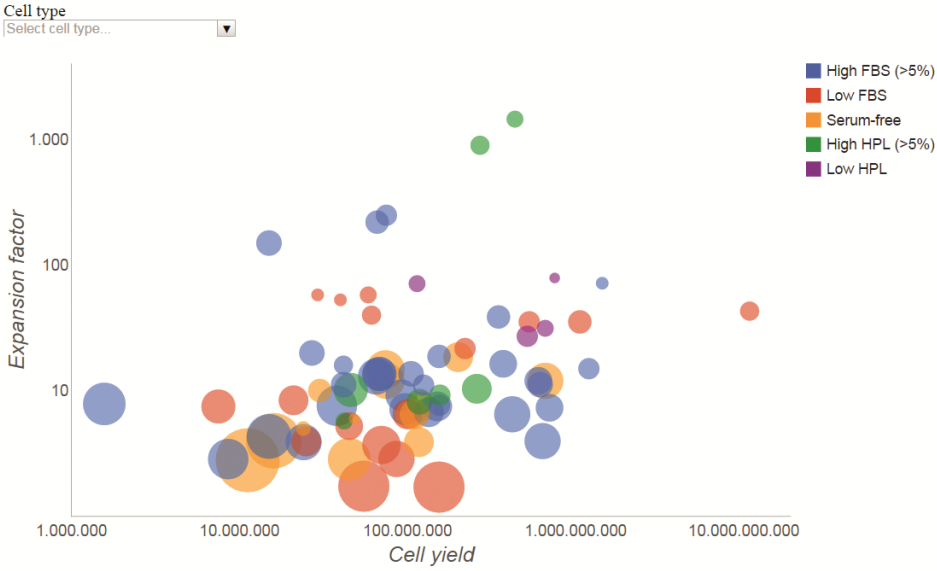

Figure 3.6: Capture of an interactive process performance map on 73 different cell expansion processes.
The y-scale indicates the expansion factor, the x-scale indicates the total cell yield, the colour of the dots indicates the source of protein supplements in the medium. The size of the circle indicates the population doubling time of the cells (larger bubbles indicate longer population doubling times).

Another interesting observation that could be made from Figure 3.3 and Figure 3.6 together was that the 5 “best in class” processes that were able to show expansion factors above 100, all originate from the same research lab where a notable lower cell seeding density was used in multi-layered flasks (30 to 40 cells/cm^2, compared to the average over het whole database of ±

3900 cells/cm^2) in combination with relatively high concentrations of supplemented protein (10% HPL or FBS), and this for 2 different cell types (BM MSC and UC MSC). It is regularly stated in literature that lower seeding densities promote faster population doublings, therefore in turn allowing larger and more efficient expansion factors (Balint et al., 2015).

3.5.2. Considering cost-effectiveness during bioprocess design

Cost of Goods (COGs) and cost breakdown structures are generally not mentioned in articles on stem cell expansion and could therefore not be included in the database. However, there exists a need for more cost-effective production methods that yield large numbers of high-quality cells at a commercially viable price in order for cell therapies to be affordable for healthcare systems and reimbursement. Therefore a cost calculation from multiple standardised large-scale expansion processes as performed multiple times in the host lab for a forthcoming clinical trial was included in order to provide a COGs reference value for the different types of processes described in the database. The calculation specifically compared the expansion of 20 million hPDCs to 350 million cells in high-glucose DMEM supplemented with 10% irradiated FBS in T175 tissue culture flasks, a hollow fibre bioreactor (Terumo BCT Quantum® Cell Expansion System, (Lambrechts et al., 2016b)) a multiplate bioreactor (Pall Integrity Xpansion, (Lambrechts et al., 2016a)) and in a spinner flask with CultiSpher-S microcarriers (unpublished results). Figure 3.7 illustrates the total cost per million of cells cultured in these vessels for the specific pre-clinical expansion process in the Prometheus lab. The reagent, disposable and labour axis provide the cost-breakdown of the total cost. The average expansion factor axis represents the expansion factor that was obtained per vessel for the hPDCs, and is included since this significantly influences process efficiency and cost. For the final axis, the number of built-in sensors was used as a measure for the monitoring capability of the vessel, since these features are increasing the COGs but facilitate the clinical translation.

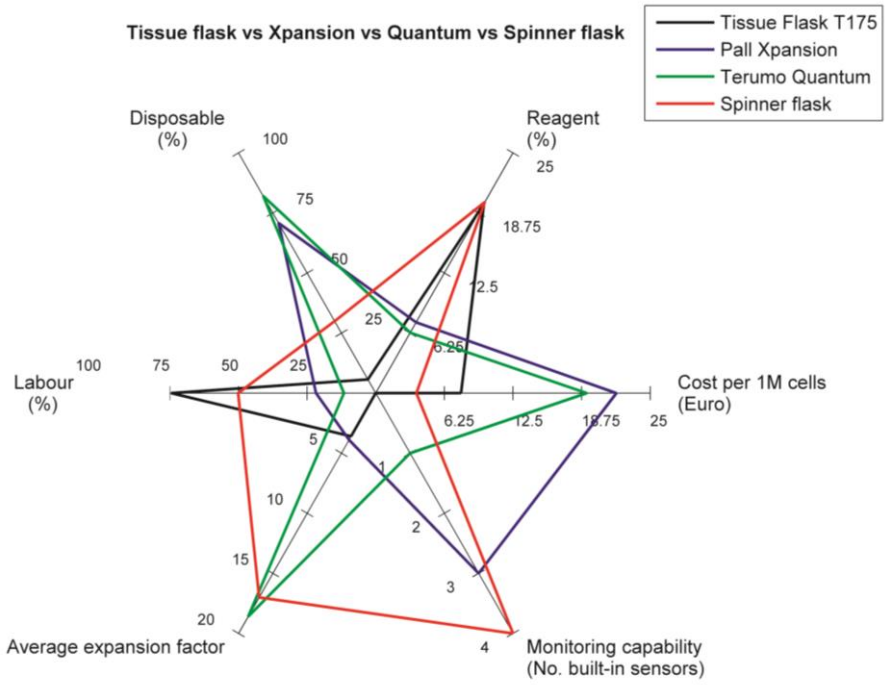

Figure 3.7: Cost breakdown structure.
Cost breakdown structure of a standardized large-scale cell expansion process of 20 million hPDCs to 350 million cells in high-glucose DMEM supplemented with 10% irradiated FBS in T175 tissue culture flasks, a hollow fibre bioreactor (Terumo BCT Quantum® Cell Expansion system a multiplate bioreactor (Pall Integrity Xpansion), and in a spinner flask with CultiSpher-S microcarriers.

Since these processes were carried out by the same operators, with a common end-goal, and with the same cell type and medium formulation, the authors believe these cost calculations form a fair comparison between multiple systems regarding COGs and cost distribution specifically for the scale of operations at Prometheus KU Leuven. These estimations could represent a manufacturing scenario for early stages of an advanced-therapy medicinal product (ATMP) development and potentially up to clinical trial phase I. It should be emphasised that these data were generated in a university setting and therefore they could potentially differ from an industrial setting regarding labour costs as well as laboratory practice. Moreover, even though the cultured cells were expanded for pre-clinical trials, the process was not yet entirely compliant to cGMP (Current Good Manufacturing Practices) which would lead to increased costs, mainly for the manual culture processes, once

the setting is switched. Even so, it is expected that the trends between the different culture processes will remain relatively similar. It can be seen that closed-system bioreactors entail high COGs, mainly due to the current high cost of the disposables (expected to eventually drop as the market grows), whereas the labour costs are reduced due to partial automation of the process. At this scale, the tissue flask-based strategy is still competitive, while further scale-up will favour microcarrier-based production.

An ongoing discussion exists in the bioprocessing field regarding the design of the most cost-effective bioprocess strategies for autologous and allogeneic cell production on the basis of "scale-out" or "scale-up". While s*cale-out* is simply doing more of the same (parallelisation of processes with the same dimensions), *scale-up* envisions a direct increase in volume or surface of the culture. In the case of an allogeneic therapy it seems that a scale-up strategy in which a transition from 2D (flask-based) culture towards microcarrier-based stirred tanks is the most attractive option, and there are bioprocess-economic models that support this strategy (Simaria et al., 2014a). The economics of allogeneic expansion for pluripotent stem cells (iPSCs and ESCs) have been recently modelled and described both for the upstream (Jenkins and Farid, 2015) as well as for the subsequent downstream operations (Hassan et al., 2015). However, this is not yet clearly addressed in the case of autologous large-scale expansion, where most likely a generic solution might not exist and optimal solutions might be case specific, based on inherent cell or donor properties as well as practical limitations (e.g. cells obtained from biopsies vs. cells required for therapy) (Hourd et al., 2014). The use of such deterministic models for the autologous case would therefore be a challenging task due to the inherent donor-related variability and uncertainty involved in these processes.

3.5.3. Integrated bioprocess design: downstream processes

MSC expansion (the "upstream" process) has gained considerable attention, addressing to a certain extent the scalability and GMP considerations. However, we are still far from whole-bioprocessing design. Downstream processing is only recently gaining attention as a result of the increasing volumes and batches of cells produced at the upstream stages. For example, the dynamic harvest of MSCs from microcarriers in suspension reactors was recently investigated providing scalable methodologies (Nienow et al., 2014), while in a follow up study the authors linked this process to the subsequent cryopreservation step (Heathman et al., 2015d). Dynamic harvest of single cells from fixed bed bioreactors was also recently described for the recovery of hPDCs that retained their regenerative potential *in vivo* (Sonnaert et al.,

2015a) and the recovered viable cell fraction per step during the harvest and volume reduction proces in a multiplate bioreactor was described in Lambrechts et al. (2015). Downstream operations are gaining importance for stem cell bioprocessing, and initial discussion on separation techniques reviewed by Diogo et al. (2012) are now translated increasingly in research results. An increasing number of bioprocesses and methods for the clarification and volume reduction of MSC suspensions using membranes and tangential (Cunha et al., 2015a; Cunha et al., 2015b) or dead-end (Tostões et al., 2015) filtration have been recently described. Moreover the use of expanded bed chromatography for the washing of MSC suspension resulted in improved efficiency (Cunha et al., 2016). This shows the rapid evolution of the field in reaching a pipeline of unit operations for (autologous) MSC manufacturing, customized per application and from patient-to-patient. By developing similar data-based visualisation tools for downstream operations as was done here for the upstream process, a whole bioprocess design approach could be further exploited.

3.5.4. Rational data-based bioprocess design

As illustrated before by the large variety in the process maps, there is growing awareness on the need for standardization given the specialised and complex components involved in cell therapy research and development (Bravery and French, 2014). The lack of standardisation, or at least some degree of harmonisation, hampers a swift transition from the development phase that is often based on trial and error, to the translational stage that requires robust and cost-effective processes (Kinzebach and Bieback, 2013). For instance, the adoption of improved standards for stem cells entering clinic (Dolgin, 2014) was recently suggested. Regarding input cell material, recent literature has highlighted the need for standardised MSC lines as calibration tool (Deans, 2015) or reference material (Viswanathan et al., 2014) while a systematic data-based approach and centralized manufacturing facilities able to conduct systematic comparability studies was advocated McKenna et al. (2014), highlighting the invasiveness of the immortalisation of the standardised MSC lines to the initial cell properties. Moreover in order to address the complex regulatory landscape, a cell therapy regulatory toolkit (online regulatory resource) was introduced for new ATMPs entering clinical trials for the EU and USA (Culme-Seymour et al., 2015). It is clear that a certain degree of standardisation would be helpful to move the field forward, however many cell-based therapies (in particular autologous therapies) will require personalised approaches where flexibility is required in order to allow customisation per patient or per therapy. Based on this work we propose and illustrate the potential of an *in-silico* data-based approach, where data related

to process performance and efficiency for MSC expansion could be concentrated, standardised and analysed based on objective quantitative criteria. This could help to obtain insights and conclusions regarding the translation of cell therapy and contribute towards efficient MSC bioprocessing and manufacturing. A similar data-based initiative was started recently by the FDA (Food and Drug Administration) to monitor manufacturing information of modified T-cells for cancer immunotherapies (CAR T) (http://www.raps.org/Regulatory-Focus/News/2016/03/16/24549/FDA-Proposes-New-Databases-to-Monitor-CAR-T-Cell-Safety-Across-INDs/). The ultimate aim is to rationalize MSC production, i.e. standardising wherever possible, but allowing calculated flexibility where needed. However, it speaks for itself that process efficiency should not be pursued at the cost of biological functionality of the cells since a high expansion efficiency is not necessarily linked to therapeutic success. It would be extremely interesting to add a measure for the therapeutic potential of the cultured cells in this type of databases, however currently there are not often objectively quantifiably biomarkers available for the *in vivo* potential of stromal (or stem) cells, either due to a lack of the proper sensors and assays, or due to a limited understanding of the mechanism of action. Even if for a specific case a potency asasy is available, it is closely linked to the intended clinical application of the cells, therefore preventing a fair comparison across multiple processes.

3.5.5. Future Challenges

The authors will attempt to keep the current database updated when new relevant publications become available. Access to the database is available upon request for collaboration on further data analysis or the addition of new parameters. As more and more data is collected in the database, more in depth data mining techniques could allow for the extraction of data-driven strategies for bioprocess improvements. From the bioprocess design point of view, the incorporation of time-series data (Viazzi et al., 2015) or process parameters that quantitatively describe the dynamic culture environment (Lambrechts et al., 2014) could provide much more insightful information on the dynamics as well as the robustness of MSC bioprocesses. For example for stirred vessels, parameters such as energy dissipation rate, shear stress or oxygen transfer characteristics could provide readouts for shear stress and mass transport properties. Unfortunately, there are very few studies reporting on these readouts for dynamic MSC expansion. For instance Nienow et al. (2016) evaluated agitation conditions across a number of stirred reactors widely used for microcarrier-based MSC expansion. By providing this kind of information

an identification of optimal bioprocess operating conditions could be also achieved.

From the cell quality attributes point of view, although ISCT criteria provide minimum cell identification criteria (Dominici et al., 2006), processes should be also linked to potency assays of increased sensitivity and functionality that could however be application specific. For instance, the performance of expanded cells in an *in vivo* setting is usually omitted and only seldom linked to its bioprocess history. There is still a need for predictive potency assays that correlate with *in vivo* activity, to ensure product comparability during manufacturing changes (Bravery et al., 2013). For most of the studies included in this paper the link with the impact of process conditions on MSC *in vivo* performance has been largely ignored, and only a handful of studies evaluated this.

3.6. Conclusion

The steady increase in MSC production scales demonstrates the continuous maturation of the field. However there are considerable challenges to be faced for the successful transition from early preclinical to late commercial stage manufacturing. A major factor contributing to this challenge is that there is no typical, one-size-fits-all manufacturing solution. Therefore we present an interactive visualisation tool that provides an integrated perspective on MSC expansion that is able to increase the understanding of scale-up and commercialization of cell production processes.

3.7. Acknowledgements

TL is supported by the KU Leuven Concerted Research Actions (GOA/13/016). MS is supported by a Ph.D. grant of the Agency for Innovation by Science and Technology (IWT/ 111457). IP is funded by Fonds Wetenschappelijk Onderzoek (FWO fellowship, project No 12O7916N).

Chapter 4. Evaluation of a monitored multiplate bioreactor for large-scale expansion of human periosteum derived stem cells for bone tissue engineering applications

Adapted from: Lambrechts, T., Papantoniou, I, Viazzi, S., Bovy, T., Schrooten, J., Luyten, F.P., Aerts, J-M. Biochemical Engineering Journal, (2016) 108: 58–68.

4.1. Positioning within the context of the PhD project

This chapter is one of two 'scale-up' chapters were the translation of the Prometheus' standard flask-based cell expansion process to a monitored and controlled bioreactor-based process is described. In this case a multiplate bioreactor is used. According to Objective 2 in Chapter 2, this translation should by all means not compromise the *in-vivo* bone healing potential of the cultured cells, as will be demonstrated here. Additionally, process monitoring data such as cell quantification by imaging or metabolic activity was used to assure process comparability to the standard flask-based culture as was envisioned in Objective 3 in Chapter 2.

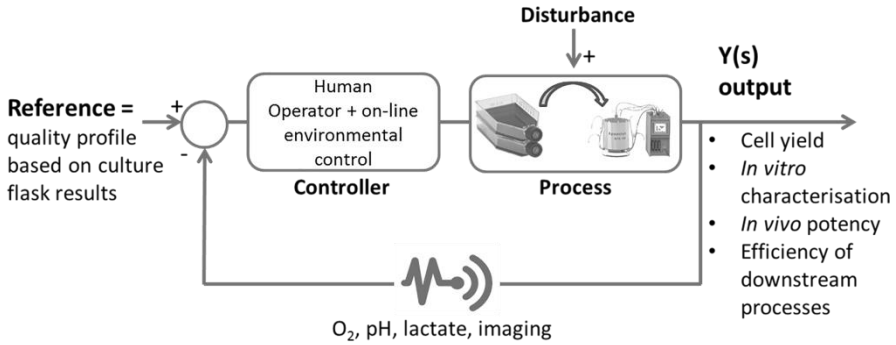

Figure 4.1: Position of Chapter 4 in the general control scheme and the larger context of this work.

4.1. Abstract

In light of the large-scale expansion of human periosteum derived stem cells for the treatment of large bone defects, a multiplate bioreactor system (Pall Integrity Xpansion) in combination with an integrated holographic imaging platform (Ovizio iLine S microscope) was evaluated. The culture process was quantitatively characterized by imaging data, metabolite concentrations and a breakdown of the cell recovery fractions. The resulting cell quality was assessed based on the minimal criteria for mesenchymal stem cells, including viability on cell culture plastic, identity markers and tri-lineage differentiation potential. Additionally, an *in vivo* bone forming potency assay was used in an ectopic mice model that resulted in compelling bone formation (11.6% ± 3.1% and 12.8% ± 3.3% for the bioreactor and control tissue culture flask

condition respectively). Therefore it was shown that the bioreactor is able to produce large quantities of cells, while maintaining satisfactory cell quality.

4.2. Introduction

Currently, more than 1300 active clinical trials are reported using cell-based therapies to treat a wide variety of indications ranging from cardiovascular to neurological disorders, as well as skeletal disorders (Heathman et al., 2015a). Around 380 of these trials use mesenchymal stem cells (MSCs) as the therapeutic cell source. While most applications require between 10^7–10^9 MSCs for a single dose (Dos Santos et al., 2014; Simaria et al., 2014a), cell expansion is traditionally carried out in 2D (monolayer) static culture set ups (e.g. tissue culture flasks or cell factories) that require extensive manual open-process interventions for media exchange and cell harvest. The high labor and infrastructure costs associated with these techniques hamper the socio-economic viability of the therapy after clinical translation. In combination with a lack of suitable potency assays related to the *in vivo* biological response of the cells (Bravery et al., 2013), the relatively low number of successful clinical translations of cell-based therapies are mainly attributed to the challenges associated with the production of the required cell numbers, while at the same time assure high and reproducible cell quality (Placzek et al., 2009; Rowley et al., 2012; Sharma et al., 2011; Simaria et al., 2014a). This highlights the rising need to develop and incorporate automated bioreactor systems for large-scale production of progenitor cells for clinical applications.

Additionally, due to the inherent complexity of biologic processes, traditional cell culture processes that were designed by a rule-of-thumb approach are difficult to adapt to an efficient and robust clinical process that is able to deliver an efficacious product to every single patient. The full potential of cell-based therapies will therefore only be able to be harnessed by a cell culture process that is standardized, scalable and able to deliver clinically relevant cell numbers, while at the same time assure potent biological functionality *in vivo* (Glassey et al., 2011; Rodrigues et al., 2011; Want et al., 2012). Recently, considerable effort is placed in developing such processes based on bioreactor systems, for example in the form of hollow fibre bioreactors (Hanley et al., 2014; Peters et al., 2013) and wave-rocking bioreactors for microcarrier-based expansion (Sutlu et al., 2010).

In this work, a monitored multiplate bioreactor (Pall Integrity® Xpansion™ equipped with Ovizio iLine S microscope) was evaluated as a platform for the clinical-scale expansion of human periosteum derived stem cells (hPDCs) and

its ability to monitor the cell expansion process was evaluated. hPDCs are a promising source of progenitor cells for the treatment of skeletal defects. During the natural bone healing process they have been shown to be the main contributors to tissue regeneration (De Bari et al., 2001a; Eyckmans and Luyten, 2006), while after *ex vivo* expansion, they have been recently shown to possess improved bone forming capabilities compared to other MSC sources (e.g. bone marrow and synovium) when seeded on calcium phosphate carriers (Roberts et al., 2014).

Using this multilayered bioreactor, limited changes to the classical planar cell culture process are required as opposed to, for example, microcarrier-based cell expansion where complex process variables need to be optimized (e.g. material/surface properties, hydrodynamics)(King and Miller, 2008). This is due to the fact that cells are seeded and cultured on a 2D cell culture surface similar to the conditions found in standard tissue culture flasks. In addition, the extensive quantitative bioreactor read-outs that can be obtained at-line, such as dissolved oxygen concentrations, pH and microscopic images, can be used to improve the control over the expansion process, ultimately leading to a more robust *in vivo* outcome (Thomas et al., 2008).

The objective of this work is the development of a clinical scale bioreactor process for the expansion of hPDCs in the Xpansion bioreactor. The advantages of thorough process monitoring are illustrated and the synergy between the multiplate bioreactor and the mounted microscope is highlighted. In addition to the standard post-harvest *in vitro* cell characterization assays that were performed, an *in vivo* potency assay was implemented which is often lacking in bioprocess studies relevant to cell therapy applications.

4.3. Materials and Methods

The experimental outline consists of 4 consecutive phases: (1) a pre-culture phase in tissue culture flasks in order to reach the amount of cells required for bioreactor seeding, (2) 7 days of bioreactor expansion with continuous monitoring of multiple process parameters, (3) cell harvest and concentration, and (4) post-harvest cell characterization in which the cells from the bioreactor are compared to a target quality profile of cells cultured in parallel in standard tissue culture flasks (Figure 4.2). The *in vitro* cell characterization is inspired on the International Society for Cellular Therapy (ISCT) minimal criteria for MSCs (Dominici et al., 2006), supplemented with a bone forming assay in order to assess the *in vivo* potency of the cells (Bianco et al., 2014). The bioreactor process was first evaluated and adapted to the needs of hPDCs in three small scale process development runs in the Xpansion-10. In a

following phase the process was translated to a larger scale bioreactor (Xpansion-50) that resembles the clinical-scale production.

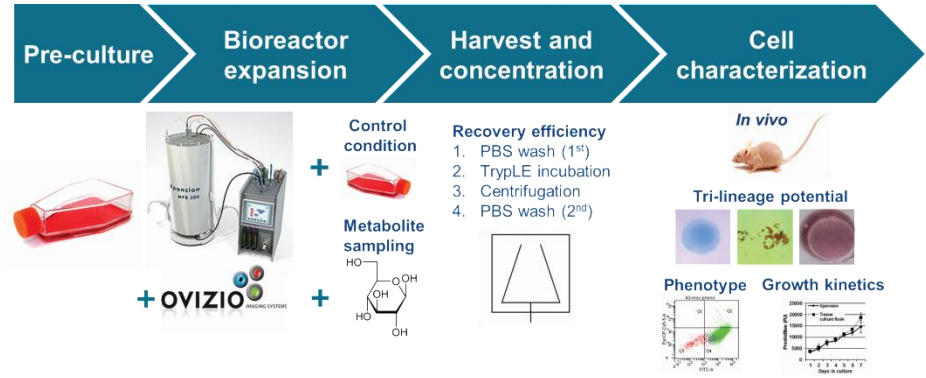

Figure 4.2: Overview of the general experimental outline with an initial tissue culture flask-based pre-culture phase, followed by the Xpansion bioreactor culture.
During the bioreactor culture the cell growth was monitored based on daily images from the Ovizio iLine S microscope and samples of the medium. Three standard tissue culture flasks were cultured in parallel as a positive control. Immediately after cell harvest and cell concentration the cell characterisation was initiated, including among others, an *in vivo* bone forming potency assay.

4.3.1. Flask-based hPDC culture

hPDCs were isolated from 4 different donors by means of enzymatic digestion of a periost biopsy as described by Eyckmans et al. (Eyckmans et al., 2010). Procedures were approved by the ethical committee for Human Medical Research (KU Leuven) and patient informed consent forms were obtained. The isolated cells were cultured in T25 flasks for the first passage in standard culture medium consisting of high glucose GlutaMAX^{TM} Dulbecco's modified Eagle's medium (Life Technologies, Merelbeke, Belgium) supplemented with 10% irradiated fetal bovine serum (FBS; HyClone, Cramlington, UK), 1% sodium pyruvate (Invitrogen) and 1% antibiotic–antimycotic (100 units/ml penicillin, 100 mg/ml streptomycin, and 0.25 mg/ml amphotericin B; Invitrogen). Cells were further cultured in T175 flasks with a seeding density of 5 700 cells/cm^2 and sub-cultured at ± 80% confluence. At passage 3, the cells from the 4 different donors were pooled all together and further expanded in T175 flasks up to passage 7 (approximately 12 total population doublings). hPDCs generally maintain linear growth curves for over 30 population doublings (De Bari et al., 2006). At all

passages, cells were harvested by trypsinization for 10 min with TrypLE Express (Invitrogen).

4.3.2. Bioreactor based hPDC culture

The Pall Life Sciences Xpansion™® (Pall Life Sciences, Brussels, Belgium) is a multiplate bioreactor that houses from 10 to 200 hydrophilised polystyrene plates of ± 612 cm^2 each (Figure 4.3). The plates are tightly packed around a central aeration column, that provides gas exchange controlled by an active gas flow controller. Based on the integrated temperature, dissolved oxygen and pH sensors, the culture conditions can be monitored and controlled (Castillo et al., 2013; Egloff and Castillo, 2012). Additionally, by making use of the holographic Ovizio iLine S microscope (Ovizio Imaging Systems, Brussels, Belgium), the cells inside the bioreactor can be visualized and critical process parameters such as cell density and morphological features can be non-invasively extracted in a quantitative way.

After passage 7, the cells were transferred to the multiplate bioreactor with a total culture surface of 6 125cm^2 (Xpansion-10) for the first 3 process development runs, and later to the Xpansion-50 with a total culture surface of 30 600 cm^2. The bioreactor and culture medium were pre-heated overnight in the incubator at 37°C in order to prevent gas bubble formation during filling. For each bioreactor run, at least 3 control tissue culture flasks were taken along as positive control for the cell expansion procedure and subsequent cell characterization. The control tissue culture flasks were seeded at the same initial seeding density as the bioreactors in order to compare growth kinetics. The inoculation densities of the bioreactor were corrected for the void volumes in the bioreactor (i.e. central aeration column and headspace) according to the manufacturer's instructions to assure a similar density on the bioreactor plates as in the control tissue culture flasks. For the Xpansion-50 bioreactor it was calculated that a little more than 85% of the cells from the inoculation volume will settle on the bioreactor plates. The seeding volume in the Xpansion-10 was 1.7 L, in the Xpansion-50 the volume was 5.7 L. After transferring the inoculation volume to the bioreactor, the bioreactor was incubated at 37°C for 7 days in parallel with the control flasks. The automated controller was only allowed to engage 9 hours after seeding in order to allow sufficient time for cell attachment, as the controller actions are accompanied by mixing of the medium.

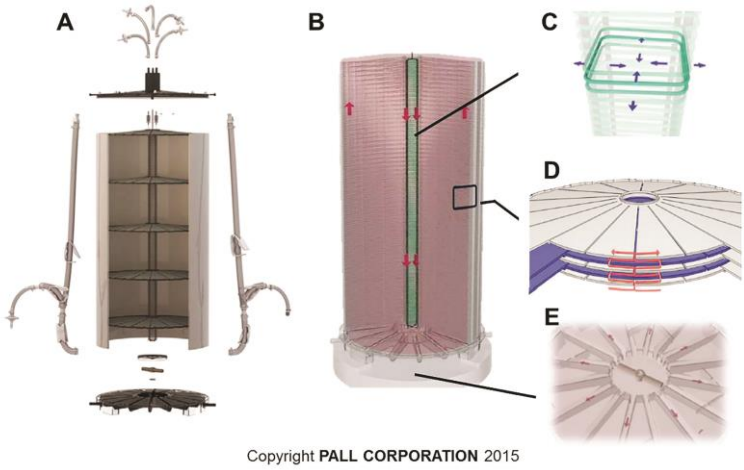

Figure 4.3: Illustration of the bioreactor design.
A) Bioreactor housing from bottom to top: bottom plate that fits on a magnetic stirrer which is installed in the incubator, magnetic impeller that drives the medium flow between the plates, cylindrical housing in which the polystyrene plates are tightly packed around the central aeration column, top plate with the connection to the gas flow rate controller, sensor probes, sampling lines and vent. The tubes for filling and draining the bioreactor are connected to the bottom plate of the bioreactor and shown on the sides. Note that the height of the housing is adapted to the number of plates for the different bioreactor scales. B) Stack of polystyrene plates inside the bioreactor housing. The red arrows indicate the medium recirculation through radial channels in the plates and through the aeration column. C) Close-up of central aeration column that provides gas exchange with the culture medium. D) Close-up of side view on three plates where the radial channels allow medium perfusion over the cells. The available culture surface per plate is 612 cm2 and the headspace between each plate is 1.6 mm, and this for every scale of the bioreactor. E) Close-up of bottom plate where the culture medium is recirculated by the impeller through the radial channels in the plates towards the top of the bioreactor. Illustration courtesy of Pall Corporation.

The cells grown in the bioreactor were harvested after 7 days, together with the control flasks. First, after draining the culture medium, the bioreactor was rinsed once with pre-heated PBS (one bioreactor volume). A pre-heated diluted TryplE concentration was used (5 times diluted in PBS), supplemented with EDTA (ethylenediaminetetraacetic acid) to a final concentration of 1.8 mM to harvest the cells from the bioreactor plates. This adapted harvest solution was optimized in T25 flasks based on a novel method that allows for the real-time quantification of the harvest kinetics by an imaging algorithm and the determination of cell yield and viability (Viazzi et al., in

preparation/press). For the bioreactor harvest a diluted harvest solution was preferred over the standard TryplE harvest as the final harvest volume is relatively large (5.6 L for the Xpansion-50, 21.9 L for example for the Xpansion-200). Therefore, to facilitate the downstream processing it was not chosen to neutralize this volume, as this would increase the volume even more, and spin down the harvested cells in the diluted TryplE solution.

Right after adding the harvesting solution to the bioreactor, the vessel was moved to the microscope platform in order to visually assess cell detachment from the plates. In parallel, one of the control flasks was harvested with the same adapted harvest solution in order to assess the effectiveness of the solution and to have a reference for the required incubation time. Once all cells were circular and started to detach from the polystyrene plates, the vessel was mechanically shaken on the Xpansion harvest station to completely detach the cells. The cell suspension was subsequently drained from the bioreactor under constant agitation in order to keep the cells in suspension. The harvested volume was then reduced by spinning down the non-neutralized cell-containing harvest solution. As a final step, the bioreactor was rinsed with PBS and placed under the Ovizio microscope again to check the harvest efficiency.

As the cell harvest in the Xpansion bioreactor is a critical step in the process, the cell recovery efficiency was identified after each step in the entire process. As shown in section 4.3.1, cell density at the day of harvest was determined by the Ovizio microscope. This density was used as the reference (100%). Viable cells were counted on samples from the waste medium drained from the bioreactor at day 7, from the 1st PBS rinse, the non-neutralized harvest volume, the suspension after volume reduction and the 2nd PBS rinse after harvest based on trypan blue exclusion.

Monitoring and control of cellular environment in the bioreactor

Temperature, pH and dissolved oxygen concentration were continuously monitored at the top plate of the bioreactor. The pH and oxygen concentration were actively controlled by the injection of gasses (CO_2, O_2 and N_2) through the central aeration column. pH was set-up to be controlled between 7.25 and 7.56 for the runs in the Xpansion-10 bioreactor, and between 7.42 and 7.56 for the Xpansion-50. These set points were based on observed culture conditions in standard tissue culture flasks. The dissolved oxygen concentration was set-up to be higher than 40% air saturation, with the main goal of preventing anoxic conditions in the bioreactor. The mixing of the culture medium is effectuated by a magnetic impeller at the bottom of the

bioreactor. The magnetic stirrer was automatically engaged (0.5 mm/s) during injection of gasses for pH or O_2 control to assure sufficient mixing. When the gas controller was idle, the agitation rate in the Xpansion-10 runs was set up in a way that it would exhaustively mix the bioreactor volume at least every 4 hours (i.e a mixing time of 20 min every 4 hours according to the manufacturers specifications). In the Xpansion-50 bioreactor continuous agitation was applied resulting at low linear speed (0.5 mm/s, 40 rpm) in order to mix the medium as much as possible. The bioreactor medium and control flask were sampled daily and lactate concentrations were determined immediately (Arkray Lactate Pro). The bioreactor was sampled via the sampling line, only after the bioreactor volume was mixed for at least 20 minutes. Samples for lactate, glucose, glutamine and glutamate were also measured on frozen samples using a YSI 2950 Biochemistry Analyser (Ankersmid M&C, Wilrijk, Belgium).

Metabolite analysis

An estimation of the oxygen consumption rate during the exponential growth phase in the Xpansion-50 bioreactor run was determined based on the measured oxygen concentration in the bioreactor. As the perceived oxygen uptake rate is influenced by the supply of external gasses, only oxygen concentration data was used during time points at which the controller was inactive. Within the exponential growth phase 7 timeframes were selected with a length of 4 hours (i.e. approximately equally spread out between day 1.5 and day 5), that were located at least 2 hours after gas injection or controller disconnection during imaging. The 4 hour timeframe was considered to have sufficient samples for a robust consumption rate calculation, while it is short enough to assume constant cell numbers. The midpoint of the 4h timeframe was used for a linear interpolation between 2 daily cell density measurements from the Ovizio microscope. Based on the interpolated cell number, a cell specific oxygen consumption rate was calculated. This oxygen consumption estimation assumed a closed system, since the contact surface of the filter on the gas vent is negligible compared to the 5.7L volume of the Xpansion-50 bioreactor.

The glucose and lactate consumption rates were calculated between consecutive daily samples and normalized to cell number to obtain cell specific consumption and production rates using the equation: $q_{MET} = \Delta met/(\Delta t.cell)$, where Δmet (mM) is the change in metabolite concentration during the time period Δt(days) and $cell$ (cells) the average number of cells during the same period. The metabolic ratios (q_{MET1}/q_{MET2}) are

calculated by dividing the average consumption or production rates of the same time period.

Process monitoring by holographic imaging

Cell growth in the bioreactor was monitored on a daily basis by disconnecting the gas and sensor lines, taking the bioreactor out of the incubator and placing it under the Ovizio microscope. The microscope set-up allows taking multiple holographic images per plate, and this for the upper ±10 plates. The OsOne software (Ovizio, Brussels, Belgium) allows to semi-automatically quantify the number of cells, the cell density on the plates and is able to provide specific morphological features per cell.

4.3.3. Post-harvest cell characterization

Growth kinetics

Growth kinetics of the harvested cells was monitored via the PrestoBlue metabolic assay (Life Technologies, Merelbeke, Belgium) as described in Sonnaert et al. (Sonnaert et al., 2015b). Cells were seeded at 5700 cells/cm^2 in a 12-well plate. Every day the normal growth medium was replaced by a 10% v/v PrestoBlue reagent supplemented growth medium. After 1 hour incubation (37°C, 95% RH, 5% CO_2) the metabolic activity in the well was quantified by fluorescence measurements (Bio-Tek SynergyTM HT, Bad Friedrichshall, Germany) with an excitation wavelength of 540nm and an emission wavelength of 590nm on 100ml supernatant in a 96-well plate. A higher metabolic activity is indicated by higher fluorescent values.

3-lineage in vitro differentiation potential

Chondrogenic differentiation of the cultured hPDCs was assessed in a micro-mass assay as described earlier (De Bari et al., 2001a). In short, $2x10^5$ cells were re-suspended in 10 µL culture medium and seeded as micro-mass in a 24-well plate. After 2 hours incubation (37°C, 5% CO_2, 95% RH) 0.5 ml standard culture medium was added. After 24 hours, the medium was replaced by chondrogenic medium consisting of DMEM/F12 (Life Technologies), 2% FBS, 1% antibiotic–antimycotic, 1% ITS Premix (Corning), 100nM dexamethasone (Sigma), 10µM Y27632 (Axon Medchem), 50µg/ml ascorbic acid, 40µg/ml proline and 10ng/ml recombinant human transforming growth factor-β1 (Preprotech, London, UK). The chondrogenic medium was refreshed every other day. Micro-masses in normal culture medium were taken along as negative control. After 7 days of chondrogenic induction the micro-masses were fixed for 1 hour in ice cold methanol and stained at room

temperature for 1 hour with a 0.1% Alcian Blue solution in 0.1M HCL at pH 1.2.

Osteogenic differentiation was assessed by seeding the cells in 24-well plates at a density of 4 500 cells/cm^2 in 0.5 ml standard culture medium. After 48 hours the medium was replaced by standard culture medium supplemented with 100 mM dexamethasone, 50 µg/ml ascorbic acid and 10 mM β-glycerolphosphate. The medium was refreshed 3 times per week for 21 days. Samples in standard culture medium were used as negative control. Cells were fixed prior to analysis in ice cold methanol for 1 hour and afterwards stained with a 2% Alizarin Red S solution in Baxter water.

Adipogenic differentiation was investigated by seeding the cultured hPDCs in 24-well plates at a density of $1x10^4$ cells/cm^2 in 0.5 mL standard culture medium. After 24 hours the medium was replaced by adipogenic medium consisting of αMEM (Life Technologies) supplemented with 10% FBS, 1% antibiotic–antimycotic, 1 µM Dexamethasone, 10 µg/ml human insulin (Sigma), 100 µM indomethacin (Sigma) and 25 µM 3-isobutyl-1-methylxanthine (Sigma). Medium was refreshed 3 times per week. At day 14, cells were fixed in 10% formaldehyde for 20 minutes, rinsed shortly with 60% isopropanol and stained with Oil Red O.

MSC phenotyping

The expression of typical MSC cluster of differentiation (CD) markers (Dominici et al., 2006) and lack of expression for the haematopoietic markers on the harvested cells was evaluated based on a hMSC Phenotyping Kit (Miltenyi Biotec). The CD marker combinations used are $CD90^+$-FITC (clone DG3), $CD73^+$-APC (clone AD2), $CD105^+$-PE (clone 43A4E1), $CD14^-$ (clone TUK4)/$CD20^-$ (clone LT20.B4)/$CD34^-$ (clone AC136)/$CD45^-$ (clone 5BI)-PerCP. The non-specific isotype control stain panel included mIgG1-FITC, mIgG1-PE, mIgG1-APC, mIgG1-PerCP (clone IS5-21F5) and mIgG2-PerCP (clone S43.10). $6x10^5$ cells per condition were washed in blocking solution (1%FBS in PBS) and the concentrated cell suspension was re-suspended in 100 µL of stain solution (1:11 antibody dilution in blocking solution) for 10 minutes at 4°C. After washing the aliquots with blocking solution again, the samples were analysed on a FACSCanto (BD Biosciences, San Jose, Ca, USA) equipped with FACSDiva acquisition software (BD Biosciences). 10 000 total events were acquired. Data analysis was done in FlowJo V10 (TreeStar Inc., Ashland, OR, USA).

In vivo bone forming potency assay and quantification

One million cells in a total volume of 35 µL culture medium were seeded on 35 mm^3 clinical grade orthopaedic 3D matrices composed of calcium phosphate particles in an open collagen network (NuOss, ACE Surgical Supply Co.,Inc, Hannover, Germany) in triplicates per condition. The scaffolds were incubated overnight (37°C, 5%CO_2, RH95%) before ectopic implantation on the back of nude mice (NMRI-nu/nu). Eight weeks later the mice were sacrificed, the scaffolds were retrieved, fixed overnight in 4% paraformaldehyde and preserved in PBS before scanning by X-ray computed tomography. All animal experiments and procedures were approved by the Animal Ethics Committee (KU Leuven). Animals were housed in accordance with the guidelines of the Animal Research Centre of KU Leuven.

The volume of newly formed bone after 8 weeks of *in vivo* implantation was determined by nanofocus X-ray computed tomography (nanoCT) performed on a Phoenix NanoTom S (GE Measurement and Control) system equipped with a diamond-tungsten target and 0.5 mm aluminum filter. The applied scan settings were 60 kV X-ray voltage, 210 mA current, 500 ms exposure time, a frame averaging of 1 and image skip of 0. Images were reconstructed with Phoenix Datos|x CT software (GE Measurement and Control) and a 3 µm voxel size. The quantification of the bone volume was based on a 2-level automatic Otsu segmentation algorithm. The match of the segmented areas was confirmed visually for each sample. In case of mismatch, manual segmentation levels were determined based on the greyscale histogram of the whole sample. All image processing was performed in CTAn (Bruker micro-CT).

4.3.4. Statistical analysis

Statistical analysis was performed using Matlab 2013a (The MathWorks, Inc., Natick, MA). Independent groups were compared by unpaired Student's t-tests, and considered statistically significant in case P-value <0.05. Error bars in figures represent standard deviation of mean.

4.4. Results and discussion

4.4.1. Monitoring cell growth

An example of a holographic image taken at the third plate from the top in the Xpansion-50 bioreactor at the final day of culture (day 7) where cells were at ±80% confluence can be found in Figure 4.4A. Figure 4.4B shows the same image after analysis by the OsOne software, where cell perimeter is indicated

and counted cells are identified. The software was able to match the cell densities with a visual assessment of the original image. The microscope was therefore used to quantitatively monitor the bioreactor processes throughout the whole culture period in terms of cell number and homogeneity of cell distribution. Figure 4.4C shows the average cell density over the 7 days culture period, based on the analysis of daily pictures of the top 5 plates of the Xpansion-50 bioreactor.

The Xpansion-50 bioreactor was seeded with a total of 160 million cells in a 5.7 L seeding volume. Taking into account the void volume in the bioreactor this would theoretically result in a seeding density of 4 400 cells/cm^2. The seeding density of the bioreactor was verified by the microscope (based on pictures at day 0 in Figure 4.4C) and was found to be around 4 500 cells/cm^2. This was close to the theoretical seeding density and matched the density used to seed the control flasks (4 400 cells/cm^2) (Figure 4.4D, day 0). Additionally, referring to the relatively small standard deviation on the microscope-based cell density estimate at day 0 in the bioreactor (Figure 4.4C), it can be stated that a homogeneous seeding density was achieved, which is important for an efficient cell expansion process. Over the 7 day culture period, a sigmoidal cell growth can be perceived with a 2 day lag period followed by an exponential growth phase, as is common after sub-culturing the hPDCs. The stagnation of growth at day 7 indicates confluence of the plates.

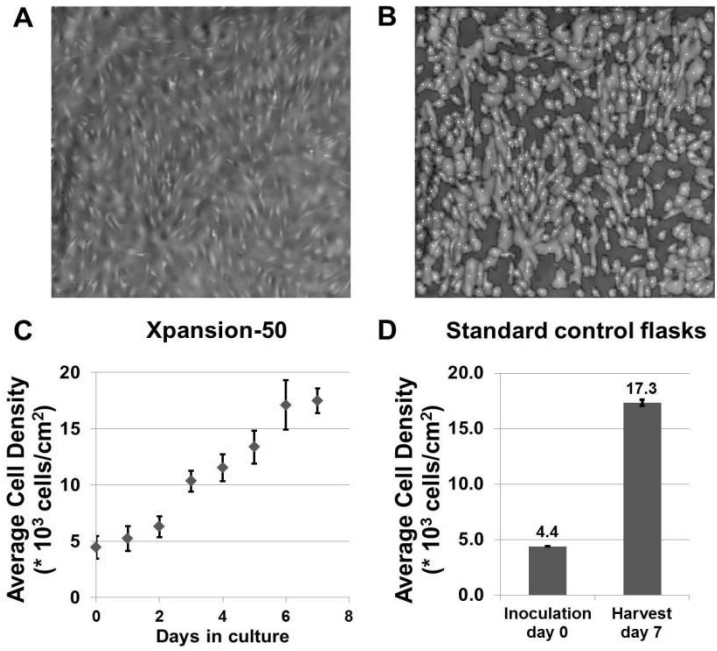

Figure 4.4: Monitoring cell growth
(A) Holographic image at the third plate from the top in the Xpansion-50 bioreactor (B) Same image as in A with cell quantifications and signature data by OsOne software (C) Growth curve of hPDCs in Xpansion-50 bioreactor based on daily microscope-based quantification of the cell density (D) Cell density quantification in the control flasks based on manual counting after TryplE harvest. All error bars represent standard deviation of the mean.

The cell density at the day of harvest was estimated to be around 17 500 cells/cm^2 in the bioreactor based on the data generated by the microscope. Given the 4 500 cells/cm^2 and 7 day culture period, this corresponds to a 86h population doubling time of the cells. In the control flasks, the resulting cell density was 17 300 cells/cm^2 based on manual cell counts after harvesting the flasks with TrypLE (corresponding to a 85h population doubling time of the cells). It can therefore be concluded that the growth kinetics and the level of confluence in the bioreactor and the control tissue culture flasks are equivalent. Population doubling times are comparable to the standard hPDC culture, however relatively high compared to typical values for MSCs in literature (Baksh et al., 2007; van Harmelen et al., 2004; Jin et al., 2013). It was demonstrated before that the continuous agitation in the bioreactor, resulting in continuous exposure of the cells to laminar flow (0.5 mm/s) would not damage cells, since hPDCs have been cultured regularly in

perfusion bioreactor at more intense flow conditions (Papantoniou et al., 2013; Sonnaert et al., 2014).

4.4.2. Monitoring metabolic activity

Dissolved oxygen tension and pH were continuously monitored over the 7 days of culture, and are shown in Figure 4.5. The short interruptions in the bioreactor sensor data are due to disconnecting the bioreactor from the controller in order to image the plates with the microscope. Small fluctuations in air saturation were caused by the injected air during pH control actions. Over the 7 day culture period the pH drops slightly. The dissolved oxygen concentration dropped gradually due to cell consumption (until around day 3 in the Xpansion-10 runs, until day 5 for the Xpansion-50). Afterwards, the controller took action to maintain the dissolved concentration above the 40% air saturation set. The resulting average cell specific oxygen consumption rate during the exponential growth phase was $1.08 \pm 0.22 \times 10^{-17}$ mol.s^{-1}.cell^{-1}. Although cell type and culture method dependent, this consumption rate is around one order of magnitude smaller compared to previously reported values in literature for MSCs (Kasper et al., 2010; Pattappa et al., 2011). When compared to a previous study on hPDCs specifically, i.e. a flow through perfusion bioreactor culture on 3D scaffolds (Lambrechts et al., 2014), the oxygen consumption rate per cell (1.1×10^{-17} mol.s^{-1}.cell^{-1}) was very close to the amount perceived in this study.

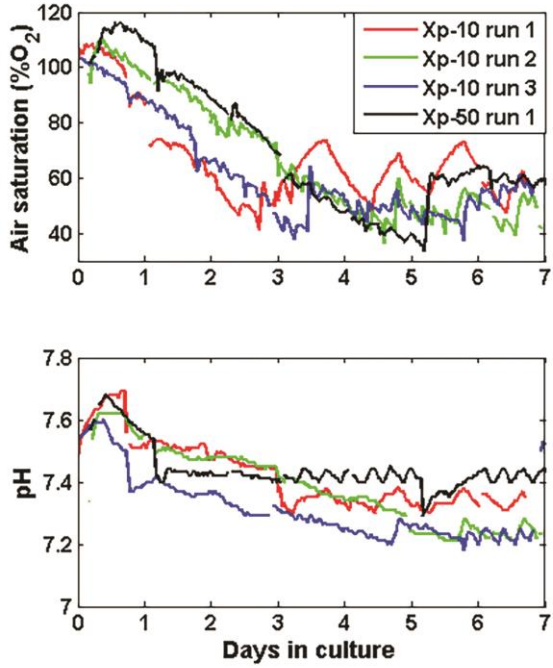

Figure 4.5: On-line dissolved oxygen concentration (top) and pH (bottom) monitoring.
A lower threshold of 40% air saturation was chosen, while for the pH a range between 7.25 to 7.56, and 7.42 to 7.56 was chosen for the Xpansion-10 and Xpansion-50 runs respectively.

Lactate, glucose, glutamine and glutamate concentrations were measured in daily medium samples both from the Xpansion-50 bioreactor and the control flask (Figure 4.6). In the Xpansion-10 bioreactor runs only lactate was measured, these production profiles showed similar trends as the Xpansion-50 data (data not shown). Metabolite concentrations in the Xpansion bioreactor were similar compared to the tissue flask condition over the 7 days culture (Figure 4.6). However, slightly higher lactate concentrations were registered in the culture flask condition. The lactate concentration, both in the bioreactor and the control flasks, remained well below the growth inhibitory level for MSCs (35.4mM) determined by Shop et al. (2009) (Schop et al., 2009). Glucose consumption rates and lactate production rates are shown in Table 4-I. As cell number quantification in the tissue flasks was done only at day 7 of culture, the cell specific consumption rates and production rates in Table 4-I for the control flasks are referring only to the last day in culture. The average cell specific rates for the bioreactor could be determined daily based

on the cell density estimates from the microscope. These rates were relatively constant over the culture period and an average is given in Table 4-I. For the sake of comparison with the control flasks, the rate at day 7 is also given for the bioreactor. The perceived lactate production and glucose consumption rates are in line with literature on other MSCs (Higuera et al., 2009).

Table 4-I: Cell specific glucose consumption rates, lactate production rates and metabolic ratios.

	Bioreactor		**Tissue culture flask**	
	Day 7	**Average**	**Day 7**	**Average**
Glucose consumption (pmol.day^{-1}cell^{-1})	5.1	8.1 ± 0.34	3.4	n.a.
Lactate production (pmol.day^{-1}cell^{-1})	9.2	13.9 ± 0.58	7.9	n.a.
Ratio qLAC/qGLUC	1.8	1.8 ± 0.37	2.3	2.5 ± 0.39
Ratio qO2/qGLUC	n.a.	0.11	n.a.	n.a.

The ratio of produced lactate over consumed glucose (q_{LAC}/q_{GLUC}), which is cell number independent, was equal to 2.54 ± 0.39 and 1.82 ± 0.37 for the tissue culture flask condition and bioreactor condition respectively, and remained stable over the whole culture. Although not significantly different, this q_{LAC}/q_{GLUC} ratio suggests that the energy production from glucose was more efficient in the bioreactor culture compared to the culture flask, and potentially indicates a different utilization of carbon sources. This difference might have been caused by the continuous mixing in the bioreactor that prevents built-up of diffusion gradients above the cell surface. The ratio of consumed oxygen over consumed glucose (q_{O2}/q_{GLUC}) in the bioreactor was equal to 0.11. This relatively low q_{O2}/q_{GLUC} ratio in non-hypoxic culture conditions, combined with the relatively high q_{LAC}/q_{GLUC} ratio suggested aerobic glycolysis as the preferred metabolic pathway during hPDC expansion (Cunha et al., 2015a; Sart et al., 2014).

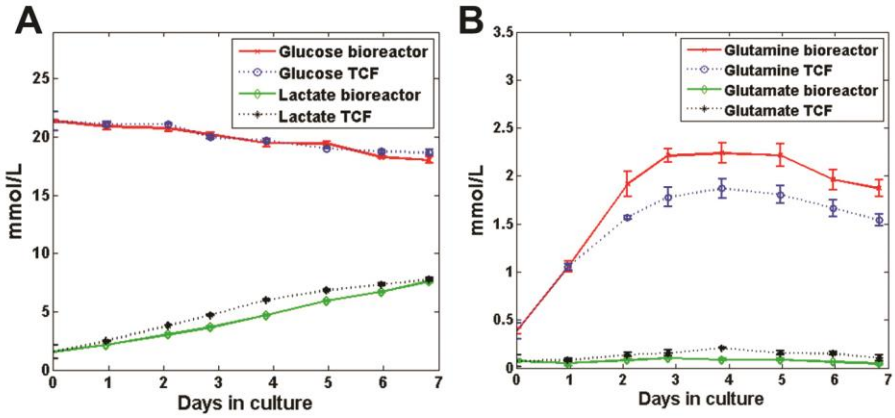

Figure 4.6: Accumulated metabolite concentration in bioreactor and tissue culture flask (TCF) over the 7 day culture process.
(A) Glucose and lactate, (B) glutamine and glutamate, continuous lines indicate bioreactor data, dashed lines indicate tissue culture flask data. Error bars represent standard deviation of the mean.

Glutamate concentrations remained quasi constant, while the glutamine concentration needed around 2 days to reach a ±2 mmol/L level (Figure 4.6). The same trend was followed in both conditions, however the glutamine concentration was generally lower in the culture flask condition. Quantification of cell specific glutamine consumption rate is difficult in Glutamax (a more stable L-glutamine L-alanine dipeptide which gets hydrolysed by cell activity and is a therefore a steady source of glutamine, but which cannot be quantified by the medium analyser) supplemented media and without information on ammonia concentrations (the end product of natural glutamine decay).

4.4.3. Bioreactor harvest and downstream processing

The average total incubation time in the adapted harvest solution for the Xpansion was 38 ± 7 minutes. This was ±2 times longer than what was required for cell detachment in T175 flasks. It is hypothesized that the increase in required incubation time was due to a less effective first PBS rinse in the bioreactor, where the serum remnants might have partially inhibited the proteolytic trypLE reaction.

Table 4-II indicates the recovered fraction of viable cells per step in the harvest process. The data is based on analysis of the third run in the Xpansion-10 bioreactor as this harvest procedure was the most exhaustively

analysed and had the furthest developed protocol. The cell count in the waste medium and 1st PBS rinse amounted up to nearly 10% of the total amount of the cells present on the plates at the time of harvest. However, these steps are generally also present in the harvest procedure in the traditional flask based process (not quantified in this study) and were therefore irrelevant regarding cell yield. More important, ± 82% of the cells were found back in the non-neutralized harvest suspension. Cells within this fraction were collected by centrifugation (290 rcf) and used subsequently for post-harvest cell characterization. Another ± 6% of the cells was found in the 2nd PBS rinse and on the plates at the end of the harvest procedure. The total of all fractions add up to ± 104%. This overestimation is probably due to the fact that two different counting methods were used (manual cell counting and the Ovizio microscope based counts). Additionally, although prevented by all means possible, counting and sampling errors are inevitable in such large volumes with in some cases relatively low cell numbers present due to the high dilution factors.

The final step in the harvest procedure was the volume reduction by centrifugation. Taking into account the ± 76% centrifugation efficiency gained in the non-neutralized harvesting suspension, in total a ± 63% final recovery efficiency of the cells present on the plates of the bioreactor was recorded in the third process development run in the Xpansion-10. Although a similar final cell density on the plates was reached in the Xpansion-50 and the same harvesting procedure was used, the final recovery efficiency in the Xpansion-50 bioreactor was around 45%. This reflects a final yield of 7 900 cells/cm^2. So, despite the high cell density gained in the Xpansion-50 bioreactor growth, many cells were lost in the downstream processing for this specific run. While the final density here was almost 4 times the density as reported for hepatic progenitor cells in the Xpansion-200 (difficult to compare due to the different cell types) (Castillo et al., 2013), more effort is required on the downstream processing. Based on the recovery efficiencies listed here, most gain can be made mainly by improving the centrifugation efficiency. Exploration of alternative volume reduction bioprocesses such as the use of continuous centrifugation (Delahaye et al., 2014) or filtration systems (Cunha et al., 2015b) could also provide solution for a higher cell recovery. In light of this, it should be noted that in case of the Xpansion-50 it was the first time this research group was handling these sizes of harvest volumes. The authors are therefore convinced that by further development of the volume reduction and centrifugation process, the total cell yield can be improved significantly.

Table 4-II: Summary of recovered viable cell fraction per step during the harvest process relative to the optically determined number of cells on the day of harvest. The (*) indicates fractions determined by the microscope, the other fractions are based on cell counts.

Step in harvest process	% of cells counted
Cell count on plates, 7 days of culture (*)	**100% = reference**
Cell count in waste medium	3.20%
Cell count in 1st PBS rinse	6.40%
Cell count in non-neutralized harvest suspension	82.40%
Cell count in 2nd PBS rinse	6.10%
Cell count of cells on plate after rinse (*)	6.20%
Total	**104.20%**

4.4.4. Post-harvest cell characterization

After each bioreactor run, the harvested cells were subjected to a standard quality check and compared to the target quality profile as derived from the tissue culture flask condition.

Growth kinetics of harvested cells

Figure 4.7 represents the average growth curve (n=4) over 7 days as determined by the PrestoBlue assay for the harvested cells after being re-seeded in 12-well plates. Growth kinetics of the harvested cells were similar for all bioreactor runs and up to day 7 no significant difference between the bioreactor condition and tissue culture flask condition was found. The lack of increased lag phase during initial culture days for the cells harvested from the bioreactor suggests that environmental stress during the bioreactor harvest procedure did not induce cell damage (Delahaye et al., 2014).

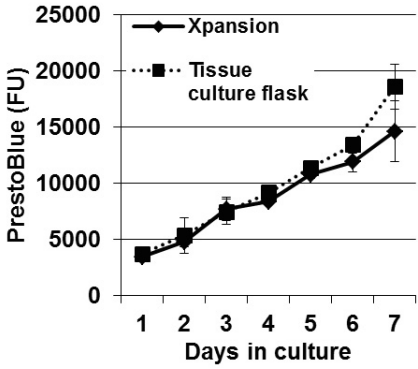

Figure 4.7: PrestoBlue-based average (n=4) growth curve of re-plated harvested cells in a 12-well plate. Error bars represent standard deviation of the mean.

In vitro 3-lineage differentiation

After each bioreactor run the *in vitro* 3-lineage differentiation potential of the cells was assessed. Both cells from the bioreactor and tissue culture flasks were able to differentiate towards the adipogenic, osteogenic and chondrogenic lineage as shown in Figure 4.8. Both in bioreactor run 3 and run 4, the *in vitro* chondrogenic differentiation was impaired compared to the tissue culture flask condition (Figure 4.8, bottom). It is hypothesized that this loss of *in vitro* chondrogenic potential was caused by an increased TrypLE exposure time as all other conditions were kept constant. It should be noted that in the case of the culture process being up-scaled with a flask or cell factory-based strategy the holding times of the cells will undoubtedly also increase. More importantly, the impaired *in vitro* chondrogenesis in run 3 and 4 did not influence the outcome of the *in vivo* results, nor the CD marker expression as shown later.

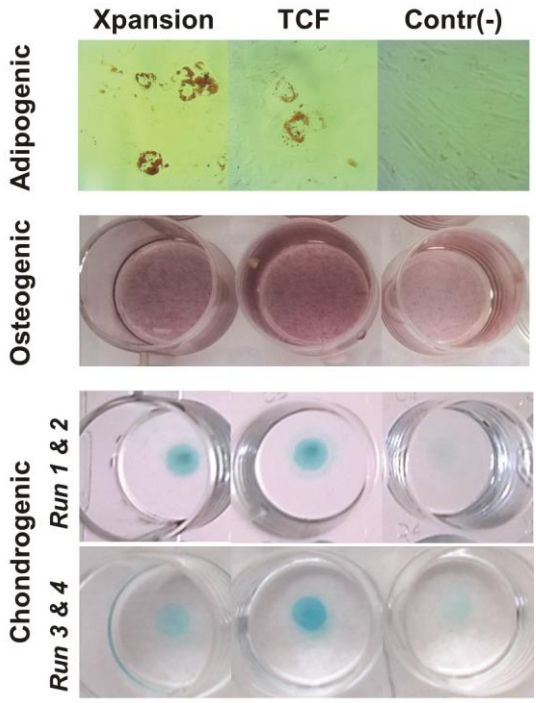

Figure 4.8: Representative images of the *in vitro* 3-lineage differentiation assay for cells from the bioreactor, tissue culture flask and a negative control in normal medium shown in the left, middle and right column respectively.
(top) Oil Red O staining after 2 weeks of adipogenic differentiation. (middle) Alizarin red staining after 3 weeks osteogenic differentiation. (bottom) Alcian Blue staining after 1 week chondrogenic differentiation in micro-mass culture.

MSC phenotype

Figure 4.9 on the left side indicates the simultaneous positivity for the standard MSC markers CD73, CD90 and CD105 for cells from the bioreactor and the control flask. On the right side the percentage of cells that are positive for at least one CD marker from the pool of hematopoietic markers CD45, CD20, CD14, CD34 are shown. Based on the flow cytometry data, cells harvested from the bioreactor showed a clear MSC like phenotype, that was close to identical the control flasks. Little variation between the different runs was perceived.

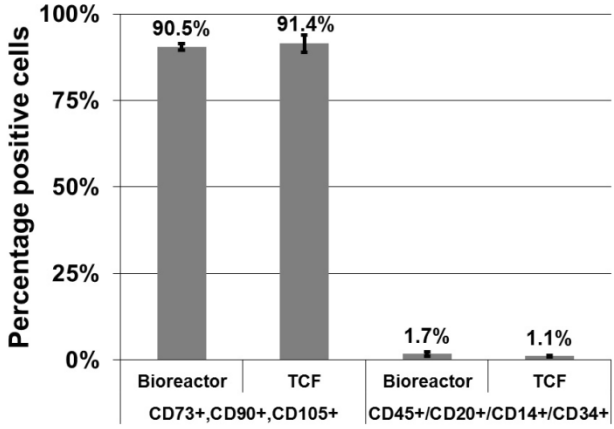

Figure 4.9: Percentage of simultaneous positivity for common MSC markers (CD73, CD90 and CD105) and common hematopoietic markers (CD45, CD20, CD14, CD34).
Error bars represent standard deviation of the mean.

In vivo bone forming potential

The *in vivo* performance for cells is a crucial aspect in the cell characterization process. As discussed by Bianco et al. (Bianco et al., 2014), the *in vitro* assays that are suggested by the ISCT (Dominici et al., 2006), and which were shown here (3.3.1-3: adherence to plastic, *in vitro* 3-lineage differentiation and (lack of) expression of certain CD markers) are of value as means to standardize MSC characterization. However, these assays are not necessarily reflecting the *in vivo* potency of the cells for specific indications. Therefore, in this work, an assay with a known mechanism of action was chosen, in order to assess the bone forming activity of the harvested cells *in vivo* (Chai et al., 2012a; Roberts et al., 2011). The amount of newly formed bone as quantified by nanoCT was normalized to the available volume in the scaffold (i.e. not taking into account the space occupied by the remaining calcium phosphate grains within the scaffold, see indications on Figure 4.10). All samples in both conditions resulted consistently in compelling ectopic bone formation *in vivo*. As quantified by the nanoCT analysis the average newly formed bone volume was 11.6% ± 3.1% and 12.8% ± 3.3% for the bioreactor and tissue culture flask respectively. Based on the boxplot it can be seen that the spread on the data is similar for both conditions, but the quartiles are closer for the bioreactor conditions. No statistical difference was found between the two conditions and the perceived quantities of newly formed bone corresponded to what was reported earlier in literature (Roberts et al., 2011). It is interesting to note that while cells from run 3 and 4 showed

impaired chondrogenic differentiation potential, they were still able to form a compelling amount of bone in vivo. This stresses the need for potency assays that are able to assess relevant biological functions and illustrates a limitation of the ISCT minimal criteria (Bravery et al., 2013). However, as the time and resources required for *in vivo* assays are considerable, more cost-effective assays should be developed that might for example look at the secretome (e.g. trophic factors) (Mastri et al., 2012).

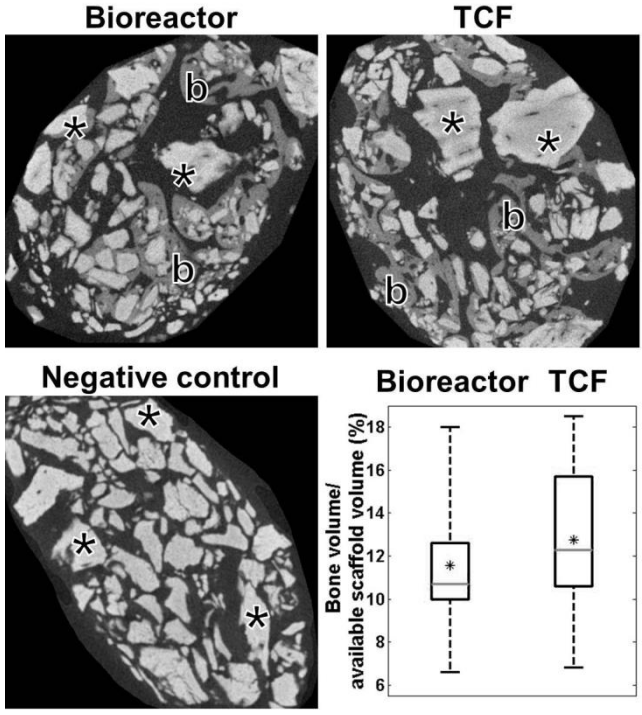

Figure 4.10: NanoCT images and quantification of bone volume.
(left top and bottom) Slides from the reconstructed nanoCT images, ”b” indicating remaining calcium phosphate grains from the implanted scaffold, “*” indicating newly formed bone tissue. The negative control consists of an implanted scaffold without cells. (bottom right) Box plot of the newly formed bone volume normalized to the available scaffold volume as determined by nanoCT imaging. Horizontal lines indicate first quartile, median and third quartile, whiskers indicate minimum and maximum, asterisk indicates average.

Although technically challenging, upscaling planar tissue culture technology is attractive for autologous tissue culture strategies (or small batch sizes of allogeneic cells) since relatively small changes to the standard culture

conditions are required. In addition, the Pall Xpansion bioreactor specifically adds a significant level of automation and control to the planar culture process, while at the same time it is scalable between 6120 cm^2 (Xpansion-10) and 122 400 cm^2 (Xpansion-200). Based on the cell densities achieved in the Xpansion-50, the theoretical cell yield for hPDCs would be around $2x10^9$ cells in the Xpansion-200 (for bone marrow MSCs, which are smaller in size, this would be more close to $3x10^9$ at a harvest density of 25 000 cells/cm^2). Although this accounts already for a considerable cell yield, allogeneic cell therapy strategies will benefit from microcarrier or suspension culture technologies, as more favourable economies of scale can be reached due to the much larger culture surface to volume ratio (Jenkins and Farid, 2015; Rowley et al., 2012; Simaria et al., 2014a; Want et al., 2012). Discussing which culture system is better in terms of cell quality is challenging as this depends heavily on specific cell type, clinical indication and bioprocess design. Recent studies have shown that hMSC expansion on planar adherent surfaces could lead to gradual loss of their therapeutic potency with altered immune modulatory properties, low survival rate post transplantation, and changes in their secretory profile and therapeutic potential due to an increasing senescent subpopulation (Bara et al., 2014; Sepúlveda and Tomé, 2014; Whitfield et al., 2013). However, similar effects could also occur during suspension culture under certain process conditions (Chen et al., 2011; Sart et al., 2013).

4.5. Conclusion

In conclusion, the Xpansion bioreactor enabled the production of large amounts of progenitor cells, while maintaining equivalent cell quality compared to the standard flask-based culture. Importantly, it was shown that these cells retained their regenerative potential resulting in compelling *in vivo* bone formation. The efficiency of the culture process for this specific cells type reached a bottleneck at the downstream level, in particular during cell recovery. However, in addition to the integrated sensors and medium sampling possibilities of the bioreactor, the transparent stacked plate design in combination with the microscope offered excellent monitoring capabilities allowing to exactly pinpoint the root cause of the bottleneck. Consequently, future efforts will be directed towards optimizing the recovery efficiency during downstream processing. The large-scale production of progenitor cells under quantitative real-time process monitoring provides a tool for the translation to robust clinical implementation and facilitates the regulatory trajectory.

4.6. Acknowledgements

The authors would like to thank Pall Life Sciences (Brussels) for the supply of the materials and the technical assistance, Kathleen Bosmans for assisting with the in vivo implantations and Jérémie Barbau (Ovizio Imaging Systems) for reviewing the manuscript. TL is supported by the KU Leuven Concerted Research Actions (GOA/13/016). IP is funded by an advanced European research council grant, ERC Rejoind / No 294191. The nanoCT images have been generated at the Department of Materials Engineering of the KU Leuven, financed by the Hercules Foundation (project AKUL 09/001).

4.7. Conflict of interest

Thierry Bovy is Global Product Manager, Integrity® Bioreactors at Pall Life Sciences.

Chapter 5. Real-time characterisation of the harvesting process for adherent mesenchymal stem cell cultures based on on-line imaging and model-based monitoring

Adapted from: S. Viazzi, T. Lambrechts, J. Schrooten, I. Papantoniou, J.-M. Aerts. Biosystems Engineering (2015) 138:104–13.

5.1. Positioning within the context of the PhD project

As the optimisation of the harvest procedure was found to have a large impact on the process efficiency in the multiplate bioreactor in Chapter 4, this Chapter focusses specifically on the use of imaging data from 2D cell culture surfaces (both tissue culture flasks and the multiplate bioreactor) for monitoring the cells detaching from the culture plastic during the enzymatic harvest of the culture vessel. The data collection, image analysis and data-based model are run in real time, enabling prediction of the optimal time to stop the enzymatic reaction. This not only provides a quantitative measure for the process operators, the enhanced data-based process control also reduces the exposure of the cells to the proteolytic enzymes, which is beneficial for cell quality, as was the goal of Objective 3 in Chapter 2.

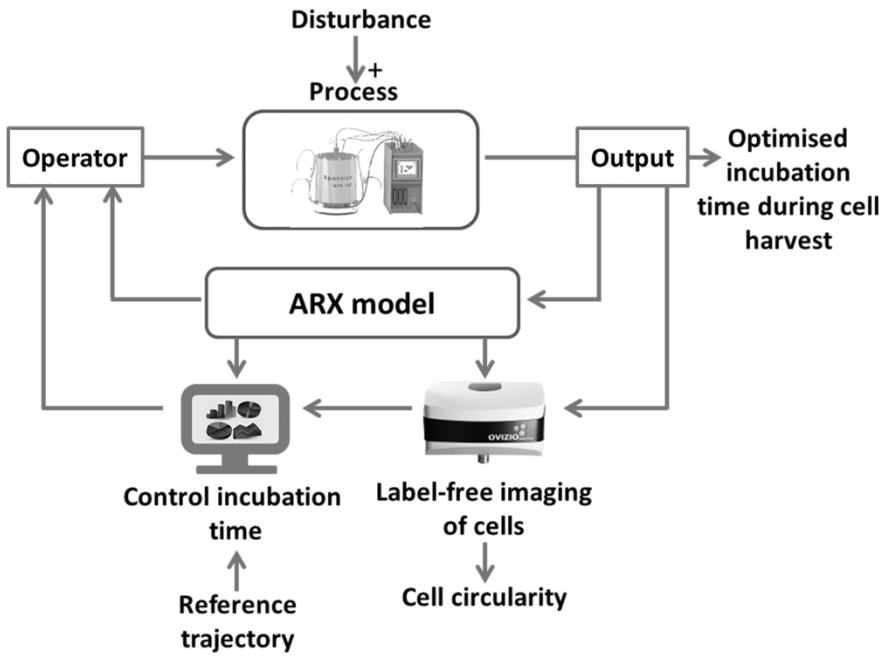

Figure 5.1: Position of Chapter 5 in the general control scheme and the larger context of this work.

5.2. Abstract

Determining the optimal time to inhibit the enzymatic reaction during cell harvesting is crucial in order to successfully detach adherent cells from the substrate before irreversible cell damage is caused by prolonged cell exposure to the enzymes. This study aimed at developing a non-invasive methodology to determine objectively and automatically the optimal time-point to inhibit the enzymatic reaction during cell harvesting. The harvesting process was monitored under a microscope and image analysis was used to measure the cells' morphology (circularity) from the images. System identification techniques were used to model the cells' circularity in response to the harvesting solution and to quantify the time when the cells become circular and reach a plateau phase (inhibition time). ARX models (Auto Regressive model with eXternal input) were used to accurately model the process, both in culture flasks and in a bioreactor ($R^2 \geq 0.98$ and 0.95 respectively), and to quantitatively determine the inhibition time. ARX models were applied to predict the inhibition time in real-time. When the model parameters converged, the median error was 21 seconds (Min 0 second, Max 75 seconds). The error decreased monotonically as new data was collected. The developed approach was generic and could be applied both in flasks and in a clinical-scale bioreactor. By automating decision-making, it will be possible to create standards and reproducibility that are necessary for large scale, robust and cost-effective cell cultures with reduced cell culture variability and consistent cell batches.

5.3. Introduction

The basic principle of autologous tissue engineering therapies consists of the isolation of progenitor cells from the patient, expansion of these cells *in vitro* until the clinically required numbers of cells is obtained, and finally proceeding to in vivo implantation at the site of injury (Koc et al., 2000). In order to get a large scale population of cells, sub culturing is used to expand the cell culture. Cells that grow adherently to the dish or flask need to be detached and collected (or "harvested") before being re-seeded and expanded (or "sub-cultured") on new culture surfaces in order to promote further growth. Adherent cells can be harvested mechanically, but this process is labour-intensive and may result in cell membrane damage and cell loss. Moreover, this procedure cannot be applied in multi-layered cell culture vessels such as cell factories used for large scale cell expansion, or in recently developed bioreactor systems such as the Pall Life Sciences Xpansion® multiplate bioreactor. Therefore, enzymatic solutions are commonly used in

order to break the connection (proteolytic reaction) both between the cells and between the cells and the surface of the vessel (Carvalho et al., 2011). However, cells must not be over-exposed to these enzymes because they can damage the cell surface, resulting in apoptosis and cell death, compromised proliferation rate and limited in vivo potential (De Smedt et al., 2008; Sutradhar et al., 2010).

The decision when to stop the proteolytic reaction is currently based on visual assessment by human operators that monitor the "roundness" of the cell via microscopy in order to determine the time-point of cell detachment (Masters and Stacey, 2007). As a result, the procedure is labour-intensive, highly operator-specific and prone to inter-operator variability and human error. Consequently current harvesting methods lack the standardisation and reproducibility that are necessary for large scale, robust and cost-effective production (Liu et al., 2010). Therefore, non-invasive, automatic monitoring systems are needed to guide operators throughout the cell culture process and in particular to improve and standardise the harvesting process with the ultimate goal of reducing cell culture variability and obtaining consistent batches of cells.

However, cell monitoring poses particular engineering challenges. Since every living organism is individually different from each other, no single organism responds like the average of a group and since living organisms are time-varying, a single organism's response to a stimulus might be different each time the stimulus is applied (Berckmans, 2008). Monitoring systems therefore have to cope with the variation between different individuals (individuality) and within the same individual (time-variance). Moreover, developing a general-purpose automated monitoring system for cells is complicated due to the different functioning principles of the available microscopes as well as due to the difference in cell density and cell types (Meijering, 2012). When using bright-field microscopy, image segmentation is also very challenging due to the low contrast between the cells and the background (Ali et al., 2012a).

In order to determine the time-point of cell detachment it is furthermore necessary to monitor the cell harvesting in real-time and both the image-processing and the modelling algorithm need to take this into account. Moreover, as the harvesting is a relatively short process, not many measurements can be used in order to determine and predict how the cells respond to the harvesting solution.

This study aimed at developing a non-invasive, automatic, on-line monitoring system that is based on a data-based (DB) modelling approach and uses non-invasive imaging technology in order to predict the optimal time for cell harvesting. The monitoring system was designed to monitor on-line the cell's response to changes in its micro-environment inflicted by a range of harvesting solutions in order to predict the optimal time-point to stop the proteolysis reaction and consequently to minimise the cells' exposure to the harvesting solution. The hypothesis of this study was that the optimal time to harvest the cells is when the cells have become circular and almost no more changes in cell morphology can be detected.

5.4. Materials and Methods

Two main experiments were performed in the present research. The first experiment was carried out on a small scale (i.e. tissue culture flasks, volume = 25 mL), the second experiment was carried out on a large scale (i.e. multi-layer bioreactor, volume = 6 L). The details of both experiments are described hereafter in more detail.

5.4.1. Small scale

Cell line and cell culture

After approval of the ethics committee for Human Medical Research (KU Leuven), human periosteum derived mesenchymal stem cells (hPDC) were isolated as described by Eyckmans and Luyten (Eyckmans and Luyten, 2006). The cells were cultured for up to seven passages in a mono-layer and in a culture medium consisting of high glucose Dulbecco's modified Eagle's medium (Invitrogen, Merelbeke, Belgium) supplemented with 10% fetal bovine serum (FBS, Gibco, Merelbeke, Belgium), 1% sodium pyruvate (Invitrogen) and 1% antibiotic-antimycotic (100 units/ml penicillin, 100 mg/ml streptomycin, and 0.25 mg/ml amphotericin B; Invitrogen). At passage 8, cells were seeded in T25 tissue culture flasks (Greiner Bio-One GmbH, Frickenhausen, Germany) at a density of 5700 cells/cm^2 and incubated at 37°C, 95% relative humidity and 5% CO_2 until they reached 70% of confluency. At this point, the harvesting procedure started.

Harvesting procedure

In this study, enzymatic harvesting was applied which is a technique that uses proteolytic enzymes to detach adherent cells from the surface of a cell culture

vessel. First, the growth medium in the vessel was aspirated and discarded. Phosphate-buffered saline (PBS) was used to wash the cells twice. Afterwards, the enzymatic harvesting solution was added to the vessel. After 15±2.5 (Mean±SD) minutes the proteolytic reaction was neutralised by adding the serum containing culture medium. The cells in the tissue culture flasks (N=33) were harvested by using different enzymatic solutions composed of different concentrations of TrypLE (Invitrogen) and EDTA (Table 5-I). Different solutions were used in order to prove that the method is generic and applicable for different cell cultures.

Table 5-I: Concentration of EDTA-TrypLE used to harvest the cells from the vessels.

Experiment	EDTA (mM)	TrypLE (times dilution)	Replication(s)
1	3.85	5	8
2	2.21	5.6	4
3	2.21	4.4	4
4	5.49	5.6	4
5	5.49	4.4	4
6	3.85	3.99	2
7	6.61	5	2
8	3.85	6.01	2
9	1.09	5	2
10	0.5	0	1

Image processing

During enzymatic treatment, the vessel was monitored under a Zeiss Primo Vert microscope (Carl Zeiss Microimaging, Oberkochen, Germany) with 4x magnification. Images (resolution = 2560x1920 pixels) were recorded every 4 seconds with a Zeiss Camera AxioCam ERc 5s (Carl Zeiss Microimaging, Oberkochen, Germany). The software Zen 2012 Lite (Carl Zeiss Microimaging, Oberkochen, Germany) was used to acquire the images from the microscope in bitmap format. All images were processed by using Matlab 2013b (Mathworks, Natick, MA) in order to extract the cells' features from the images, following the procedure described in Figure 5.2.

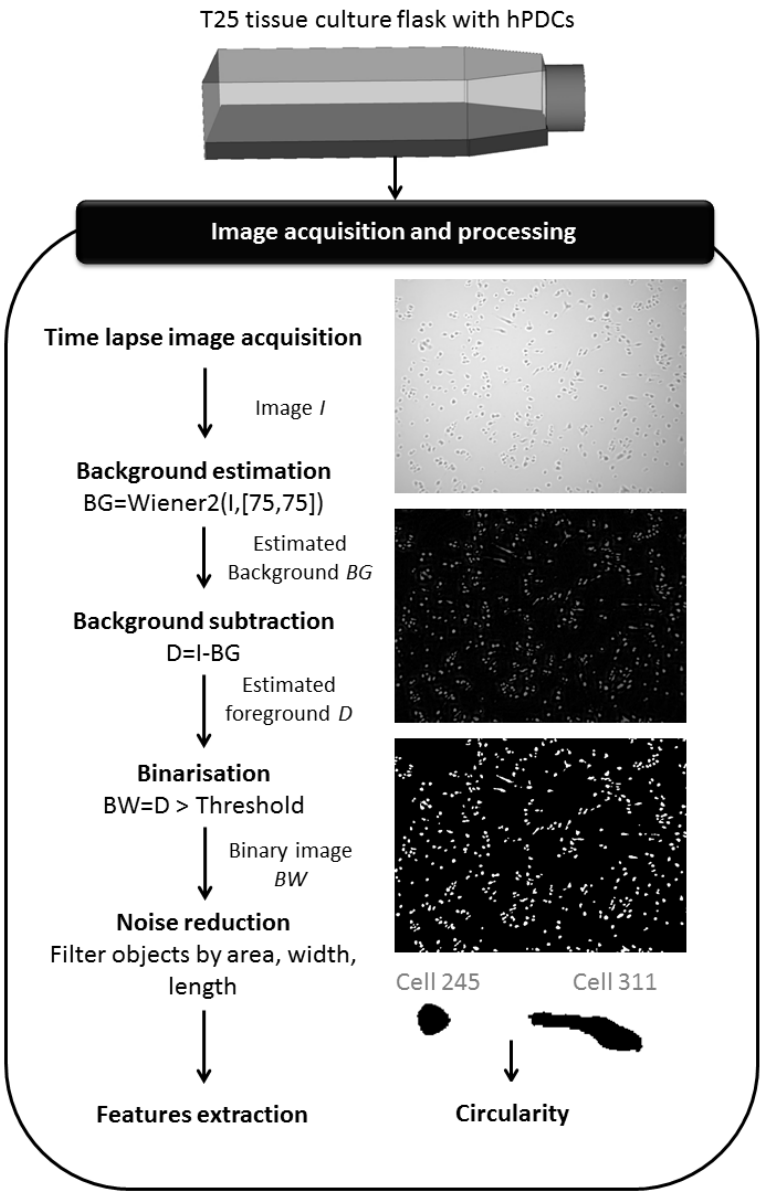

Figure 5.2: Schematic illustration of image processing.
The raw image was first pre-processed by background estimation using a Wiener filter with a window larger than the size of the cells. The estimated background was then subtracted from the original image. The final images were binarised by the optimal threshold. The noisy objects were removed by an object deletion filter. The remaining objects were reduced to a morphological feature describing the circularity of each cell.

The background was first estimated from the raw images by applying a Wiener filter to the original image (Wiener, 1949) with a window (W=75) larger than the size of the cells. The Wiener filter was used because it adapts to the local image variance, performing more smoothing when the variance is small. The estimated background was then used to compensate the illumination inhomogeneity by being subtracted from the original image. The corrected images were binarised by using an optimal threshold. The threshold was calculated from 10 images that had been acquired before the experiment. After segmentation, the detected objects still contained artefacts. These noisy (non-cell) objects were removed by eliminating all objects that did not meet specific criteria, namely area (between 100 and 3000 pixels), length (at least 5 pixels) and width (at least 5 pixels).

5.4.2. Bioreactor scale

Cell line and cell culture

The same cell type was used for the second experiment. However, at passage 8, the cells were seeded at a density of 5700 cells/cm^2 on a Pall Life Sciences Xpansion® multiplate bioreactor (Pall Life Sciences, Brussels, Belgium) with a total culture surface of 6125 cm^2 (compared to 25 cm^2 in the first experiment). The Xpansion™ bioreactor is a large scale 2D cell expansion system in which adherent cells can be cultured in an automatically controlled environment (i.e. control of pH, O_2 and CO_2 level) with a surface of up to 122400 cm^2. Moreover, in combination with the Ovizio iLine S microscope (Ovizio image technology, Brussels, Belgium), the cells on the top plates of the bioreactor could be visualised on-line.

Harvesting procedure

The harvesting performed in the bioreactor is similar to the flask-based process. The cell culture medium is drained from the bioreactor after which the bioreactor is rinsed with PBS once. Subsequently the preheated harvesting solution (3.85 mM EDTA/5 times diluted TrypLE) is pumped into the bioreactor and the whole setup is moved to the Ovizio iLine S digital holographic microscope for time-lapse imaging. The harvesting solution with the suspended cells is drained from the bioreactor upon visual confirmation of cell detachment.

Image processing

During cell detachment, the multi-layer bioreactor was monitored by using the Ovizio iLine S digital holographic microscope with 5x magnification. OsOne

3 software (Ovizio image technology, Brussels, Belgium) was used to acquire the image at 5 frames/second at a resolution of 1024x1024 pixels. The images were extracted from the OsOne system as bitmap images. The Ovizio microscope allows 3D cell reconstruction, but only 2D images were required for processing (Figure 5.3). All images were processed by using Matlab 2013b (Mathworks, Natick, MA) in order to extract the cells' features from the images. The images were filtered by using a low pass filter in order to correct irregular illumination. The resulting images were smoothed by using a Gaussian filter (W=3) and binarised by using an optimal threshold. The threshold was calculated from the first 10 images. After segmentation, the noisy (non-cell) objects were removed from the images by eliminating all objects that did not meet specific criteria, namely area (between 50 and 2000 pixels), length (at least 5 pixels) and width (at least 5 pixels).

a) b)

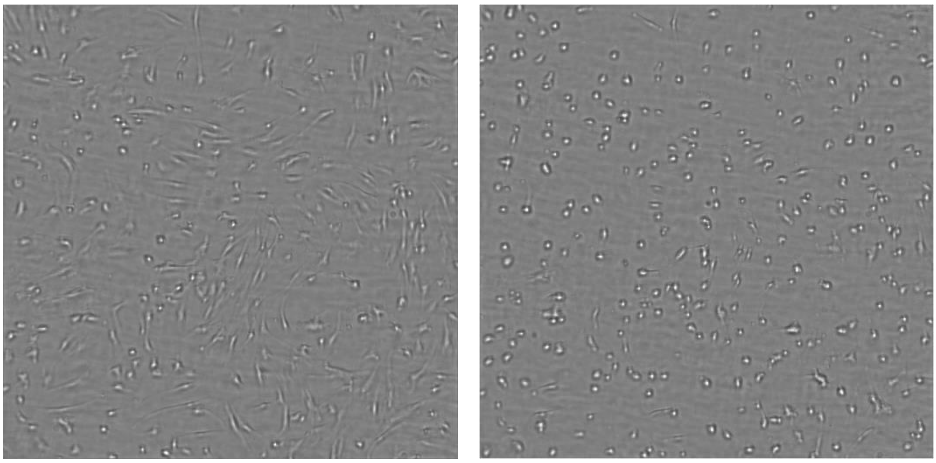

Figure 5.3: Images acquired during the harvesting from the Xpansion® bioreactor (Pall Life Sciences, Brussels, Belgium).
At the beginning, the cells had an elongated shape a) while most of the cells became round at the end of the harvesting procedure b).

5.4.3. Features extraction

Features extraction aims at reducing redundant information within an image to a few variables that retain all relevant information. These representative variables describe each image as a point in an N-dimensional feature vector

space, where N is the number of extracted features. Cell circularity was calculated as 4π*area/perimeter^2 (Friel, 2000) for each of the segmented cells. The average cell circularity was used to monitor the status of the cell population when exposed to the harvesting solution (Figure 5.4).

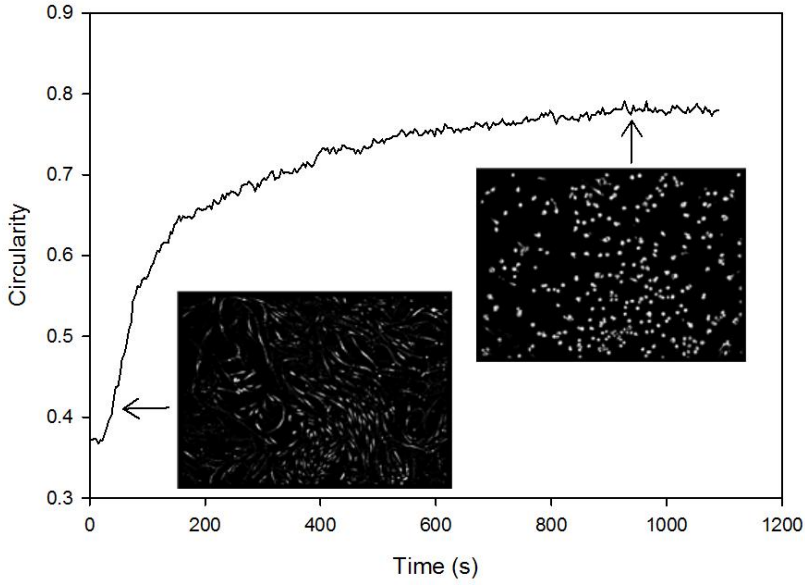

Figure 5.4: Cell circularity measured during harvesting. At the beginning, the adherent cells had an elongated shape, while they adopted a circular shape when in suspension.

5.4.4. Modelling

Model-based monitoring

Model-based monitoring methods do not necessarily require *a priori* knowledge of the actual system physics in order to determine the system dynamics. The system is considered as an object in which different variables interact and produce observable signals that are the output of the system. The output of the system depends both on external signals that are manipulated by the observer (inputs) and on external signals that can only be observed by their influence on the output (disturbances) (Ljung, 1999). Modelling consists in determining the relation between input and output of the system. The determined relation can be used for different applications such as control, prediction or error detection. The purpose of the application affects the choice of the appropriate method for modelling the system.

The aim of this study was to predict the optimal time-point for cell harvesting by monitoring changes in the cell's circularity (output) in response to the enzymatic harvesting solution (input). Cell circularity as measured by image analysis remained approximately constant when cells had been grown in a cell culture medium before the harvesting solution was added. Upon addition of the enzymatic harvesting solution, cell circularity changed to a new value. This response is described in control theory as an unitary step-response (Tay et al., 1998). The transient response of the system was specified by six attributes; namely delay time, rise time, peak time, maximum overshoot, maximum undershoot and settling time (Tay et al., 1998). The settling time was defined as the time required for the response curve to reach and stay within a range of certain percentage (Tay et al., 1998). In this study the percentage was set to 5% and the settling time was considered as the plateau in which the cells should be harvested.

Off-line vs. on-line modelling

In contrast to on-line modelling in which the model parameters are estimated recursively as time progresses, off-line modelling uses all data available after the experiment for parameter estimation. In this study, off-line modelling was necessary initially in order to validate the model estimation of the experimental data and to calculate the dynamic information used to measure the performance of the on-line model.

On-line and real-time modelling, instead, was necessary in order to predict the optimal time for harvesting the cells while the process is still ongoing. In order to focus on the main system dynamics, the structure of the model was fixed as a first-order structure and only the input-output delay and the model parameters were estimated. Once the model parameters converged within a range of a certain percentage (5%), the model was considered stable and the settling time was calculated and used as the optimal time for harvesting the cells. Both off-line and on-line modelling approaches are described hereafter in more detail.

Off-line modelling: ARX model

In this study, the linear, discrete-time Auto Regressive model with eXternal input (ARX) was selected as a parametric model structure in order to describe the cell response to the enzymatic solution. The ARX model is most efficient in estimating the model parameters because it solves linear regression equations in analytic form. It can be used if there is a good signal-to-noise

ratio. The ARX model predicts the output as a linear function of measurable data (Ljung, 1999):

$$\boldsymbol{y(k)} = \frac{\boldsymbol{B(d)}}{\boldsymbol{A(d)}}\boldsymbol{u(k-n_k)} + \frac{\boldsymbol{1}}{\boldsymbol{A(d)}}\boldsymbol{e(k)} \quad (1)$$

where *y* is the output, *u* is the input, *e* is the error, *A* is the model denominator, *B* is the model numerator, *d* is the number of parameters and *k* is the backward shift operator.

The ARX model can be solved by using Least Squares (LS) where *nb* and *na* are the numbers of parameters in the numerator and denominator of the parametric model:

$$\begin{bmatrix} y(k) \\ y(k+1) \\ \vdots \\ y(k+n-1) \end{bmatrix} = \begin{bmatrix} -y(k-1) & \cdots & -y(k-na) & u(k-1) & \cdots & u(k-nb) \\ -y(k) & \cdots & -y(k-na+1) & u(k) & \cdots & u(k-nb+1) \\ \vdots & \ddots & \vdots & \vdots & \ddots & \vdots \\ -y(k+n-2) & \cdots & -y(k-na+n) & u(k+n-2) & \cdots & u(k-nb+n) \end{bmatrix} \begin{bmatrix} a_{na} \\ a_{na-1} \\ \vdots \\ a_0 \\ b_{nb} \\ b_{nb-1} \\ \vdots \\ b_0 \end{bmatrix} + \begin{bmatrix} e(k) \\ e(k+1) \\ \vdots \\ e(k+n-1) \end{bmatrix}$$

(2)

Equation 2 can be written in compact format as follows:

$$\boldsymbol{y} = \boldsymbol{Z\vartheta} + \boldsymbol{e} \quad (3)$$

The LS estimation of the parameters $\widehat{\boldsymbol{\vartheta}}$ is used to resolve this equation:

$$\widehat{\boldsymbol{\vartheta}} = \left(\boldsymbol{Z^T Z}\right)^{-1}\boldsymbol{Z^T y} \quad (4)$$

The input-output delay *nk* was estimated by using the cross-correlation function (CCF). The CCF is the product-moment correlation as a function of the input (*u*)-output (*y*)-delay (Chatfield, 2004) where *N* is the length of the time-series, $\bar{u}$ is the mean input and $\bar{y}$ the mean output:

$$ccf(n_k) = \frac{\frac{1}{N}\sum_{k=1}^{N-n_k}(u_k-\bar{u})(y_{k+n_k}-\bar{y})}{\sqrt{\frac{1}{N}\sum_{k=1}^{N}(u_k-\bar{u})(u_k-\bar{u})\frac{1}{N}\sum_{k=1}^{N}(y_k-\bar{y})(y_k-\bar{y})}} \quad (5)$$

Off-line modelling: model identification and evaluation

System identification requires to collect the data from the experiment and to select a model structure (order) that represents the system as appropriately as

possible based on a cost function. Different criteria exist to determine the structure and goodness of fit of a model from experimental data. The Young Information Criterion (YIC) was used to determine the degree of the polynomials *A(d)* and *B(d)* and the time delay *nk* (Young et al., 2008). The YIC combines the model residual variance with the parameter efficiency and is defined as:

$$YIC = ln\frac{\hat{\sigma}^2}{\sigma_y^2} + \ln\left(\frac{1}{n_\vartheta}\sum_{i=1}^{n_\vartheta}\frac{\hat{p}_{ii}}{\hat{\vartheta}_i^2}\right) \quad (6)$$

where $\hat{\sigma}^2$ is the variance of the model residuals, σ_y^2 is the variance of the measured output, n_ϑ is the number of estimated parameters and $\hat{p}_{ii}$ is the i^{th} diagonal element of the covariance matrix.

In order to quantify the goodness of fit, the coefficient of determination (R^2) was calculated (Nash and Sutcliffe, 1970):

$$R^2 = 1 - \frac{\sigma_e^2}{\sigma_y^2} \quad (7)$$

where σ_e^2 is the variance of the estimated noise and σ_y^2 the variance of the measured output. R^2 was used to compare how the models fitted to different time series.

On-line modelling: Kalman filter

The Kalman filter (Kalman, 1960) was used to recursively estimate the 1st order ARX model parameters whenever new data was acquired. The principle of the Kalman filter is that the estimation of new parameters $\hat{\boldsymbol{\vartheta}}(\boldsymbol{k+1})$ at time $\boldsymbol{k+1}$ depends on the predicted error and on the previous parameter estimation $\hat{\boldsymbol{\vartheta}}(\boldsymbol{k})$ at time $\boldsymbol{k}$.

Considering equation (3), when new data arrives in form of input and output, the new problem consists in estimating the new parameters $\boldsymbol{w}$ based on the old data [**y Z**] and the newly gathered data [$\tilde{y}$ $\tilde{z}$]. The problem is solved by minimising the 2-norm of the following equation:

$$\min_{\boldsymbol{w}} \left\| \begin{pmatrix} \boldsymbol{y} \\ \tilde{y} \end{pmatrix} - \begin{pmatrix} \boldsymbol{Z} \\ \tilde{z}^T \end{pmatrix} \boldsymbol{w} \right\|_2^2 \quad (8)$$

That resulted in:

$$\boldsymbol{w} = (\boldsymbol{Z^T Z} + \tilde{z}\tilde{z}^T)^{-1}(\boldsymbol{Z^T y} + \tilde{z}\tilde{y}) \quad (9)$$

The formula can be computed by using the Woodbury-Sherman-Morrison equation (Sherman and Morrison, 1950) and after some simplifications, the formula can be described as follows:

$$\boldsymbol{w} = \hat{\boldsymbol{\vartheta}}(\boldsymbol{k}+\mathbf{1}) = \hat{\boldsymbol{\vartheta}}(\boldsymbol{k}) + \boldsymbol{G}[\tilde{y} - \tilde{z}^T\hat{\boldsymbol{\vartheta}}(\boldsymbol{k})] \quad (10)$$

where $[\tilde{y} - \tilde{z}^T\hat{\boldsymbol{\vartheta}}(\boldsymbol{k})]$ is the error of the prediction and $\boldsymbol{G}$ is the gain:

$$\boldsymbol{G} = \frac{(\boldsymbol{Z^T Z})^{-1}\tilde{z}^T}{1+\tilde{z}^T(\boldsymbol{Z^T Z})^{-1}\tilde{z}} \quad (11)$$

On-line modelling: model convergence

The model parameters of $\hat{\boldsymbol{\vartheta}}(\boldsymbol{k})$ and the input-output delay *nk* were monitored over time (**Figure 5.5**).

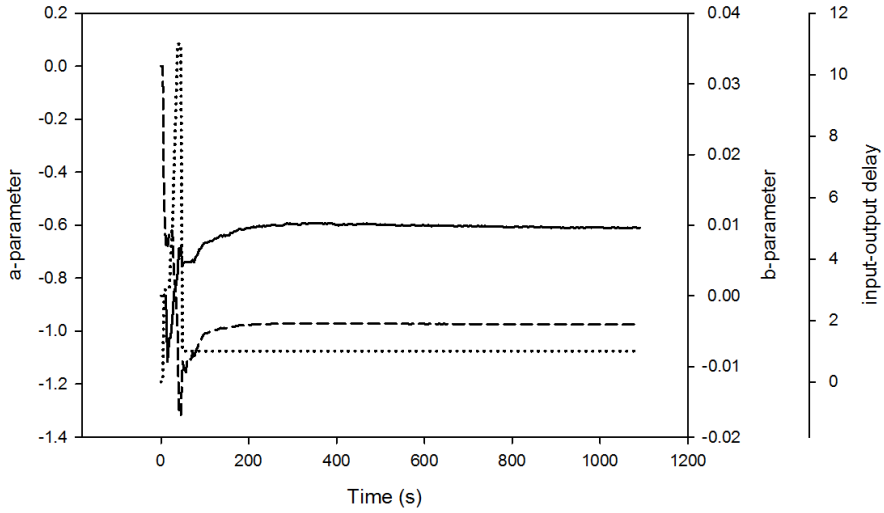

Figure 5.5: Example of parameters estimation over time.
The a-parameter (dashed line) and b-parameter (continuous line) as well as the input-output delay (dotted line) converged after 350 seconds. After this moment, it was possible to predict the time for harvesting the cells by calculating the settling time of the model.

A sliding window of 10 samples was used to calculate whether the parameters reached convergence or not. The parameters were considered converged if the variance of the parameters within the time window was less than 5%.

5.4.5. Algorithm

The final on-line and real-time algorithm that monitored the cell circularity in response to micro-environmental changes and that was used to predict the time when there were no more significant morphological changes (i.e. the

settling time) was developed in Matlab 2013b (Mathworks, Natick, MA) and reads as follows:

1. Watch microscope acquisition folder
2. When a new time-lapse image is detected:
    a. Load image
    b. Pre-process image
    c. Segment image
    d. Calculate mean circularity *y(k+1)*
    e. Calculate the predicted value $\hat{y}(k+1)$:
    $\hat{y}(k+1) = \alpha^T \hat{\vartheta}(k, n_k)$
    f. Calculate the error *e(k)* between the predicted and the measured circularity*:*
    $e(k+1) = \hat{y}(k+1) - y(k+1)$
    g. Calculate the gain ***G***:

$$\boldsymbol{G} = \frac{\left(\boldsymbol{Z^T Z}\right)^{-1} \alpha^T}{1 + \alpha^T (\boldsymbol{Z^T Z})^{-1} \alpha}$$

    h. Re-estimate the model parameters $\widehat{\boldsymbol{\vartheta}}_{\boldsymbol{n_k}}(\boldsymbol{k+1})$ based on the new data for the different time delay *nk*:
    $\widehat{\boldsymbol{\vartheta}}_{\boldsymbol{n_k}}(\boldsymbol{k+1}) = \widehat{\boldsymbol{\vartheta}}_{\boldsymbol{n_k}}(\boldsymbol{k}) + \mathbf{G*e}$
    i. Calculate the variance of the parameters in a time window of size 10
    j. If the variance is less than 5%, calculate the settling time (ST)

5.5. Results

5.5.1. Small scale

10 different experiments with different levels of replication and with different harvesting solutions were performed. A total of 33 datasets were gathered. For each dataset, the cell circularity in response to the micro-environmental changes was modelled and the settling time was calculated (Figure 5.6).

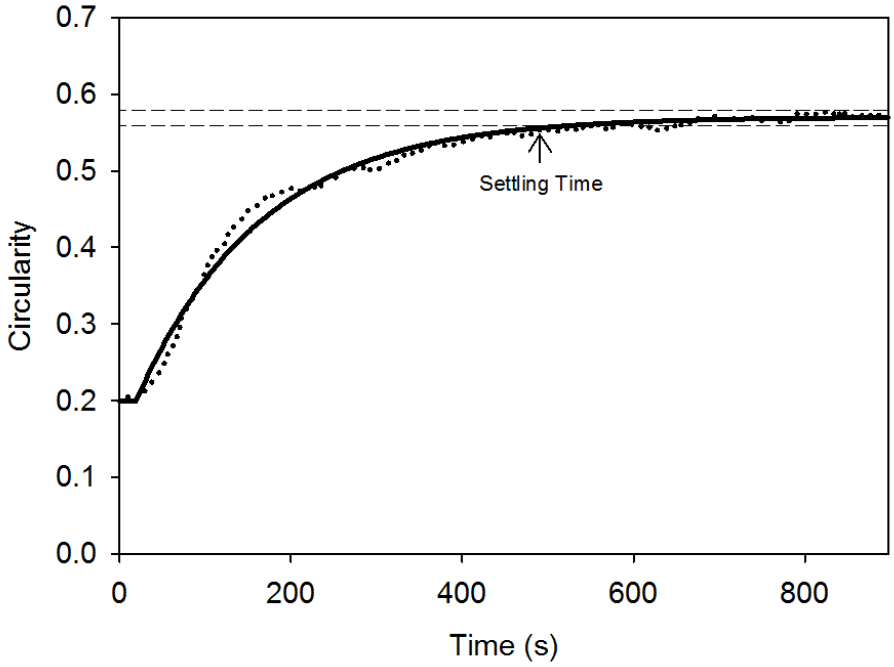

Figure 5.6: Example how cell morphology was modelled as a response to the harvesting solution.
The dotted line is the measured circularity, while the continuous line is the modelled one. The settling time is calculated as the time required for the response curve to reach and stay within 5% range of the signal.

The model structure, the order of the parameters and the input-output delay were selected by means of the YIC, a criterion that provides an indication for the best parsimonious model (see above). Based on the selected model, the coefficient of determination (R^2) and the settling time were calculated. As it is documented in Table 2, the estimated off-line models fitted the data very well with a $R^2 \geq 0.98$. The estimated model structures were either represented by a first-order or by a second-order polynomial. However, while the second-order was estimated, the equivalent first-order model had a YIC (and R^2) very close to the second-order one. The input-output delay varied between 0 and 10 data points (0 to 40 seconds), while the settling time varied between 344 and 978 seconds, with a median of 470 seconds. The settling time was used as a reference for the on-line and real-time prediction of the harvesting time.
Experiment 10 used a harvesting solution that only consisted of EDTA. Since this solution does not contain enzymes, it was not powerful enough to initiate the proteolytic reaction and was considered as negative control: no change in

morphology was noticed and no cells could be harvested. Therefore, no model was estimated for this condition since no input-output relation existed in the system of interest.

The on-line model required to recursively estimate the parameters as new data was continuously gathered. The model was considered stable once the variance of the parameters was less than 5% in a time window of size 10. The stability of the parameters was reached after a median of 474 (Min: 238, Max: 698) seconds. Once the model was stable, the settling time was calculated. The on-line modelling approach was applied to the same 33 experimental datasets that were used for the off-line modelling.

Using the estimated model at the time of convergence to model the data, the coefficient of determination resulted in a median R^2 of 0.983 (Min: 0.923, Max: 0.997). The absolute error between the settling time predicted at the time of convergence in the on-line model approach and settling time calculated off-line had a median of 21 seconds (Min 0 second, Max 75 seconds) (Table 5-II). As it can be seen in Table 5-II, the on-line prediction tends to under-estimate the settling time. However, after the parameters reached convergence, the monitoring did not stop but continuously re-estimated the settling time whenever new data was acquired. The error therefore decreased monotonically with new data being used for parameter estimation (Figure 5.7).

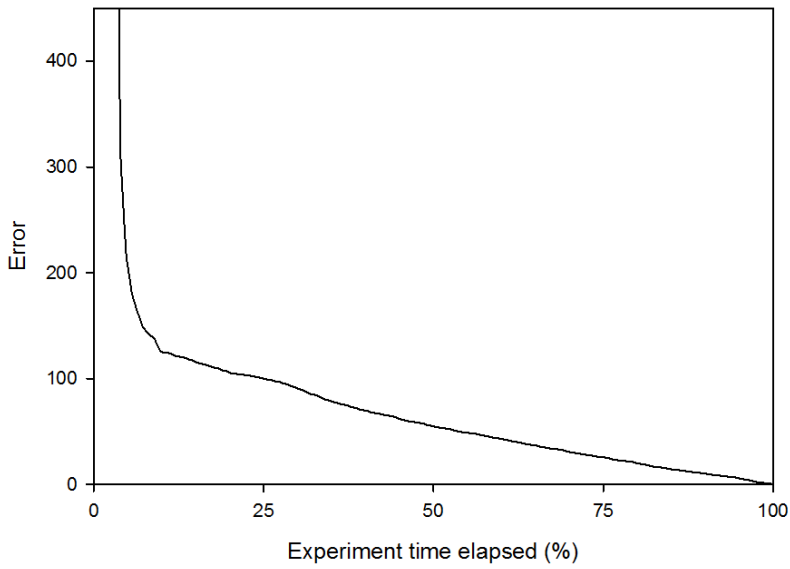

Figure 5.7: Average estimation error (N=32) in seconds related to the elapsed time of the experiment. The error is monotonically decreasing with new data being used.

Table 5-II: Results of the small scale harvesting modelled off-line and on-line.
For each experiment, the results of the model based on the lowest YIC are presented and consist of the model order (i.e. number of *a* parameters), the input-output delay *nk*, the YIC, the R^2 and the calculated settling time. For the on-line experiment, the input-output delay, the R^2 and the settling time calculated at the time of parameter convergence are presented. Furthermore, the error between the estimated settling time (on-line) and the reference one (off-line) is shown. [a]No change in morphology was measured after the harvesting solution was applied. No cells were harvested at the end of the experiment. "#" stands for the model order.

		off-line					on-line			
Exp	Repl	#	nk	YIC	R^2	ST (s)	nk	R^2	ST(s)	Error ST (s)
1	1	1	8	-14.964	0.994	978	10	0.943	940	-38
1	2	1	8	-14.204	0.992	545	10	0.959	557	12
1	3	2	1	-13.925	0.998	390	0	0.984	390	0
1	4	2	2	-12.497	0.995	427	0	0.979	409	-18
1	5	2	7	-13.969	0.998	597	2	0.991	597	0
1	6	1	7	-15.965	0.998	473	7	0.997	450	-23
1	7	2	10	-15.204	0.999	488	6	0.992	465	-23
1	8	1	5	-14.032	0.993	390	5	0.992	375	-15
2	1	1	1	-11.799	0.981	474	1	0.98	473	-4
2	2	1	4	-13.82	0.993	367	4	0.993	367	0
2	3	1	3	-14.74	0.994	469	5	0.977	394	-75
2	4	2	7	-15.473	0.999	469	5	0.982	413	-56
3	1	1	0	-14.316	0.993	518	3	0.923	461	-57
3	2	1	0	-13.339	0.987	344	0	0.979	314	-30
3	3	1	5	-13.36	0.99	689	4	0.99	715	26
3	4	2	7	-14.023	0.998	367	3	0.991	367	0
4	1	1	1	-12.034	0.981	344	1	0.98	344	0
4	2	1	3	-16.442	0.998	397	4	0.995	401	4
4	3	2	5	-14.422	0.999	454	0	0.98	428	-26
4	4	2	2	-14.863	0.998	439	0	0.982	439	0
5	1	1	0	-14.083	0.993	430	1	0.981	362	-68
5	2	1	10	-14.025	0.994	499	10	0.994	503	4
5	3	1	0	-13.003	0.984	470	0	0.977	428	-42
5	4	2	8	-15.68	0.999	439	4	0.99	439	0

6	1	1	2	-14.068	0.993	428	3	0.99	394	-34
6	2	2	7	-15.277	0.999	389	6	0.978	324	-65
7	1	1	1	-14.137	0.992	624	1	0.992	624	0
7	2	1	7	-14.628	0.995	473	9	0.964	473	0
8	1	1	4	-13.534	0.99	510	6	0.973	537	27
8	2	1	7	-15.144	0.996	526	8	0.993	481	-45
9	1	1	4	-14.82	0.995	621	4	0.995	621	0
9	2	1	0	-13.86	0.992	571	0	0.99	541	-30
10[a]	1									

5.5.2. Bioreactor scale

The cells' morphological response to the harvesting solution in the Xpansion® bioreactor was similar to the one in the flasks (Figure 5.8). The cells started to react to the solution and circularity increased over time.

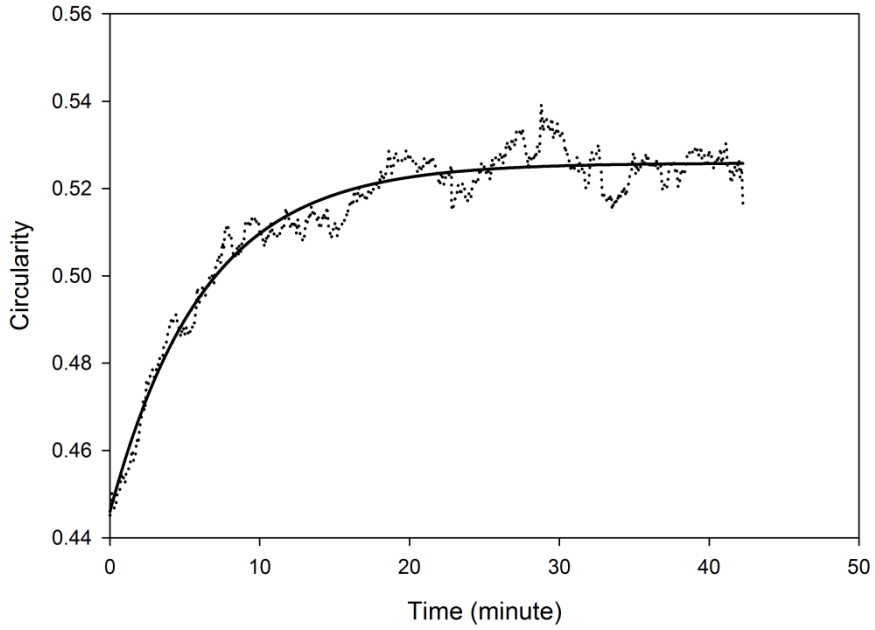

Figure 5.8: Cell circularity measured and modelled as a response to the enzymatic solution during the harvesting from the Xpansion® bioreactor. The dotted line is the measured circularity, while the continuous line is the modelled one.

This reaction could be quantified by measuring the average cell circularity. The cell response to the harvesting solution resulted in a first order-model with a YIC of -18.01. The model fitted the data with a R^2 of 0.95. The settling time was calculated as 17 minutes from the start of the reaction.

The parameters converged after 16 minutes and 20 seconds and the settling time at this point was estimated for 16 minutes and 40 seconds. Due to the higher noise in the data, the convergence of the parameters was slower compared to the one obtained in the T25 flasks (see 5.4.1) and the estimation error was around 20 seconds.

The process dynamics were slower compared to the flasks, probably because the presence of more FBS containing medium residue, due to the single rinse (compared to double in the flasks), slowed down the reaction. Therefore, the harvest procedure needs be optimised to reduce the settling time to be closer to the time used for T25 flasks.

5.6. Discussion

This work used image analysis and DB modelling techniques in order to develop an on-line and automatic monitoring system that measured morphological changes in cells during harvesting and that predicted the optimal time-point to stop the enzymatic reaction (i.e. harvesting). By measuring the cell surface it was possible to monitor the detachment status of the cell. The measure of circularity reflects this process as the cell changes from being attached to being detached. The time required for the cell to react varied from experiment to experiment, depending on the harvesting solution itself, but also on the time needed to place the vessel under the microscope, to focus the image and to start the recording. In fact, the input-output delay represented the time in which the enzymatic solution started to react with the substrate.

The morphological changes in response to the harvesting solution were modelled as the system- response to a unitary step. The used ARX model that was fixed to a 1^{st} order and was sufficiently complex to determine the input-output relation, even though a second-order model was deemed more optimal in some experiments based on the YIC cost function. The chosen models fitted the data well, as a $R^2 \geq 0.98$ was determined. The dynamic information extracted from the model could therefore be used to interpret the physical information of the underlying biological process. The time constant of the model represented the speed of the cell response to the reaction rate, the steady state gain reflected the circularity level cells reach at the end of the reaction while the settling time was the time where no more morphological changes were noticeable and which was considered the optimal time for

harvesting the cells. Defining the plateau as the optimal time-point for harvesting the cells, is in accordance with literature (Wilson and Walker, 2010) and with the empirical procedure currently followed by the operators. Future works will need to validate if a different percentage (in this study 5%) should be employed in order to calculate the settling time and how this percentage influences the cell yield. Future works will also need to check if the reaction rate (correlated with the model's time constant) influences the cell quality. However, this optimisation can only be carried out if a quantitative measurement, as presented in this study, is available.

By on-line monitoring cell morphology it was possible to predict the optimal harvesting time-point as soon as the model parameters converged with a prediction error of 21 seconds (Min 0 second, Max 75 seconds). A minimum of 60 (238 seconds) and a maximum of 174 (698 seconds) data-points were required to make prediction of the cell behaviour. Of course, as more data was collected, the increased confidence in the parameters decreased the error monotonically. In order to further reduce this error, a higher sampling rate may be used, however, this needs to be balanced in regard to the time needed for processing the data in real-time.

The main challenge in automating cell culture procedures is the high cell variability that requires the ability to make adaptive decisions based on the status of the cells at each given time (Ker et al., 2011). As it was shown in the results, the cells responded differently even when the same harvesting solution was used, demonstrating the high cell variability even in controlled conditions. Time-lapse imaging is a non-invasive method that allows collecting information about the status of the cell population based on the morphological information and making predictions about the cell behaviour (Matsuoka et al., 2013).

When using bright-field microscopy, as it was used in the small scale experiment of this study, image segmentation is very difficult due to the low contrast between the cells and the background (Ali et al., 2012b). In addition, the fastness of the harvesting process required efficient image processing algorithms. The cells morphology needed to be calculated within 4 seconds in order to facilitate real-time monitoring. To improve the threshold-based segmentation (Meijering, 2012) an estimation of the background was used in order to remove the shading from the images.

A major advantage of the developed method is that it is generic and can be applied not only to a wide range of harvesting solutions, but also to different cell culture systems across different scales. This study demonstrated that the same procedure could be used in a large scale bioreactor, obtaining a result similar to the small scale cell culture flasks. The only part of the procedure

that is microscope specific and that needs to be adapted or tuned is the image segmentation because it is highly dependent on the applied microscope technology. Automatic monitoring tools based on live cell monitoring, as presented in this study, are needed to develop applications that standardise and optimise processes in cell culture. This becomes even more crucial in autologous cell-therapy applications were cell donor variability could be robustly dealt with by using this kind of data-based approach.

5.7. Conclusion

This study aimed at developing a non-invasive, automatic, on-line monitoring system that uses microscopy, DB modelling approach and imaging technology in order to predict the optimal time for harvesting adherent mesenchymal stem cell cultures. This allowed determining in real-time the optimal time-point to inhibit the enzymatic reaction of the harvest. Furthermore, the quantification of the harvesting process will allow collecting descriptive parameters for further process optimisation.

The approach was tested at two different scales, namely in flasks and in a large scale bioreactor, and with different microscope technologies (bright-field and holographic). The results showed that the method is generic and scalable. By enabling automatic decision-making based on objective measurements, it will be possible to create standards and reproducibility that are necessary for large scale, robust and cost-effective cell cultures with reduced cell culture variability and consistent cell batches.

5.8. Acknowledgment

The authors would like to thank Pall Life Sciences for providing the Xpansion® bioreactor. This work was supported by the KU Leuven Concerted Research Actions (GOA/13/016), by the ENDEAVOUR project G.0982.11N of the Research Foundation Flanders (FWO Vlaanderen), and by the TETRA IWT LIMSY project 120154.

Chapter 6. Large-scale progenitor cell expansion for multiple donors in a monitored hollow fibre bioreactor

Adapted from: Lambrechts T., Papantoniou I., Rice B., Schrooten J., Luyten F. P, Aerts J.-M. Cytotherapy (2016) 18:1219–33.

6.1. Positioning within the context of the PhD project

This is the second 'scale-up' chapter in which the translation of the standard Prometheus flask-based cell expansion process to an automated closed-system bioreactor is described (see Objective 2 in Chapter 2). While Chapter 4 evaluated the translation to a multiplate bioreactor where the cells are cultured on large plastic plates similar to the standard culture flasks, this chapter assesses a hollow fibre bioreactor where the cells grow inside perfused hollow fibres. The cell quality characterisation is similar to the characterisation used in Chapter 4, however here multiple donors were evaluated. The effect of donor-related variability on large-scale cell expansion and process comparability is discussed (Objective 3 in Chapter 2) and potential strategies to take this variability into account while determining the feed rate and harvest timing are investigated.

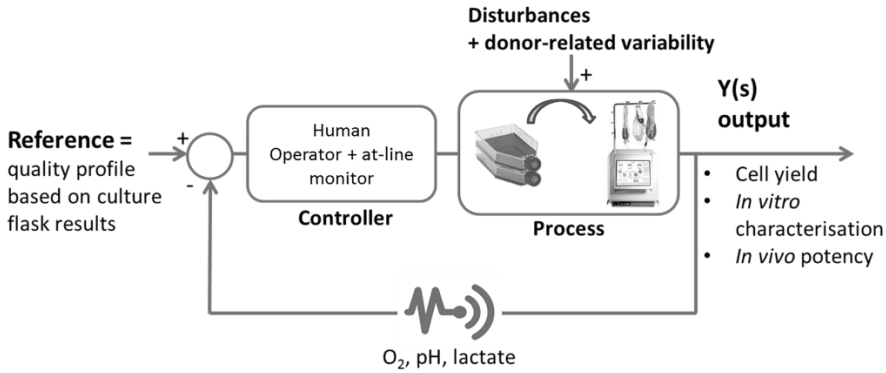

Figure 6.1: Position of Chapter 6 in the general control scheme and the larger context of this work.

6.2. Abstract

Background: With the increasing scale in stem cell production, a robust and controlled cell expansion process becomes essential for the clinical application of cell based therapies. The objective of this work was the assessment of a hollow fibre bioreactor (Quantum® Cell Expansion System from Terumo BCT) as a cell production unit for the clinical-scale production of human periosteum derived stem cells (hPDCs).

Methods: We aimed to demonstrate comparability of bioreactor production to standard culture flask production based on a product characterisation in line with the International Society of Cell Therapy (ISCT) *in vitro* benchmarks

and supplemented with a compelling quantitative *in vivo* bone-forming potency assay. Multiple process read-outs were implemented in order to track process performance and deal with donor-to-donor-related variation in nutrient needs and harvest timing.

Results: The data show that the hollow fibre bioreactor is capable of robustly expanding autologous hPDCs on a clinical scale (yield between 316 million and 444 million cells starting from 20 million after ± 8 days of culture), while maintaining their *in vitro* quality attributes compared to the standard flask-based culture. The *in vivo* bone-forming assay on average resulted in 10.3 ± 3.7% and 11.0 ± 3.8% newly formed bone for the bioreactor and standard culture flask respectively. The analysis showed that the Quantum system provides a reproducible cell expansion process in terms of yields and culture conditions for multiple donors.

6.3. Introduction

An increasing number of clinical trials (Culme-Seymour et al., 2012; Heathman et al., 2015a) demonstrate that cell-based therapies are becoming a reality, destined to revolutionize the healthcare industry. Mainly based on hematopoietic and mesenchymal stromal cells (MSCs), a large number of cell-based therapies are currently being developed for the treatment of multiple conditions ranging from skeletal defects (e.g. PREOB® by Bone Therapeutics), to oncological (Curran et al., 2015; Maus et al., 2014), to cardiovascular (e.g. C-CURE® by Celyad (Bartunek et al., 2013)) and liver disorders (e.g. HepaStem® by Promethera). However, there is growing awareness of the numerous bioprocessing challenges that need to be addressed in order to translate initial clinical successes, which were most often based on manual laboratory-scale cell culture processes, into an industrial process that can guarantee the production of cell-based therapies with manageable cost of goods, and robust and predictable *in vivo* performance (Galipeau, 2013; Hourd et al., 2014; Kaiser et al., 2015).

Although clinical dose sizes vary significantly across therapeutic applications, most MSC- based therapies require between 10^7 and 10^9 cells for a single dose (Jung et al., 2012; Simaria et al., 2014a) while the number of cells that can be sourced from a single donor is generally much lower, e.g. approximately one thousand MSCs per mL of bone marrow (Beitzel et al., 2013; Fennema et al., 2009). Therefore, a cell expansion step is required that is able to produce a high number of cells with a reproducible cell quality (Rowley et al., 2012; Sharma et al., 2011). With an increasing scale of culture volumes the choice to translate from manual flask-based culture to bioreactors, be it multi-plate

bioreactors, perfusion bioreactors or stirred vessels, is inevitable (Bovy et al., 2015). However, the high level of automation and precision that is essential for the desired process reproducibility often conflicts with the complexities entailed in live cell-based products. As more process steps are required for larger numbers of cells, not only is variability introduced by the process itself proportional to the scale of expansion (Hanley et al., 2014), but with the use of large-scale automated bioreactors the monitoring and control of biological variability also becomes more important. Since MSCs generally possess only a limited expansion capacity before critical cell characteristics start to deteriorate (Bara et al., 2014; Siddappa et al., 2007), cells are sourced from multiple donors, resulting in variable process input. Especially for autologous ("patient-specific" compared to "universal" or allogeneic) therapies, where donor-to-donor variation is expected to affect each batch for example in terms of nutrient requirements or optimal timing of harvest, the lack of process reproducibility poses a significant challenge to the development of a clinical production process that should assure a minimal number of cells with a defined quality level.

In the first phase of this work, the Quantum system was evaluated as a tool to scale-up a standard tissue culture flask-based expansion step for an autologous bone tissue engineering therapy under development in our lab. The expansion process should assure the maintenance of a set of MSC quality characteristics such as their pluripotency and differentiation potential (Dominici et al., 2006; Oliveira et al., 2014). But more importantly, these cells should maintain an unimpaired regenerative potential when implanted in an *in vivo* potency assay. Secondly, monitoring tools were implemented in order to track changes in bioreactor process conditions, either induced by process variations or biological variation. Finally, a case study on the clinical-scale expansion of three different donors is presented allowing to compare bioreactor process reproducibility.

6.4. Materials and methods

6.4.1. General experimental workflow

The evaluation of the large-scale bioreactor-based expansion step fits in the development of an autologous bone tissue engineering therapy, based on human periosteum derived stem cells (hPDCs). Only a small number of cells (between $1x10^4$ and $1x10^5$) can be obtained via a biopsy of the periosteum of the patient, while it is hypothesised that for a tibia defect of 3 cm wide around 300 million cells are required (Eyckmans et al., 2010; Eyckmans and Luyten, 2006). The general experimental workflow (Figure 6.2) consists of an initial

pre-culture phase (section 6.4.2 for details) in which the cells from a periost biopsy are expanded by standard flask-based culture to be able to seed the bioreactor surface with a minimum initial seeding density. The second phase is the bioreactor-based expansion process (section 6.4.3 for details). Three flask-based control conditions were included in parallel with the bioreactor culture in an effort to provide appropriate experimental comparators, namely those associated with seeding density, substrate characteristics, and fluid (medium) handling. The third phase consists of the post-harvest cell characterisation (section 6.4.6), for which an *in vitro* and *in vivo* quality profile was determined, starting directly after harvesting the bioreactor.

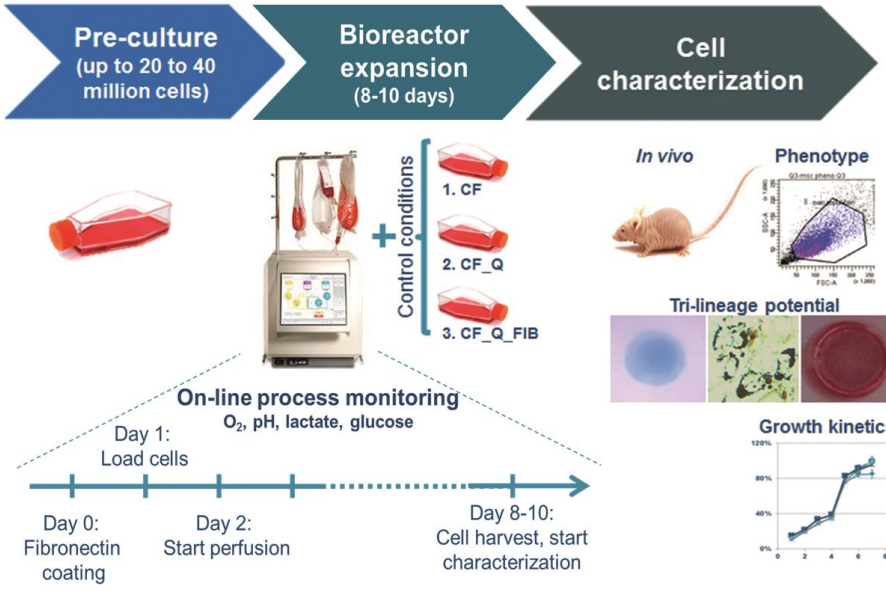

Figure 6.2: General experimental work flow with an initial flask-based pre-culture phase, followed by the Quantum system bioreactor culture.
During bioreactor culture the cell growth was monitored based on daily lactate measurements, and three tissue culture flask-based control conditions were taken along in order to investigate the effect of flow rate, lowered seeding density and fibronectin coating. Immediately after cell harvest the cell characterisation was initiated, including among others an in vivo bone-forming potency assay.

In total, data from nine runs in the Quantum system are discussed in this work (Table 6-I). The first three runs were used to fine-tune the process based on the results of a pool of cells from four individual donors (Table 6-I) in order to compare the result of changes to the process settings, while limiting the biological variability. This data will be referred to as the process development data. For the subsequent six runs, the process parameters were fixed and three

other donors (2 individual runs per donor, Table 6-I) were randomly selected for an assessment of the process reproducibility. This data will be referred to as the individual donor data.

6.4.2. Standard flask-based hPDC culture

Human periosteum-derived stem cells (hPDCs) are a promising source of adult stem cells for skeletal cell therapies as they are the main contributors to the natural bone healing process (Roberts et al., 2014) and possess extensive *in vitro* expansion capabilities as hPDCs generally maintain linear growth curves for over 30 population doublings (De Bari et al., 2001a; De Bari et al., 2006; Eyckmans and Luyten, 2006). hPDCs are able to differentiate to the osteogenic, chondrogenic and adipogenic lineage *in vitro* and generally have a high expression of CD105, CD90 and CD73, even after large-scale expansion (Lambrechts et al., 2016a). Furthermore, in comparison to stromal cells derived from the bone marrow or synovium, they have been shown to possess superior bone-forming potential when seeded on calcium phosphate carriers (Roberts et al., 2014).

hPDCs were isolated by overnight enzymatic digestion (0.2% type IV collagenase, InvitrogenTM) of a periost biopsy that was obtained from a patient as described earlier (Eyckmans et al., 2010). Subsequently, periosteal cells were collected by centrifugation, seeded in a 6-well plate and non-adherent cells were removed after 5 days by changing the medium. Procedures were approved by the ethical committee for Human Medical Research (KU Leuven) and informed consent was obtained from the patients. The isolated cells were cultured in T25 flasks for the first passage in standard culture medium consisting of high glucose GlutaMAX™ Dulbecco's modified Eagle's medium (Life Technologies, Merelbeke, Belgium) supplemented with 10% irradiated fetal bovine serum (FBS; HyClone, Cramlington, UK), 1% sodium pyruvate (Invitrogen™) and 1% antibiotic–antimycotic (100 units/ml penicillin, 100 mg/ml streptomycin, and 0.25 mg/ml amphotericin B; Invitrogen). For the standard flask-based conditions, cells were further cultured in T175 flasks with a seeding density of 5 700 cells/cm^2 and sub-cultured at ± 80% confluence up to passage 7 (approximately 12 total population doublings). For the process development data were a pool of cells was used, the cells from four different donors (average age 29 ± 11 years, Table I) were pooled together at passage 3 and further expanded in T175 flasks up to passage 7. At all passages, cells were harvested by trypsinisation for 10 min with TrypLE™ Express (Invitrogen).

Table 6-I: Overview of bioreactor runs, donor details, culture conditions and expansion process results

Donor	Pool of 4 Donors (process development)			Donor 1		Donor 2		Donor 3		Average Bioreactor	Average TF	Average TF_Q	Average TF_Q_FIB
Run	1	2	3	4	6	5	8	7	9				
Donor age-gender	20-M, 47-F, 23-M, 25-F			44-F		23-M		17-F					
Number of cells seeded	4E+07	4E+07	2E+07	2E+07	2E+07	2E+07	2E+07	2E+07	2E+07				
Culture time (days)	9.84	7.90	9.93	7.89	7.88	8.21	8.21	8.10	8.10				
Total harvest (cells)	3.36E+08	4.44E+08	3.72E+08	4.49E+08	4.03E+08	3.23E+08	3.54E+08	3.35E+08	3.27E+08	3.71E+08			
1st harvest (cells)	2.11E+08	4.40E+08	3.56E+08	4.44E+08	3.99E+08	3.16E+08	3.51E+08	3.31E+08	3.25E+08	3.53E+08			
Harvest efficiency	62.8%	99.1%	95.7%	99.1%	99.0%	97.9%	99.1%	98.9%	99.1%	94.5%			
Final cell density (cells/cm2)	16 000	21 143	17 714	21 357	19 205	15 381	16 864	15 952	15 586	17 689	16 886	11 999	21 587
Expansion factor	8.4	11.1	18.6	22.4	20.2	16.2	17.7	16.8	16.4	16.4	3.0	15.1	21.7
Pop. doublings	3.1	3.5	4.2	4.5	4.3	4.0	4.1	4.1	4.0	4.0	1.5	3.7	4.3
Pop. doubling time (days)	3.2	2.3	2.4	1.8	1.8	2.0	2.0	2.0	2.0	2.2	5.3	2.3	2.1

6.4.3. Bioreactor culture

Approximately 24 h hours before seeding the bioreactor, the cell expansion set was loaded in the environmentally controlled housing, and the lines and hollow fibres were automatically primed with phosphate-buffered saline (PBS). Directly after priming, the lumen of the hollow fibres was coated with 5 mg fibronectin (BD Biosciences) overnight. Before loading the cells in the bioreactor, the PBS and remaining fibronectin was washed out of the system with standard culture medium. The medium was then actively equilibrated with the bioreactor conditions by rapidly circulating it through the gas transfer module (37 °C, 20% 0_2, 5% CO_2 and 75% N_2). After an automated gas bubble removal step, 100 mL inoculum was transferred to a cell inlet bag, connected to the bioreactor and automatically loaded into the lumen of the hollow fibres that has 21 000 cm^2 of available culture surface. The cells were allowed to attach for 24 h without medium circulation in the lumen, but with oxygen and nutrient supply through circulation in the external hollow fibre circuit. The system was then programmed to start feeding the cells in the internal circuit with fresh culture medium at a flow rate of 0.1 ml/min. The progression of the bioreactor feed rate was determined at-line based on lactate concentrations (Lactate Pro, Arkray) of medium samples taken from the external bioreactor circuit at least twice a day, but more often towards the end of the culture. One sample per day was frozen and later analysed offline for lactate and glucose (YSI 2950 Biochemistry Analyzer). Increases in the feed rate were aimed to keep the lactate concentration in the bioreactor under a level of 8 mmol/L, based on the maximum concentration observed in flask-based experiments. As the lactate concentrations approached this limit, the feed rate was doubled through the interface of the bioreactor system.

As the donor-specific growth rate does not allow a fixed time point for harvesting of the bioreactor, the time of harvest was determined by a distinct shift from the exponential growth curve reflected by visual determination of a consecutive downward deviation of the last two lactate measurements from the straight line on a semilog-plot of the lactate production rate based on all previous measurements (n-2) (see Figure 6.6C for an example). At the time of harvest, the bioreactor was washed with PBS before adding 180 ml TrypLE Express (Invitrogen) at 37°C to the system and incubating for 15 minutes. After incubation with TrypLE Express, cells were harvested by rapidly adding media to the system and concurrently collecting the approximately 450 mL cell product in the pre-attached cell harvest bag (resulting on average in a cell suspension of 0.8 million cells/ml directly from the bioreactor). In general, the harvest process, including washing, 15 min TryplE incubation time and spinning down the neutralised harvest suspension took around 45 minutes and

resulted in a single cell suspension as determined by microscopic inspection. A second harvest process, performed with trypsin-EDTA (0.25%, Life Technologies), ensured that all cells were recovered from the bioreactor, thus allowing an estimation of the initial harvest efficiency. Cells recovered from the second harvest were not used for subsequent analysis.

6.4.4. Control conditions

Three different flask-based cultures were taken along during the bioreactor culture in order to elucidate possible differences between the Quantum system bioreactor expansion and the current gold standard, or flask-based, expansion of mesenchymal stem cells. In this way, primary causes of any observed differences in cell quality could be more easily identified, thus providing opportunity to optimize future bioreactor processes in an informed manner. Accordingly, in addition to the bioreactor condition, the experimental design incorporated the following three conditions: (1) standard tissue culture flasks according to pre-culture protocols described above in 2.2 (*CF*), (2) tissue culture flask condition at the same initial seeding density as in the bioreactor (*CF_Q*) to account for the lower seeding density in the bioreactor, and (3) a tissue culture flask condition at the same initial seeding density as in the bioreactor with an additional fibronectin coating (1 µg/cm^2) as present on the surface of the hollow fibres of the bioreactor (*CF_Q_FIB*). This last condition was omitted for the runs with the individual donors. For the lower seeding density conditions, an anticipated initial loss of 30% of the loaded cells in the bioreactor dead volume (according to the manufacturer's information) was taken into account. A comparison of the cell characterisation from these culture conditions allows the assessment of the individual effect of seeding density (CF vs CF_Q), fibronectin coating (CF_Q vs CF_Q_FIB) and the effect of dynamic feed rate (CF_Q_FIB vs bioreactor) on the cell phenotype and *in vivo* potency.

6.4.5. Growth kinetics calculations

Growth kinetics for the bioreactor culture and control flasks were calculated as follows:

$$Expansion\ factor = EF = \frac{number\ of\ cells\ harvested}{number\ of\ cells\ seeded}$$

$$Number\ of\ population\ doublings\ per\ passage\ = PD = log_2(EF)$$

$$Population\ doubling\ time = PDT = \frac{culture\ time}{PD}$$

Note that the population doubling time is calculated based on the initial and final cell number and therefore includes lag phase and possible stationary phase of growth, because only initial and final cell numbers could be quantified in the bioreactor.

Metabolite analysis

Metabolic production and consumption rates (q_{MET}) were calculated between every two concentration measurements from the external lumen of the hollow fibre bioreactor. The concentration for these small molecule metabolites were equal between the outer side and lumen of the hollow fibre (validated by sampling both sides) as the hollow fibres allow diffusion of small molecules through the fibre. The volume of the lumen and the outer side was provided by the manufacturer (189.1 mL and 305.4 mL respectively). For the q_{MET} calculation, the outgoing flow rate was assumed to be equal to the ingoing flow rate as specified by the user, minus an evaporation term as specified by the manufacturer. Metabolite ratios q_{MET1}/q_{MET2} were calculated between every measured sample. Accumulated rates were calculated by aggregating all quantities (mM) produced or consumed between samples. Oxygen consumption rates were calculated based on the slope of the measured oxygen concentration over the whole culture, normalised to the initial and final cell number.

6.4.6. Post-harvest cell characterisation

Post-harvest growth kinetics

Harvested cells were re-plated at a density of 5 700 cells/cm^2 in a 12-well plate. The growth kinetics were monitored daily by a PrestoBlue® metabolic assay (Life Technologies, Merelbeke, Belgium) of 10% w/w PrestoBlue reagent in culture medium. After 1 h of incubation the metabolic activity of the cells was quantified by fluorescence measurements (Bio-Tek Synergy™ HT, Bad Friedrichshall, Germany) with an excitation wavelength of 540 nm and an emission wavelength of 590 nm on 100 ml supernatant in a 96-well plate. A higher metabolic activity is indicated by higher fluorescent values.

3-lineage differentiation potential

The 3-lineage differentiation potential of the cultured hPDCs was assessed as described earlier (Lambrechts et al., 2016a). All experimental conditions were

performed in triplicate. In short, the chondrogenic differentiation cells were cultured for 7 days as micromasses in a 24-well plate with a chondrogenic medium consisting of DMEM/F12 (Life Technologies), 2% FBS, 1% antibiotic–antimycotic, 1% ITS pre-mic (Corning), 100nM dexamethasone (Sigma), 10µM Y27632 (Axon Medchem), 50µg/ml ascorbic acid, 40µg/ml proline and 10ng/ml recombinant human transforming growth factor-β1 (Preprotech). After 7 days of chondrogenic induction, micromasses were fixed in methanol, stained with a 0.1% Alcian Blue solution in 0.1 M HCL at pH 1.2. After washing with Milli-Q, the micromasses were destained in 6 M guanidine (Sigma) and quantified by measuring the absorbance of 100 µL samples at 620 nm.

The osteogenic differentiation was induced by culturing the cells for 21 days in standard culture medium supplemented with 100 mM dexamethasone, 50 µg/ml ascorbic acid and 10 mM β-glycerolphosphate. Afterwards, cells were fixed in ice-cold methanol and stained with a 2% Alizarin Red S solution in Baxter water. Non-specific staining was washed away with distilled water. Quantification was performed by dissolving the staining with 10% cetylpyridinium chloride in Baxter water until complete dissolution. Absorbance was measured at 570 nm in 100 uL samples.

Adipogenic differentiation was assessed by culturing the harvested cells in 24-well plates for 14 days in adipogenic medium consisting of αMEM (Life Technologies) supplemented with 10% FBS, 1% antibiotic–antimycotic, 1 µM dexamethasone, 10 µg/ml human insulin (Sigma), 100 µM indomethacin (Sigma) and 25 µM 3-isobutyl-1-methylxanthine (Sigma). At day 14, cells were fixed in 10% formaldehyde, rinsed shortly with 60% isopropanol and stained with Oil Red O.

MSC phenotyping

Harvested cells were assessed based on a combined positivity for typical MSC cluster of differentiation (CD) markers and lack of expression for haematopoietic markers. The used antibody panel was CD90-FITC (clone DG3), CD73-APC (clone AD2), CD105-PE (clone 43A4E1), CD14 (clone TUK4)/CD20 (clone LT20.B4), CD34 (clone AC136), CD45 (clone 5BI)-PerCP (all from Miltenyi Biotec). Dead cells were excluded based on a viability dye (Zombie Aqua™, BioLegend®) excited by the fluorescent laser (BD FACSCanto™). Antibody titration was performed according to the protocol of Hulspas (2010). Automatic single-colour compensation was performed by the acquisition software (BD FACSDiva™) using compensation beads (UltraComp eBeads affymetrix eBiosceince), except for the viability

dye as it works based on internalisation of the dye in the cell. The gating was based on FMO (Fluorescence Minus One) controls (Herzenberg et al., 2006), except for the viability dye where the gating was based on the signal of a 50-50 mixture of healthy cells and heat/cold-killed cells.

In vivo ectopic mouse model

After every bioreactor run, clinical grade orthopaedic 3D matrices composed of calcium phosphate particles in an open collagen network (NuOss^{TM}, ACE Surgical Supply Co.,Inc.) with a volume of 35 mm^3 were seeded each with 1 million cells per scaffold in a total volume of 35 µL (generally 3 to 4 scaffolds per culture condition per experimental run). To allow cell attachment, the scaffolds were incubated overnight (37° C, 5% CO_2, RH 95%) before randomised ectopic implantation on the back of nude mice (NMRI-nu/nu). After 8 weeks of *in vivo* implantation, the scaffolds were retrieved, fixed overnight in 4% paraformaldehyde and preserved in PBS before X-ray computed tomography and histology. All animal experiments and procedures were approved by the Animal Ethics Committee (KU Leuven) and the animals were housed in accordance with the guidelines of the Animal Research Center of KU Leuven.

Quantification of bone formation

The volume of newly formed bone in the explanted NuOss scaffolds was assessed by nanofocus X-ray computed tomography (nano-CT) on a Phoenix NanoTom® S (GE Measurement and Control) system equipped with a diamond-tungsten target and 0.5 mm aluminium filter. The scan settings applied were 60 kV X-ray voltage, 210 mA current, 500 ms exposure time, a frame averaging of 1 and image skip of 0. Images were reconstructed with Phoenix Datos|x CT software (GE Measurement and Control). The resulting reconstructed images had a 3 µm voxel size. CTAn (Bruker Micro-CT) was used for image processing and quantification of the bone volume based on a 2-level automatic Otsu segmentation algorithm. Resulting segmentation was checked visually, and in the rare case of mismatch, manual segmentation levels were determined based on the greyscale histogram of the whole sample. 3D visualisation of reconstructed CT images was done in CTvox (Bruker micro-CT). After nano-CT analysis, the samples were decalcified in a 0.5 M EDTA (ethylenediaminetetraacetic acid) solution for two weeks, dehydrated, embedded in paraffin and sectioned (6 µm thick at 8° angle). Hematoxylin and eosin staining was performed using a standard protocol and a qualitative assessment was done, both on bright field and fluorescent images (as in (Martin and Mastrogiacomo, 2002)), based on features of mature bone

formation (presence of osteocytes and osteoblast lining, blood vessel ingrowth, and onset of bone marrow compartments).

6.4.7. Statistical analysis

Data analysis was performed using MATLAB® 2013a (The MathWorks®). Independent groups were compared by unpaired Student's t-tests, and considered statistically significant when $P < 0.05$. All error bars in figures show standard deviation of the mean.

6.5. Results

6.5.1. Biological evaluation of Quantum system bioreactor cultured cells

Cell yield and growth rate

On average the total cell yield from the bioreactor was 371 ± 46 million hPDCs, reflecting an average cell density at harvest of 17 700 ± 2 200 cells/cm^2 (see Table 6-I for details per run). The average harvesting efficiency in the bioreactor was 94.5%. The average cell density at harvest of the standard control flasks (CF) was comparable at 16 900 ± 4 900 cells/cm^2. However, in the control flasks at the seeding density of the bioreactor (CF_Q), it was noted that efficient cell growth was not always sustained for certain donors, resulting in a significantly lower average cell density at harvest of only 12 000 ± 5 600 cells/cm^2. The control flasks at the seeding density of the bioreactor but with an additional fibronectin coating (CF_Q_FIB) show an average harvesting density of 18 800 ± 3 500 cells/cm^2. Average population doubling times (Table 6-I) were not significantly different for all conditions with the same seeding density.

Post-harvest growth kinetics

Cells from all conditions showed excellent viability at time of harvest (> 95% determined by trypan blue exclusion), and 24 h after re-plating the harvested cells no apparent differences in cell morphology could be perceived. Growth kinetics of the harvested cells were monitored over 7 days in which all conditions showed a similar sigmoidal growth curve as expected (data not shown).

3-lineage *in vitro* differentiation potential

For all process development runs, all conditions showed a clear maintenance of their *in vitro* differentiation potential towards the osteogenic, chondrogenic and adipogenic lineage (Figure 6.3 A, B, C). Both the osteogenic and chondrogenic assays, showed no significant difference based on Alizarin Red and Alcian Blue staining respectively. In a qualitative assessment of the adipogenic differentiation, no apparent differences could be observed between the bioreactor condition, the standard control flask (CF) and the control flask at low seeding density (CF_Q). However, cells cultured on the fibronectin-coated flasks (CF_Q_FIB) produced notably smaller and less frequent lipid deposits.

Immunophenotyping by flow cytometry

Figure 6.3 D represents the CD-marker expression as generally cited according to the minimal criteria for defining multipotent MSCs (Dominici et al., 2006). All samples generally showed a high simultaneous expression of CD105, CD73 and CD90, while at the same time the combined expression for CD45, CD20, CD14 and CD34 is very low at this passage. When comparing the marker expression separately, the average CD105 expression is significantly lower ($p = 0.03$) for the bioreactor condition in a pair-wise comparison to the CF_Q condition, while for the other markers no difference could be perceived. No apparent differences could be perceived in the marker expression between the different donors.

In vivo bone forming potency

Nano-CT-based quantification of the newly formed bone was carried out and normalised to the available scaffold volume, i.e. not taking into account the space occupied by the remaining calcium phosphate grains within the scaffold. Figure 6.4 A-C indicates the result of the 3D segmentation of nano-CT images of newly formed bone from the remaining calcium phosphate grains and shows the distribution of the newly formed bone throughout the whole scaffold. In the process development runs, on average the nano-CT quantification resulted in a relative bone volume of 10.3%, 11.0%, 10.2% and 9.4% for the bioreactor, CF, CF_Q, and CF_Q_FIB condition respectively (Figure 6.5 A). For the donor-specific data (Figure 6.5 B-D), intra-donor results do not differ significantly either between the different culture conditions, or between the two different batches. However, there is a significant ($p = 0.0006$) and consistent inter-donor variability regarding bone-forming potential, where donor 1 produces on average 8.8% ± 2.4% of newly

formed bone, donor 2 5.8% ± 1.7%, and donor 3 no bone at all for all conditions in both batches.

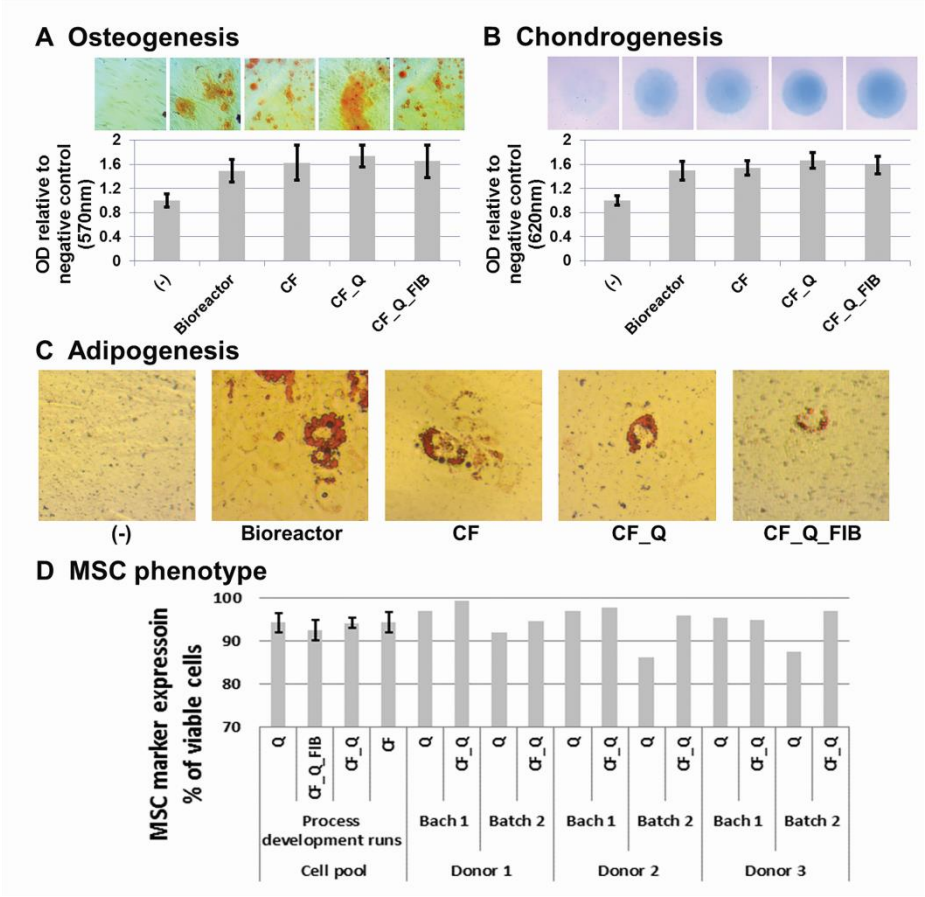

Figure 6.3: In vitro post- harvest cell characterisation:
(A) Alizarin red staining and quantification after 3 weeks osteogenic differentiation. (B) Alcian Blue staining and quantification after 1 week chondrogenic differentiation in micro-mass culture. (C) Oil Red O staining after 2 weeks adipogenic differentiation. Quantifications of staining was normalised to the negative control. (D) Percentage of viable cells with simultaneous expression of CD73, CD90, CD105 and combined lack of expression for CD45, CD20, CD14 and CD34 after immunophenotyping by flow cytometry. The data for the different culture conditions during the three process development runs is averaged. CF = Control Flask, CF_Q = Control Flask at same seeding density as the bioreactor, CF_Q_FIB= Control Flask at same seeding density as the bioreactor with fibronectin coating.

The quality of the newly formed bone was assessed based on hematoxylin and eosin (H&E) staining on paraffin slides of the decalcified explants. As the nano-CT images suggested, newly formed bone tissue was found in similar quantities as reported earlier (Roberts et al., 2011). The imaged sections (Figure 6.4D) suggest that characteristic features of mature bone (osteocytes, hematopoietic compartments and osteoblast lining) were generally present.

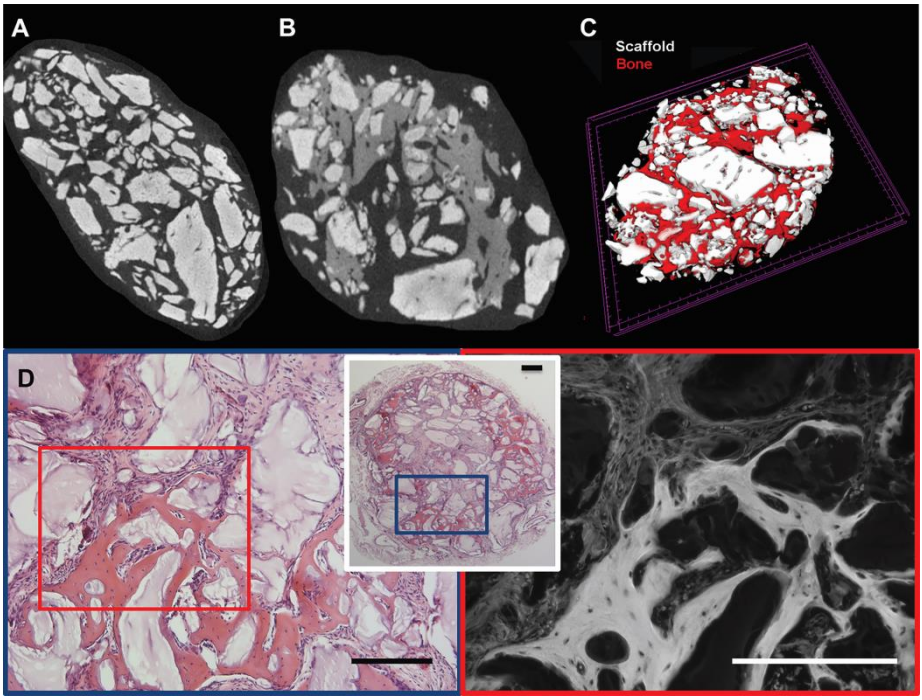

Figure 6.4: Qualitative assessment of bone formation
(A) Reconstructed nano-CT image of a negative control (scaffold implanted without cells). (B) Reconstructed nano-CT image of an implanted scaffold with cells from the bioreactor. (C) 3D visualisation of 200 µm thick stack of reconstructed nano-CT images where the newly formed bone volumes are shown in red. (D) H&E on decalcified explants after 8 weeks implantation with cells from the bioreactor condition. Scale bars are 250 µm. Image on the left is H&E staining under bright field. Image on the right show H&E staining under red fluorescent light where bone tissue becomes bright grey under fluorescent light as described in Martin et al. (2002).

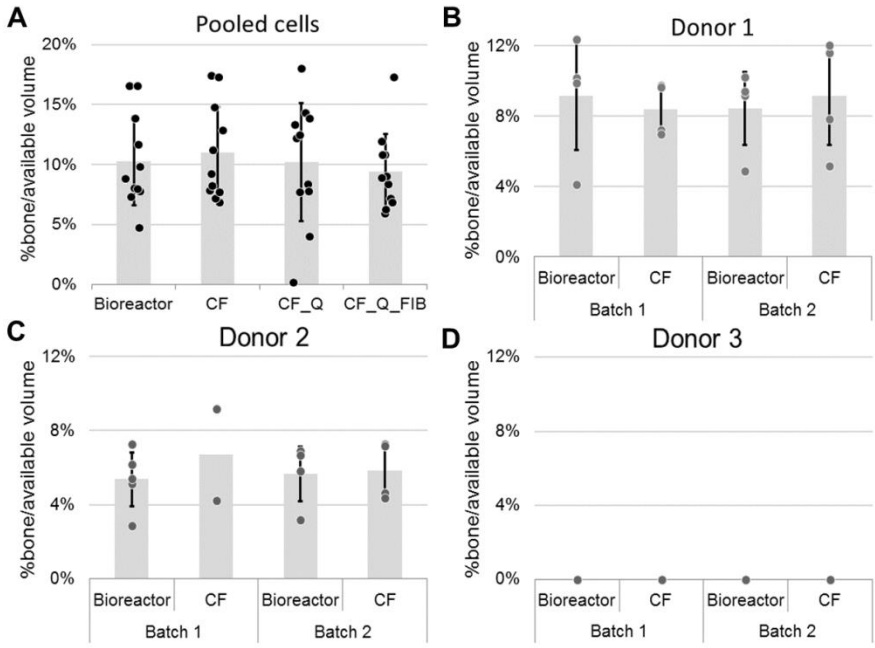

Figure 6.5: Quantification of newly formed bone volume per available scaffold volume as determined by nano-CT imaging.
Bars represent average result with standard deviations. (A) Comparison of average process development data per culture condition. (B-D) Comparison of the results of donor-specific runs per batch and per culture condition. CF = Control Flask, CF_Q = Control Flask at same seeding density as the bioreactor, CF_Q_FIB= Control Flask at same seeding density as the bioreactor with fibronectin coating.

6.5.2. Evaluation of bioreactor process and influence of donor-to-donor variability

The cell expansion process was monitored by sampling media from the extracapillary bioreactor circuit. In the process development runs and the first batch of the donor-specific runs, the medium feed rate was doubled every time that the measured concentration approached 8 mmol/L lactate. For the second batch of the donor-specific experiments, the medium feed rate as determined for the first batch was reproduced in the second batch. This means that the feed rate was equal for the same donor, but that donors with a higher lactate production received a more aggressive feed rate strategy, and therefore had a higher total medium volume spent at the end of the run (Table 6-II). For example, donor 2 in Figure 6.6A and 5B required around 6.2 L medium, compared to a less metabolically active donor such as donor 3 that required only 4.8 L in order to keep the lactate concentration below 8 mmol/L.

Additionally the at-line lactate measurements were used to provide an objective estimation of the optimal moment of harvest for the donor-specific runs (Figure 6.6C). A distinct deviation of the lactate production rate from the exponential lactate production curve was used as a signal for the determination of the time of harvest. For all donors, this moment was detected at comparable time points relative to the start of the culture (on average 8.1 ± 0.14 days), however it can be seen from the decreasing lactate production rate that the initial process development run was unintentionally grown over-confluent (Figure 6.6C), which is also suggested by the lower harvest efficiency and higher perceived population doubling time for this run (Table 6-I).

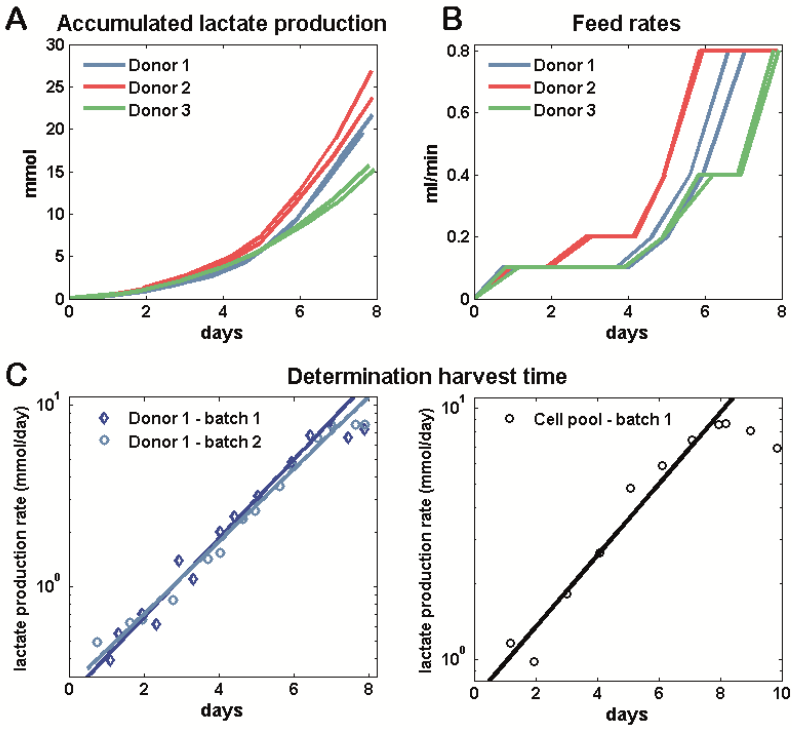

Figure 6.6: Lactate production, feed rates and harvest timing.
(A) Accumulated lactate production per donor. (B) Resulting medium feed rates in bioreactor. (C) Semilog-plot of the lactate production rate based on all previous measurements except for the last 2, to determine a shift from the exponential growth in order to have a donor independent time for harvesting the bioreactor. (Left) Data for donor 1. (Right) Example of the first process development run that was grown over-confluent.

The bioreactor circuit was slightly modified in order to be able to measure the dissolved oxygen concentration (dO_2) and pH by welding in an ethylene oxide sterilized sensor connection that was developed in-house into the waste line, directly after the hollow fibre. As the medium was continuously fed in the bioreactor, the same volume was discarded through the waste line where the dO_2 and pH could be measured with a delay proportional to the feed rate. As for the metabolite measurements, it can be seen in Figure 6.7, that the dO_2 and pH measurements followed very similar trends, for both inter- and intra-donor conditions. The pH followed the same slightly downward trend for all donors as expected for CO_2-buffered culture medium at increasing cell concentrations, but there was a rather large difference between the average values across the batches for donors 2 and 3. This difference was due to the fact that an *in situ* 1-point recalibration of the pH sensor was not possible in this setup and the sensor had to be calibrated before sterilisation and implementation in the system.

Table 6-II summarises the metabolic profile of the donor cells, as measured during the different bioreactor runs. While the q_{lac}/q_{gluc} ratios were relatively similar indicating a preference for aerobic glycolysis (ratio close to 2, and at the same time the dissolved oxygen concentration does not drop below 10%) as was shown earlier for proliferating hPDCs (Lambrechts et al., 2016a), it is clear that donor 1 and 2 were metabolically more active compared to donor 3. Donor 3 had a higher q_{lac}/q_{gluc} ratio, suggesting that the energy production from glucose was less efficient compared to the other donors, and potentially indicates a different utilisation of carbon sources.

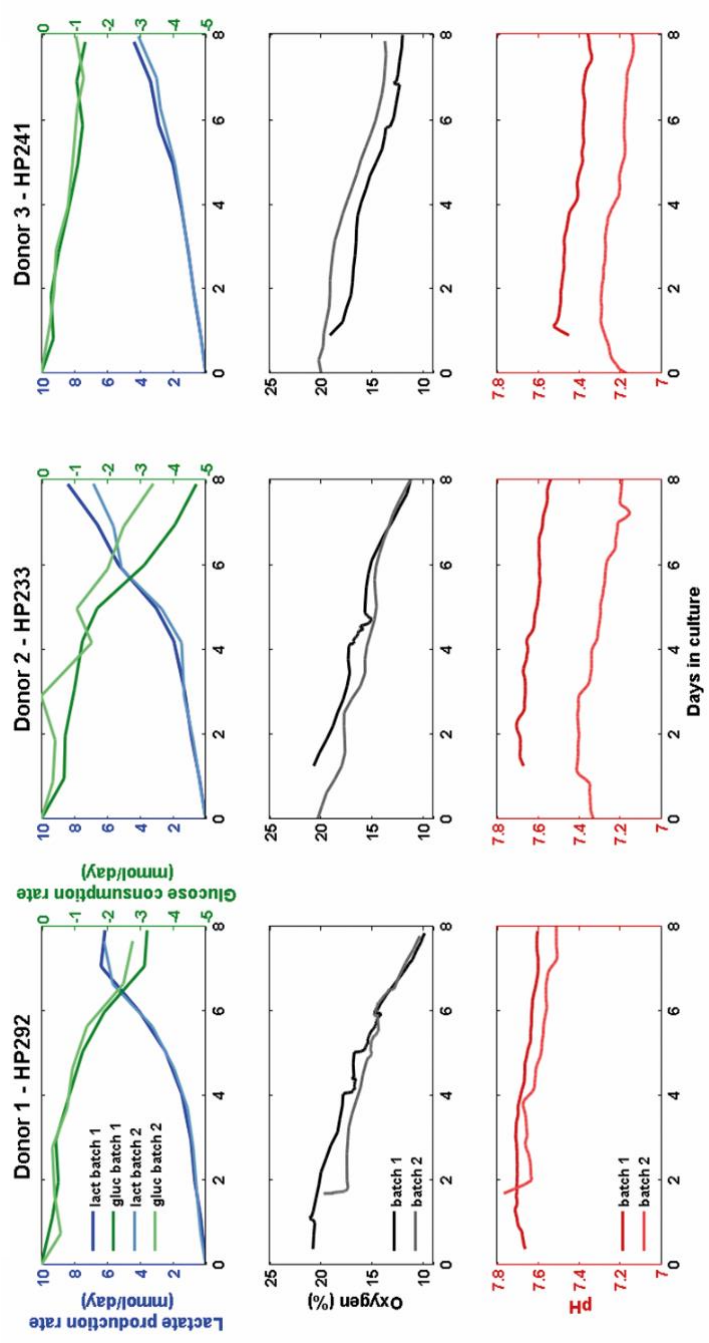

Figure 6.7: Lactate production rate and glucose consumption rate over time in the bioreactor for the two batches of the three different donors. (Middle) Dissolved oxygen concentration as measured in the bioreactor. (Bottom) pH as measured in the bioreactor.

Table 6-II: Overview metabolic data and medium consumption for different donors

	Donor 1		Donor 2		Donor 3	
Batch	1	2	1	2	1	2
Maximum lactate concentration in system (mmol/L)	8.8	7.4	9.5	7.8	8	7.8
Accumulated lactate production (mmol)	21.6	19.6	26.8	23.7	15.7	15.2
Accumulated glucose consumption (mmol)	11.4	9.5	16.8	10.4	6.7	6.2
Average daily ratio q_{LAC}/q_{GLUC}	1.7 ± 0.4	1.8 ± 0.7	1.4 ± 0.4	1.9 ± 0.6	2.2 ± 0.8	2.3 ± 0.7
Average cell specific 0_2 consumption rate (mol s^{-1} $cell^{-1}$)	1.03E-15	8.76E-16	1.12E-15	8.18E-16	8.59E-16	9.08E-16
Total medium volume used (mL)	5 127	5 124	6 337	6 114	4 869	4 772
mL medium used/100K cells	1.14	1.27	1.96	1.73	1.45	1.46

6.1. Discussion

In the first part, this study pursued a comparative and quantitative evaluation of the post-harvest quality of hPDCs expanded in the Quantum system hollow fibre bioreactor compared to three different tissue culture flask conditions (CF, CF_Q, CF_Q_FIB). This was attempted by using a pool of cells from 4 different donors with known behaviour in 2D cultures. Secondly, it was attempted to integrate lactate, O_2 and pH readouts that would allow to non-invasively monitor process conditions during cell expansion, and on which objective donor-specific decisions for feed rates and time of harvest could be based. Lastly, cells derived from three different donors were cultured in the monitored bioreactor in order to assess process-inherent and donor-to-donor variability.

6.1.1. Cell expansion

Regarding cell yield, the average cell density at harvest per available culture surface was comparable between the standard TF and bioreactor condition, $1.69 \pm 0.5 \times 10^4$ and $1.77 \pm 0.2 \times 10^4$ cells/cm^2 respectively. Interestingly, the variability on the outcome was lower for the bioreactor condition, suggesting a more controlled expansion process. The final cell density is very similar to the density obtained for hPDCs in another large-scale bioreactor (Pall® Xpansion®) in a recent study (Lambrechts et al., 2016a). For the CF_Q condition, in certain cases using the same low seeding density as in the bioreactor failed to initiate exponential cell growth, resulting in a significantly lower average final cell density at harvest ($1.2 \pm 0.6 \times 10^4$ cells/cm^2). The CF_Q_FIB condition (evaluated only during the process development runs) on the other hand resulted on average in a final cell density that was not significantly different from the corresponding bioreactor runs ($2.16 \pm 0.4 \times 10^4$ cells/cm^2). It is therefore hypothesised that the fibronectin coating of the bioreactor is able to promote more efficient cell growth potentially through more efficient cell attachment and cell spreading on fibronectin-coated surfaces as described earlier (Ogura et al., 2004).

Clearly, as the Quantum system bioreactor culture is able to start from a low initial seeding density, the expansion efficiency (reflected in the expansion factor calculation, Table 6-I) is significantly higher in the automated process, 16.4 on average, compared to 3.0 for the standard flask-based culture. It is hypothesised that the efficient culture from low seeding densities are facilitated in the bioreactor by improved cell-to-cell communication through the more 3 dimensionally-structured hollow fibres resulting in more cells per volume compared to the flat surface of a flask. Additionally, the load of the bioreactor-based culture on the down-stream processing is low, as the hollow fibre design allows concentrated cell suspension at harvest (in this work around 370 million cells in ± 450 ml neutralised harvest suspension that can be further processed in a benchtop centrifuge, compared to multiple litres for example in stacked-plate bioreactors (Lambrechts et al., 2016a)).

hPDC population doubling times in the bioreactor were 2.0 days (leaving out the first run that was grown over-confluent based on the harvest efficiency and lactate production rates as shown in Figure 6.6C) and were generally faster than the ones observed in the TF_Q condition (2.3 days), however the difference is not significant. Jones et al. (Peters et al., 2013) and Rojewski et al. (Rojewski et al., 2013) experienced a slower cell growth for bone marrow-derived hMSCs in the Quantum system bioreactor compared the standard culture, whereas Hanley et al. (Hanley et al., 2014) and Lechanteur et al.

(Lechanteur et al., 2014) reported faster cell expansion in the Quantum system bioreactor for bone marrow-derived hMSCs. The bioreactor process reached in all cases the minimum process target of 300 million cells required for the hypothetical tibia defect of 3 cm as introduced above, and outperformed the standard culture flask conditions regarding cell yield and expansion efficiency. We believe that there is still potential to drive the bioreactor yield even higher after further process optimisation, e.g. by being able to better monitor the confluence level in the bioreactor, or by further optimising the seeding homogeneity within the hollow fibres.

6.1.2. Cell quality – *In vitro* assays

The tri-lineage differentiation potential did not show significant differences in the osteogenic and chondrogenic differentiation. Qualitatively, the adipogenic differentiation of the cells harvested from CF_Q_FIB condition appeared to be reduced, which might be caused by the fibronectin as previously reported in literature (Martino et al., 2009; Ogura et al., 2004; Singh and Schwarzbauer, 2012; Wang et al., 2010), however this effect was not apparent in the bioreactor where a similar coating was used. It is plausible that the culture plastic has a different affinity for the coating compared to the hollow fibres, however it is difficult to assess the resulting fibronectin concentration after coating.

Immunophenotyping by flow cytometry showed in general a high simultaneous expression of CD105, CD73 and CD90, while there was almost no expression of CD45, CD20, CD14 and CD34 for all conditions. The bioreactor condition showed a tendency to have a slightly lower CD105 expression (on average 94 ± 3,4% compared to 97 ± 1.5% for the CF_Q condition). A loss of CD105 is regularly seen in bioreactor literature (not only in the specific case of the Quantum bioreactor (Hanley et al., 2014; Peters et al., 2013), but also in spinner flask culture (Jing et al., 2013; Dos Santos et al., 2014)). However, no in-depth mechanisms of action are known. Dos Santos et al. (2014) showed that after re-plating the cells harvested from a spinner flask again in static culture conditions, the CD105 expression recovered to normal levels, and therefore hypothesised that this reversible loss was related to shear stress conditions.

6.1.3. Cell quality – *In vivo* assay

The *in vivo* bone-forming potency of the cells was assessed based on the ectopic implantation of harvested cells seeded on calcium-phosphate carriers in nude mice, which was shown previously to be a valid model for bone tissue

engineering (Chai et al., 2012b; Eyckmans et al., 2010; Roberts et al., 2011). No significant differences in the amount of bone formation and tissue development were perceived between cells from the bioreactor condition and the three control flask conditions during the process development runs, both quantitatively based on nano-CT imaging (Figure 6.6A), and qualitatively based on histology (Figure 6.7). For example, the newly formed bone per available scaffold volume for the bioreactor and the standard tissue culture flask condition was 10.3 ± 3.7% and 11.0 ± 3.8% respectively. More striking was the difference in bone-forming potential between the different donors (Figure 6.6B,C,D). While the intra-donor variability was low, i.e. the average percentage of newly formed bone between two different batches and between two different culture conditions (bioreactor and TF culture) within one donor was similar, the inter-donor variability on the other hand was large (8.8 ± 2.4%, 5.8 ± 1.7% and 0% for donors 1, 2 and 3 respectively). Donor 1 produced on average significantly more bone than donor 2 for both batches and both conditions, while donor 3 produced no bone at all in all conditions. It is clear that this lack of bone-forming potential is not due to the difference in culture conditions specifically, since both the standard culture flask and the bioreactor condition show the same behaviour. Although it is difficult to predict how these cells would have performed in an orthotopic *in vivo* model where more appropriate cell stimuli were provided, the example of this specific donor is highlighting risks entailed in autologous tissue engineering strategies. Thorough cell characterisation is required, ideally with a predictive power regarding the *in vivo* potency, before large-scale expansion is pursued. This will help prevent large sunk costs and unnecessary surgical interventions for the patient.

6.1.4. Process comparability

Apart from the practical advantage of a bioreactor-based cell expansion process, e.g. the reduction of open processes that requires expensive GMP facility resources, reduced work load, small footprint, etc., one of the main drivers for increased automation is to enhance the robustness and reproducibility of the culture process, directly leading to a more uniform cell quality and subsequent less variable *in vitro* and *in vivo* potency (Santoro et al., 2010; Trainor et al., 2014). In this study it was shown that the bioreactor condition is able to reduce the overall process variability by a factor of 2.5 regarding cell yields (normalised per available surface) compared to the flask-based condition, demonstrating therefore a much higher potential capability to produce cell batches within specification limits. Similar findings regarding automated cell expansion processes were reported earlier (Archibald et al., 2015; Liu et al., 2010; Paull et al., 2015; Terstegge et al., 2007).

Controlled cell expansion methods are essential for the development of cost-effective and robust production processes for commercial cell-based products (Archibald et al., 2015; Liu et al., 2010). Especially in the case of autologous therapies, where a decentralised multi-centre production model is almost inevitable, process consistency and reproducibility is a critical issue in order to assure uniformity of the product (Foley and Whitaker, 2012; Hourd et al., 2014). For decentralized production of autologous cells, where cells from different donors might behave differently during culture (Heathman et al., 2015b; Siddappa et al., 2007), additional process monitoring and control is required that is able to assess the level of similarity between two different runs, and ultimately facilitate the demonstration of comparability between different production sites and even between different donors.

In this work, the implemented oxygen and pH measurements showed that culture conditions could be replicated over multiple bioreactor runs and that a greater process understanding can be achieved in order to better control the critical process parameters (EMA, 2014; FDA, 2011). Additionally, process read-outs were used to make consistent decisions, for example the lactate-based feed rate strategy and harvest timing for different donors. These ultimately increased production efficiency by reducing medium consumption and optimising final cell density. Although requiring a small adaptation to the current bioreactor system, on-line monitoring such as done here for O_2 and pH is preferred from a manufacturing point of view, as up-to-date information can be obtained from the system at any time without the manual handlings that are currently still required for lactate and glucose sampling. In future studies continuous process verification could be used as a basis for active donor-specific process control. For example, the perceived ±10% drop in dissolved oxygen concentration (Figure 6.7) could be counteracted with a feedback control loop that would increase the medium circulation rate in the external space between the hollow fibres in order to increase the homogeneity in terms of oxygen availability over the length of the hollow fibres, without increasing the shear stress on the cells inside the hollow fibre lumen. Additionallyrecently explored oxygen-based cell number quantification techniques could also be applied (Lambrechts et al., 2014).

6.2. Conclusion

In conclusion, these data show that hPDCs can be reproducibly expanded in the Quantum system bioreactor on a clinical scale. At the same time the main cell quality attributes, assessed with both *in vitro* assays based on the ISCT minimal criteria and an *in vivo* bone-forming potency assay, remained very consistent between the bioreactor and standard flask-based culture.

Additionally, it was shown that the bioreactor culture resulted in a more robust outcome regarding cell yield (showing a reduction of the overall process variability on cell yield by a factor of 2.5 compared to the standard flask-based culture) and showed good process reproducibility based on process analytics such as O_2, pH, lactate etc. Although all donors reached the minimally required cell yield (350 million cells) and showed limited intra-donor variability for the different batches and culture conditions, large inter-donor differences were observed regarding for example nutrient requirements and *in vivo* potential (8.8 ± 2.4%, 5.8 ± 1.7% and 0% newly formed bone per available scaffold volume for donors 1, 2 and 3 respectively) that would have significant implications for clinical translation.

6.3. Acknowledgements

The authors would like to thank Kathleen Bosmans for her assistance with the in vivo implantations, Greet Kerckhofs for her expertise on the nano-CT image processing, Lennert Ceysens for his help with the flow cytometry samples and Johan Vanhulst for the production of the sensor connection. Part of this work was supported by the Bone4Kids Fund and an advanced European research council grant ERC Rejoind (No. 294191). TL is supported by the KU Leuven Concerted Research Actions (GOA/13/016). IP is funded by Fonds Wetenschappelijk Onderzoek (FWO fellowship, project No 12O7916N). The X-ray computed tomography images were generated at the facilities of the Department of Materials Engineering of the KU Leuven, financed by the Hercules Foundation (project AKUL 09/001).

6.4. Disclosure of interest

Brent Rice is an employee of Terumo BCT.

Chapter 7. Model-based cell number quantification using online single-oxygen sensor data for tissue engineering perfusion bioreactors

Adapted from: T. Lambrechts, I. Papantoniou, M. Sonnaert, J. Schrooten, J.-M. Aerts. Biotechnology and Bioengineering. (2014) 111:1982–92.

7.1. Positioning within the context of the PhD project

In Objective 3 (Chapter 2) it was hypothesised that by making use of routine process data, more information on critical process parameters and critical quality attributes of the cells could be derived, on which in turn more informed process control decisions can be based. While imaging technology was used in Chapter 4 and 5 to assess the number of cells inside the bioreactor, more 3D bioreactor configurations such as the Quantum hollow fibre bioreactor from Chapter 6 cannot be non-invasively imaged during the culture. This chapter therefore focusses on the use of data from a single oxygen sensor in perfusion bioreactors in order to non-destructively monitor the amount of cells inside the bioreactor. The measured response to changes in the perfusion flow rate are translated by means of a data-based transfer function model to an estimate on the number of cells.

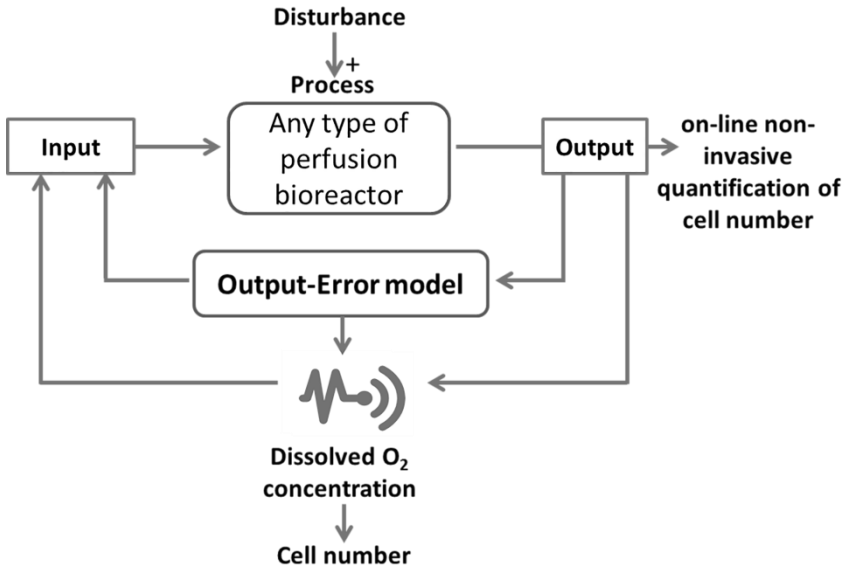

Figure 7.1: Position of Chapter 7 in the general control scheme and the larger context of this work.

7.2. Abstract

On-line and non-invasive quantification of critical tissue engineering (TE) construct quality attributes in TE bioreactors is indispensable for the cost-effective up-scaling and automation of cellular construct manufacturing. However, appropriate monitoring techniques for cellular constructs in bioreactors are still lacking. This study presents a generic and robust approach to determine cell number and metabolic activity of cell-based TE constructs in perfusion bioreactors based on single oxygen sensor data in dynamic perfusion conditions. A data-based mechanistic modelling technique was used that is able to correlate the number of cells within the scaffold (R^2=0.80) and the metabolic activity of the cells (R^2=0.82) to the dynamics of the oxygen response to step changes in the perfusion rate. This generic non-destructive measurement technique is effective for a large range of cells, from as low as $1.0x10^5$ cells to potentially multiple millions of cells, and can open-up new possibilities for effective bioprocess monitoring.

7.3. Introduction

The translation of promising lab-scale cell based regenerative medicine and tissue engineering (TE) therapies to large-scale commercial production is hampered by a lack of robust and cost-effective manufacturing processes that can deliver effective, regulatory-compliant and safe cellular products (Brindley et al., 2012; Mason and Manzotti, 2010). Bioreactors for 3-dimensional (3D) TE have demonstrated their potential as a cost-effective and highly automated production platform showing great promise for both the up and scale-out strategies (Martin et al., 2009; Dos Santos et al., 2013). Due to a combination of increased surface area per volume and improved nutrient transport while closer mimicking the natural niche of the cells, 3D bioreactors contribute to a higher productivity compared to traditional 2D cell culture (Martin et al., 2004; Tandon et al., 2013; Wendt et al., 2005). Additionally, in light of recent stringent quality control guidelines by the European Medicines Agency (CAT, 2010) and the US Food and Drug Administration (DeFrancesco, 2012), bioreactors will provide an indispensable means for process control as they allow a more precise physicochemical control of the cellular microenvironment, directly contributing to the enhancement of construct quality and reproducibility prerequisites for consistent clinical outcomes (Kirouac and Zandstra, 2008; Martin et al., 2009; Rodrigues et al., 2011).

Despite these advantages, the use of bioreactor systems in a clinical setting remains minimal (Salter et al., 2012). This is attributed to the lack of robust

bioprocess control in the closed system 'black box' bioreactor (Wendt et al., 2009). Multiple bioprocess monitoring techniques exist, primarily originating in the biopharmaceutical bioreactor industry, that can quantitatively measure physicochemical process parameters, such as temperature, pH, dissolved O_2, glucose concentration and metabolic activity (Bluma et al., 2011; Rolfe, 2006; Starly and Choubey, 2008; Ward et al., 2013; Zhou et al., 2013). However, a direct transfer of the biopharmaceutical monitoring and control strategies to TE bioreactors is not straightforward. Firstly, in the biopharmaceutical field the product is usually an antibody or protein expressed by cultured cells that are destructively harvested at the end of the culture step, while in the case of TE the cells will be (part of) the end product themselves (Mason and Hoare, 2007). Secondly, contrary to the biopharmaceutical industry, the production process of TE constructs is more dynamic since the cell population will not only proliferate but will also go through a phase of differentiation. Furthermore, the smaller scale of TE products will require sensitive tools, especially in the case of autologous therapies where small cell numbers are cultured and a more batch-dedicated monitoring and control strategy will be required (Glassey et al., 2011).

Therefore, *functional* bioprocess control in TE bioreactors, in the sense that it allows direct control over the critical quality attributes (CQAs) of the TE construct, such as proliferation rate, extracellular matrix production, differentiation stage, construct permeability, etc., remains a challenge due to inadequate online, non-invasive and cost-effective monitoring tools (Glassey et al., 2011; Koutinas et al., 2012; Placzek et al., 2009; Read et al., 2010; Vojinović et al., 2006). Depending on the bioreactor setup and cell carrier or scaffold design under consideration, this can be attributed to the high technicality and/or cost of direct, online and non-destructive measurement of TE construct CQAs. For example imaging techniques for real-time bioprocess control in 3D TE scaffolds are limited by the resolved depth of the sample or the lack of label-free techniques (Jaccard et al., 2014; Ward et al., 2013), surface plasmon resonance or mass spectrometry techniques needs specialized setups and have issues with complex culture medium samples (Jacquemart et al., 2008; Weber et al., 2012), while biomass probes are limited to certain cell carrier materials and are unable to distinguish between viable and non-viable cells (Kiviharju et al., 2007).

Because the CQAs are the effectual culture parameters upon which the release criteria of the TE construct should be based in a clinical setting, the development of such monitoring tools will be indispensable for the cost-effective production of regulatory compliant and clinically useful TE constructs. As a solution to the lack of direct CQA measurements some

studies use information on culture parameters that can conveniently be measured to indirectly estimate CQAs in fermentation and biopharmaceutical bioreactors (Dorresteijn et al., 1996; Junker and Wang, 2006; Meuwly et al., 2006; Papas et al., 2007), but applications for TE bioreactors and especially for perfusion bioreactors are limited. For example Santoro et al. (2011) used isothermal microcalorimeters in a static culture system to correlate heat production caused by biological processes to cell number and proliferation rate. When focusing on perfusion bioreactors, Janssen et al. (2006) used the difference in dissolved O_2 concentration in the culture medium across a perfused scaffold to estimate the number of cells, assuming an exponential cell growth rate. Santoro et al. (2012) improved this measurement by directly relating the difference in O_2 concentration to experimental data based on DNA quantification. However, the main disadvantage of the latter two measurements is that two O_2 sensors are needed. This decreases the cost-effectiveness, but also by relying on the absolute difference between the sensors small measurement perturbations cause large changes in the estimated number of cells, resulting in a limited measurement resolution in the low cell number range.

The aim of this study is to use a data-based mechanistic (DBM) modelling approach as a cost-effective tool to online monitor the amount of cells on a scaffold during 3D perfusion culture, based on single-sensor non-invasive O_2 concentration measurements in the micro-environment of the cellular construct under dynamic flow rate conditions. It is hypothesized that with this DBM approach, which is novel to the TE field, the number of cells within the scaffold can be estimated in a robust way based on a dynamic discrete-time transfer function model that describes the relation between the measured O_2 response (output) and the dynamic perfusion condition (input).

7.4. Materials and Methods

7.4.1. Scaffolds

Porous bio-inert Ti6Al4V scaffolds (Ø=6mm; h= 6mm; ±80% porosity), applied as geometrical backbone for 3D cell seeding and culture, were produced by selective laser melting as described by Van Bael et al. (2011). The cell-seeded volume per scaffold, taking into account a 80% porosity, is equal to 0.136 cm^3. The scaffolds were cleaned in an ultrasonic bath consecutively in pure acetone, 70% ethanol and distilled water. Subsequently the scaffolds underwent an oxidation treatment for 24 hours in a 5M sodium hydroxide solution at 60°C, and were rinsed with distilled water. Before use, the scaffolds were autoclaved and pre-wetted with culture medium by vacuum

impregnation, incubated for 2 hours in a 37°C incubator at 95% humidity and dried overnight in a non-humidified incubator to create a customized cell seeding and attachment surface (Impens et al., 2010).

7.4.2. Pre-culture of human periosteum derived stem cells (hPDC) and scaffold seeding

Human periosteum derived stem cells (hPDC) were isolated as described by Eyckmans and Luyten (2006) after approval of the ethics committee for Human Medical Research (KU Leuven). The cells were pre-cultured in monolayer in culture medium consisting of high glucose Dulbecco's modified Eagle's medium (Invitrogen) supplemented with 10% fetal bovine serum (FBS; Gibco), 1% sodium pyruvate (Invitrogen) and 1% antibiotic–antimycotic (100 units/mL penicillin, 100mg/mL strepto- mycin, and 0.25mg/mL amphotericin B; Invitrogen). For up to 7 passages, cells were trypsinised for 10 minutes with Tryple Express (Invitrogen). At passage 8, $2x10^5$ (28 000 cells/cm²) or $4x10^5$ (56 000 cells/cm²) cells were seeded in the scaffolds in 5 different batches using biphasic static drop-seeding as described by Impens et al. (2010) with a 45 minute incubation time during the two seeding steps. This seeding procedure generally results in a seeding efficiency of 44% ± 3.5%. The variability in cell density on the scaffolds is attributed to the use of two different seeding densities, the inter batch variability and the intrinsic variation in seeding efficiency.

After the seeding procedure, the scaffolds were incubated under static conditions in 12-well plates with growth medium for up to 4 days. As part of the cell seeding evaluation randomly selected Live-Dead® viability/cytotoxicity staining (Invitrogen) was performed after seeding to evaluate homogeneity.

7.4.3. Bioreactor setup

For the O_2 measurements the scaffolds were transferred to an in-house developed perfusion bioreactor system (Figure 7.2A) in which culture medium from a disposable medium reservoir (50-mL Falcon tubes; BD Biosciences) containing 10 ml culture medium was pumped through the scaffold in the perfusion chamber by a computer controlled peristaltic pump (PC-24; Ismatec SA). The dissolved O_2 concentration in the culture medium at the inlet of the perfusion chamber was kept constant at incubator conditions (5% CO_2, 37°C) with the aid of an oxygenator consisting of gas permeable tubing. The O_2 concentration at the perfusion chamber inlet was checked with a Fibox3 sensor (PreSens Precision Sensing GmbH). It is important to note

that this data was used only as a control for a constant dissolved O_2 concentration at the inlet of the perfusion chamber and is not used in further analysis. A second O_2 sensor (NeoFox, Ocean Optics) was placed at the outlet of the perfusion chamber to register the outgoing O_2 concentration after perfusion through the cell seeded scaffold.

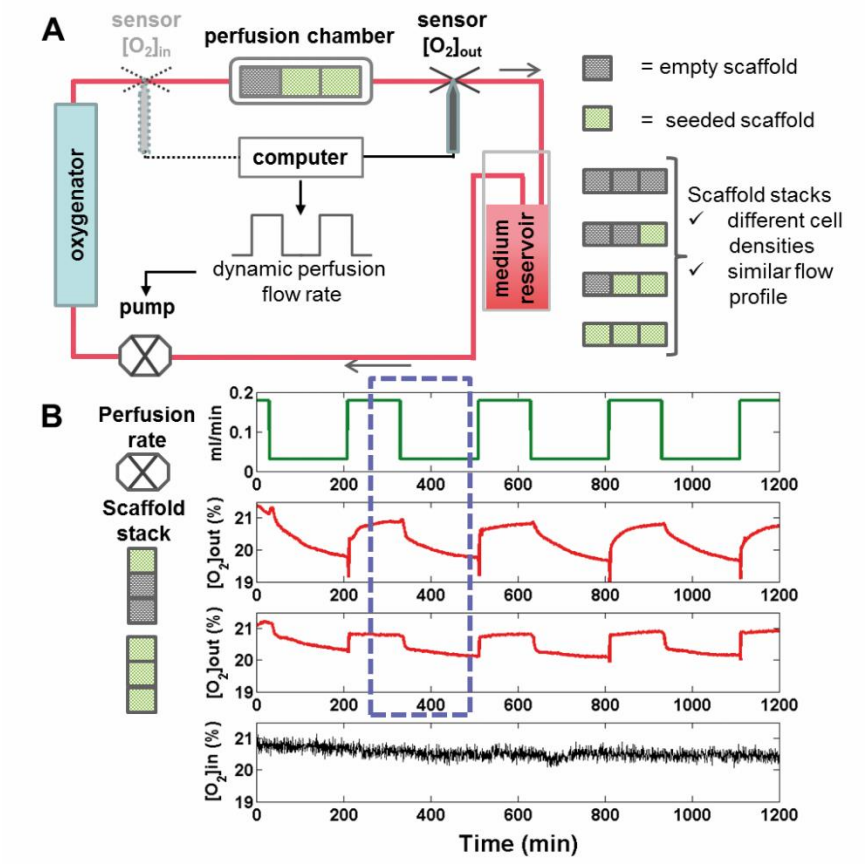

Figure 7.2: Overview of bioreactor setup and data interpretation
(A) Bioreactor setup in which stacks of scaffolds are dynamically perfused. The O2 sensor at the outlet registers the resulting fluctuations in O_2 concentration in the medium, the sensor at the inlet is solely used as a control for the constant input conditions. (B top) The applied dynamic perfusion rate consisting of 4 steps of 5 hours (0.18ml/min for 2h, 0.03ml/min for 3h). (B) Typical examples of the resulting dynamic O_2 profile for a stack of scaffolds containing $1.0x10^5$ and $4.0x10^5$ cells. The box indicates the part of the data considered in the modelling analysis, with the perfusion flow rate as model input and resulting O_2 concentration as model output. The bottom graph in B shows the constant O_2 input conditions during the dynamic perfusion condition as captured by the sensor at the perfusion chamber inlet. This data is not

used for further analysis. .(Note that the positions of the scaffold stacks are switched compared to the signal that is shown in B).

Dynamic perfusion of scaffolds

The pump was programmed to apply a stepwise dynamic perfusion flow rate, consisting of 4 consecutive 5h "*steps*" in which a pump speed of 0.18 ml/min is applied for 2h, followed by 0.03 ml/min for 3h (Figure 7.2B). This dynamic flow rate condition is exploited as a shift or dynamic pulse experiment in which the cell population is subjected to a change in process parameters aiming at investigating culture characteristics (Sagmeister et al., 2013). By applying step changes in flow rate, the measured dissolved O_2 concentration per unit volume of medium is altered due to cellular consumption proportional to the residence time of the medium in the scaffold. The resulting dynamic O_2 response to the perfusion rate steps can be measured by a single sensor at the perfusion chamber outlet (Figure 7.2B). This measurement will be used for further analysis with the data-based mechanistic modeling approach. The bottom of Figure 7.2B shows an example of a sensor measurement at the inlet of the perfusions chamber. This data is not used in further processing, but it illustrated the constant O_2 input conditions during the dynamic perfusion conditions (i.e. the effectiveness of the oxygenator).

The design of the steps in flow rate was based on a mathematical relation between the applied flow rate and resulting O_2 concentration at the perfusion chamber outlet (Equation 6) and was chosen in this way that predicted variations in the measured outlet O_2 concentrations would be easily perceived by the sensor. In a preliminary validation experiment it was shown that the number of cells attached to the scaffold did not significantly change (based on DNA content) after being exposed to the fluid flow within the perfusion bioreactor, irrespective of the used perfusion rate (range tested was between 0.2 ml/min and 4 ml/min, Figure 7.3A). Additionally, to underline the non-destructive and non-invasive nature of the step changes in the perfusion conditions, its effect on the metabolic activity and cell number was assessed. In a setup where one group of scaffolds (n=3) was subject to a constant perfusion rate of 0.18 ml/min for 7 days while another group of scaffolds (n=3) was subject to one dynamic perfusion step every 24h for 7 days (high flow rate 0.18 ml/min, low flow rate 0.03 ml/min for 3h), no significant difference in metabolic activity and DNA content between the two groups was observed (Figure 7.3B).

For the O_2 measurements, a total of 21 combinations of 3 seeded and/or non-seeded scaffolds were stacked on top of each other in the bioreactor (Figure 7.2A) and dynamically perfused for 20 h (4 steps), resulting in 21 different

time series of dynamic O_2 measurements. By stacking combinations of 3 seeded and non-seeded scaffolds, a large number of different cells densities could be measured (between $1x10^5$ and $6.5x10^5$ cells) without altering the flow profile inside the perfusion chamber.

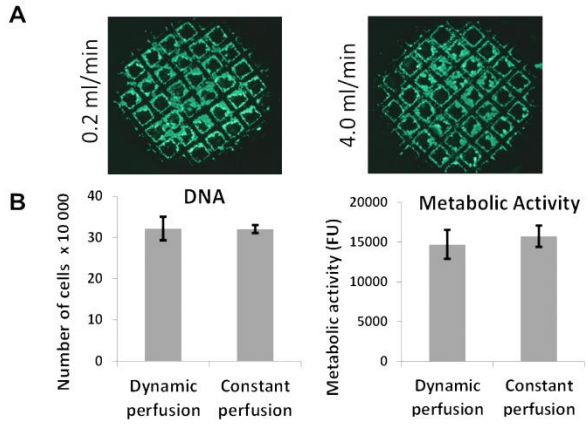

Figure 7.3: Validation experiment for the influence of the dynamic perfusion flow on the cells within the scaffold.
(A) Live/dead staining after replacing the seeded scaffold from static conditions to the perfusion bioreactor at different flow rates. (B) The number of cells in the scaffolds (determined by DNA quantification) and the metabolic activity of the cells (determined by a PrestoBlue metabolic activity assay) after 7 days of culture in dynamic perfusion conditions did not significantly differ from the constant perfusion condition.

7.4.4. Metabolic activity and DNA content analysis

Immediately after the 20h dynamic perfusion culture period in the bioreactor, the stacked scaffolds were separately transferred to a 12-well plate and submerged in a 10% PrestoBlue (Life Technologies) metabolic activity assay according to the manufacturer's instructions. After 2h incubation, the metabolic activity of the cells in the scaffolds was quantified by fluorescence measurements (Bio-Tek Synergy™ HT) with an excitation wavelength of 540nm and an emission wavelength of 590nm on 100µL supernatant in a 96-well plate. A higher metabolic activity is indicated by higher fluorescent values. Subsequent to the metabolic activity assay, the DNA content on the scaffolds was obtained by a highly quantitative and selective DNA assay (Quant- iT™dsDNA HS kit; Invitrogen) as described by Chen et al. (2012). In short, after rinsing the scaffolds with PBS, they were lysed in 350µL lysis buffer (Qiagen) supplemented with 3.5µL β-mercaptoethanol (Sigma) and frozen at -80°C. Afterwards the scaffolds were thawed at room temperature

and a Qubit® Fluorometer (Invitrogen) was used to quantify the DNA content for each sample in 10µl supernatant diluted in 90µl miliQ water.

7.4.5. Data-Based Mechanistic (DBM) Modelling of single sensor dynamic O_2 data

A data-based mechanistic (DBM) modelling approach was used to infer information on cell numbers within the scaffold based on the O_2 measurements under dynamic perfusion conditions. Contrary to the often used mechanistic simulation models that start from a model structure as it is perceived based on a priori knowledge of the modeller (deductive approach), the data-based approach infers its model structure directly from the observed data (inductive approach) (Young, 1999). This approach significantly reduces the model complexity and facilitates parameter estimation. After the "black-box" model identification stage, the resulting model is mechanistically interpreted in physically meaningful terms.

In this study a discrete-time, linear, single-input, single-output transfer function (TF) model was used to describe the time series data of the response of the O_2 sensor at the perfusion chamber output to the step variations in the perfusion flow rate (Young, 1984):

$$y_t = \frac{B(z^{-1})}{A(z^{-1})} u_{t-\delta} + \xi_t \qquad (1)$$

where t refers to the value of the associated variable at the t^{th} sampling point; y_t is the model output or the observed time series from the O_2 sensor (%O_2); $u_{t-\delta}$ is the model input or the dynamic perfusion flow rate (ml/min) shifted over a time delay δ; ξ_t is the additive noise, assumed to be a zero mean, serially uncorrelated sequence of random variables with variance σ^2 accounting for measurement noise, modelling errors and effects of unmeasured process inputs. $B(z^{-1})$ and $A(z^{-1})$ are polynomials of model parameters that describe the influence of the exogenous input u_t on the process:

$$B(z^{-1}) = b_0 + b_1 z^{-1} + \ldots + b_n z^{-n} \qquad (2a)$$

$$A(z^{-1}) = 1 + a_1 z^{-1} + \ldots + a_m z^{-m} \qquad (2b)$$

where b_i and a_j are the model parameters; z^{-1} is the backward shift operator defined as $z^{-1} y_t = y_{t-1}$; and n, m are the orders of the respective

polynomials. For each data set of O_2 measurements the b_i and a_j model parameters were estimated using a refined instrumental variable method (Young, 1984) for model orders n and m ranging from 1 up to 2 and time delays δ ranging from 0 up to 10 resulting in 44 (2 x 2 x 11) possible TF models. The resulting models were evaluated principally, but not solely, based on Young Identification Criterion (YIC) which is a combined measure for the goodness of fit (model residuals) and the parametric efficiency (ill-conditioning). More negative YIC values for a certain model structure suggest better model fits (Pedregal et al., 2007; Young, 1984). Other criteria that were used in combination with YIC, were goodness of fit (expressed as the coefficient of determination, R_T^2), the model stability (quantified via the poles of the TF) and the reliability of the model parameter estimates (calculated based on the 95% confidence intervals around the parameter estimates).

The TF model parameters or combinations thereof can be used to evaluate the dynamics of the model. For example the steady state gain (SSG) that will be used later, is a parameter describing the model dynamics that represents the steady level achieved by the output of the transfer function $y(t)$ following a sustained unit step in the input variable $u(t)$ (Figure 7.4) (Pedregal et al., 2007). For a 1st order TF with one a- and b-parameter the SSG is calculated as:

$$SSG = \frac{b_0}{1 + a_1} \qquad (3)$$

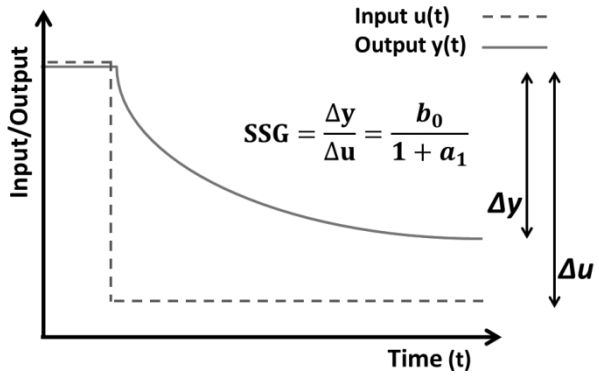

Figure 7.4: Graphical interpretation of the steady state gain (SSG) and calculation for 1st order transfer functions.

7.4.6. Mechanistic model of the perceived drop in O_2 concentration

With the goal of linking the TF model parameters to the dynamics of a physical system, a mechanistic model was used to describe the O_2 distribution along the length of a perfused scaffold. In this study the perfusion setup is not diffusion limited (Péclet number is equal to 106 at lowest perfusion rate, assuming water at 37°C as the diffusion medium for O_2 with a diffusivity constant of $3x10^{-9}$ m^2/s), therefore the mass conservation law with a Michaelis-Menten consumption kinetics can be written like (Truscello et al., 2011):

$$\rho \boldsymbol{v} \frac{dpO_2}{dx} = OCR_{max} \frac{pO_2}{k_m + pO_2} \qquad (4)$$

where ρ is the medium density; $\boldsymbol{v}$ the flow speed; pO_2 the partial O_2 pressure; x the coordinate relative to the scaffold length; OCR_{max} the maximum volumetric O_2 consumption rate of the cells and k_m the Michaelis-Menten constant corresponding to the concentration at which the O_2 consumption rate is equal to half of OCR_{max}. Assuming a near normoxic condition in the incubator and relatively high flow rates ($pO_2 \gg k_m$), the right hand side of the equation can be replaced by a constant consumption term equal to the maximum consumption rate OCR_{max}. In this case the equation can be solved analytically:

$$\Delta pO_2 = \frac{L \cdot OCR_{max}}{v} \qquad (5)$$

where L is the length of the scaffold. Substituting $OCR_{max} = OCR_{max,cell} \cdot \rho_{cell} = OCR_{max,cell} \cdot N_{cell}/V$ and $v = Q_m/\pi r^2$ results in:

$$\Delta pO_2 = \frac{OCR_{max,cell} \cdot N_{cell}}{Q_m} \qquad (6)$$

where $OCR_{max,cell}$ is the maximum O_2 consumption rate per cell (mol/cell·s); ρ_{cell} is the cell density (cell/m^3); N_{cell} is the total number of cells in the scaffold (cell), V(m^3) is the scaffold volume; r is the scaffold radius (m); Q_m the medium flow rate (m^3/s). A conversion between molarity (mol/L) and partial pressure (atm) is done with a Henry's constant for O_2 in water at 310 K equal to 959.3 L·atm/mol. As the mechanistic model describes the O_2 gradient in a volume with a homogeneous cell distribution, which was not the case for

the scaffold stacks used in the oxygen measurements, a normalization of the measured oxygen drop based on the cell-seeded volume of the scaffold stack is required when comparing the results of the mechanistic model and the sensor measurements.

7.4.7. Statistical analysis and numerical methods

Data analysis was performed using Matlab 2011b (The MathWorks Inc.) in combination with the Captain toolbox (Taylor et al., 2007). Independent groups were compared by the unpaired Student's t-test (two-tailed), and considered statistically significant in case $p < 0.05$.

7.5. Results

A total of 21 different scaffold combinations with cumulative cell numbers ranging between $1.0x10^5$ and $6.5x10^5$ cells were dynamically perfused in the bioreactor. This resulted in time series data of the dynamic O_2 response to the dynamic perfusion flow rate as shown in Figure 7.2B. Differences in the O_2 response measurements for different cell densities can already be observed when comparing the signal for a scaffold stack with 1 seeded scaffold and 3 seeded scaffolds (respectively $1.0x10^5$ and $4.0x10^5$ cells in Figure 7.2B). These differences were quantified by the DBM modeling approach and the DBM model parameters were used to make an estimate of the number of cells within the scaffold. Due to the initial 1h adjustments period needed for the bioreactor system to reach equilibrium with the incubator conditions (37°C, 5% CO_2), data derived from the first step of the dynamic perfusion regime (minute 0 to minute 300) were not taken into account. Therefore, the first part of the second step (between minute 300 and 500 of the measurements as indicated by the box in Figure 7.2B) was used for the DBM model.

The dynamic O_2 response data could be accurately described by means of a 1st order discrete-time, linear single-input single-output TF model, resulting in a R_T^2 of 0.93 or higher for every dataset (Figure 7.5). The 1st order model structure with one a- and b-parameter was chosen to fit the measured data based on a generally lower YIC value compared to a 2nd order model structure with two a- and b-parameters. For the TF model parameters it was found that the steady state gain (SSG) showed a strong positive linear correlation (R^2=0.80) with the number of cells inside the perfused scaffolds, with the cell number being based on the DNA quantification on the scaffold after the 20h dynamic perfusion cycle (Figure 7.6A). Additionally, the SSG also showed a strong positive linear combination with the total metabolic activity of the cells within the scaffold (R^2=0.82) (Figure 7.6B) as could be expected from earlier

studies where a correlation between metabolic activity and the number of cells was found (Zhou et al., 2013).

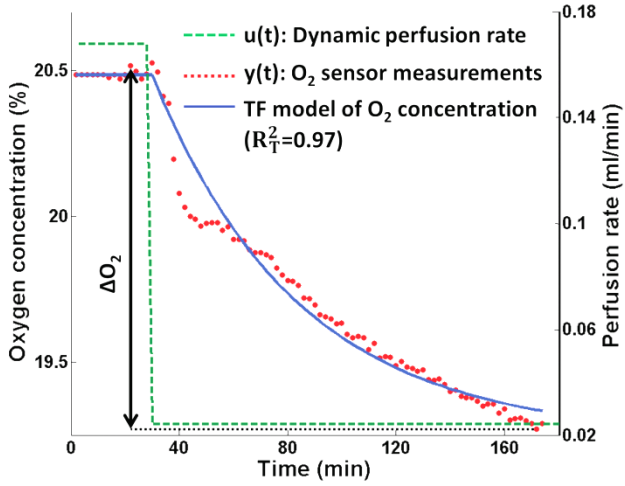

Figure 7.5: Typical example of the transfer function model resulting from the data-based mechanistic modeling approach (± 4.0x10^5 cells).
The green dashed line represents the model input or the dynamic perfusion flow rate on the right axis. The red dots represent the O_2 sensor time series and the blue line represents the resulting transfer function model of the oxygen concentration on the left axis. The arrow ΔO_2 indicates the height of the perceived drop in O_2 due to the dynamic perfusion rate as will be used in Figure 7.7 and 7.8.

To corroborate the data-based relation between the SSG model parameter and the number of cells within the scaffold, the mechanistic model describing the expected drop in O_2 concentration (Equation 6) was used to physically interpret the data-based TF model. The mechanistic model showed that when the perfusion speed was lowered during the step change perfusion condition, the drop in O_2 concentration was proportional to the number of cells in the scaffold, assuming a constant O_2 consumption rate per cell (Figure 7.7). The drop in O_2 concentration was quantified in the time series data by subtracting the lower steady state O_2 concentration after the step in flow rate from the higher steady state O_2 concentration before the step in flow rate (as indicated by the ΔO_2 arrow in Figure 7.5). After normalizing this drop for the cell-seeded volume of the scaffold stack, the mechanistic model was able to accurately fit (R^2=0.75) the data. From the model fit a cell specific O_2 consumption rate of 1.09x10^{-17} mol/cell·s^{-1} could be calculated.

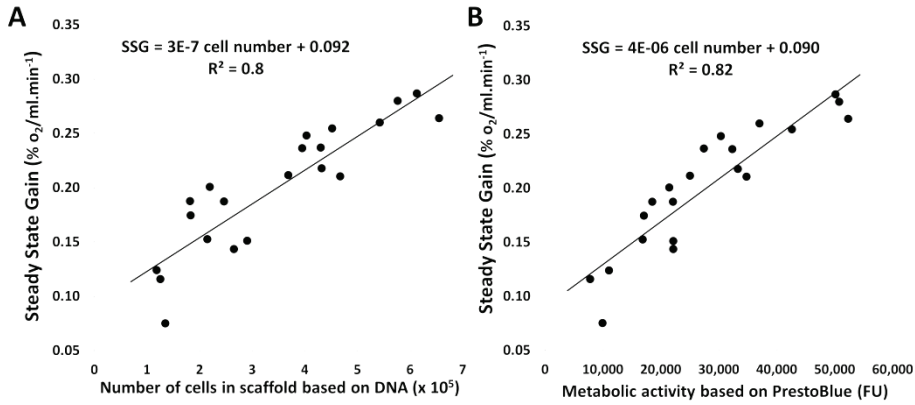

Figure 7.6: Correlation between Steady Sate Gain (SSG) and the number of cells in the scaffold, and the SSG and the metabolic activity of the cells.
(A) Correlation between the steady state gain derived from the transfer function model parameters and the total number of cells within the scaffold based on DNA quantification (R^2=0.80). (B) Correlation between the steady state gain derived from the transfer function model parameters and the total metabolic activity of the cell in the scaffold as determined by the PrestoBlue assay (R^2=0.82). The graphs show the results for all 21 O_2 measurement time series.

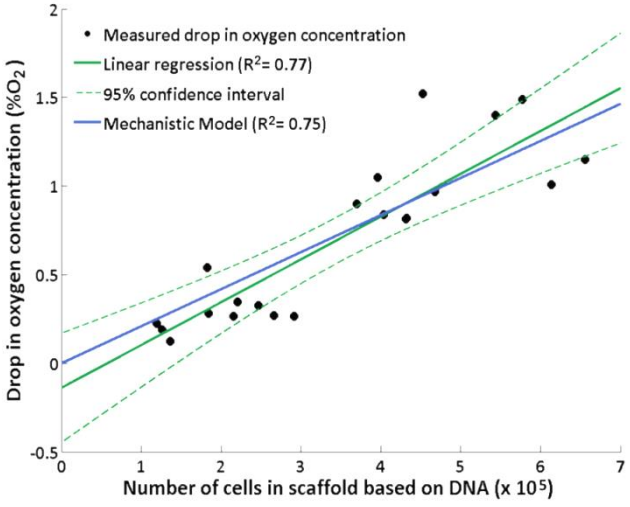

Figure 7.7: Fit of the mechanistic model as described in Equation 6, on data from the measured drop oxygen concentration.
The drop in oxygen concentration is quantified by subtracting the lower steady state O_2 concentration after the flow rate step from the higher steady state O_2 concentration before the flow rate step and normalized for the cell-seeded volume of the scaffold stack. Based on the parameters of the fitted model a cell specific O_2 consumption rate of $1.09x10^{-17}$ mol/cell.s^{-1} could be determined.

From the correlation between the number of cells in the scaffold and the SSG (Figure 7.6A), and the number of cells and the drop in O_2 concentration (Figure 7.7), a linear correlation between the SSG and measured drop in O_2 concentration was obtained as can be seen in Figure 7.8A. Further, when looking closer to the units of the SSG ($\%O_2/ml.min^{-1}$) it is possible to calculate the O_2 drop from the value of SSG. When the O_2 drop, estimated via the SSG as determined from the data-based model (normalized for cell-seeded volume as before), is compared to the O_2 drop as expected from the mechanistic model, it can be appreciated in Figure 7.8B that the same trend is followed. These correlations between the SSG parameter of the TF model and the mechanistic model is important as it makes the purely data-based TF model more interpretable in a mechanistic sense.

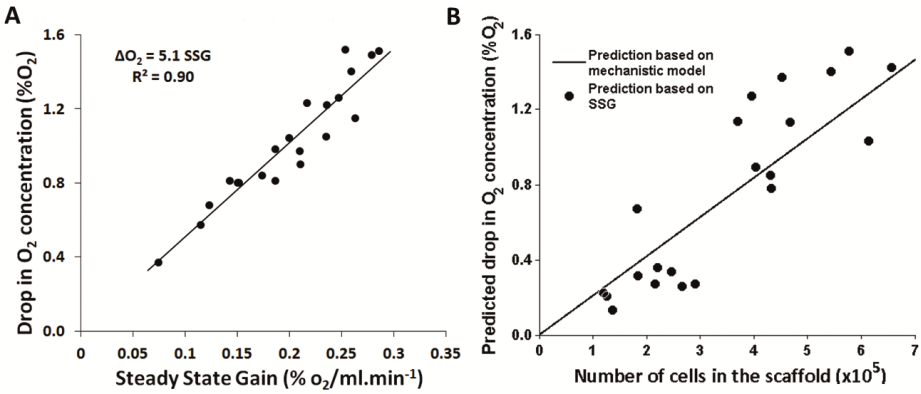

Figure 7.8: Correlation between the drop in oxygen concentration and the number of cells in the scaffold and the Steady State Gain.
(A) Correlation between the Steady State Gain derived from the transfer function model parameters and the drop in oxygen concentration as perceived in the time series data (R^2=0.90). (B) Expected drop in oxygen concentration based on the prediction of the mechanistic model and the prediction via the Steady State Gain normalized for the cell-seeded volume of the scaffold stack

7.6. Discussion

This study showed that a data-based mechanistic modelling approach can be successfully applied on O_2 sensor data to accurately determine the number of cells in a scaffold in 3D perfusion culture in a non-invasive and on-line way. It can be observed (Figure 7.6A) that by combining step changes in perfusion flow rate with a DBM modelling approach a range of cell numbers can be accurately determined. It was shown that the lowest detectable limit with this single sensor approach is approximately 5 times lower than reported in similar 3D bioreactor setups in literature that make use of two O_2 sensors (Janssen et

al., 2006; Santoro et al., 2012) (Table 6-I). In case the absolute difference in O_2 concentration between two sensors is taken as a measure for a certain amount of cells in the double sensor setup, small perturbations in the readings can cause relatively large deviations in the estimated number of cells. The single sensor approach described here, in combination with the SSG parameter that relatively describes the dynamics of the signal between two steady states, is less affected by fluctuations in the read-out. The subsequent increased accuracy and lower detection limit of this single sensor approach could open up new bioprocess control possibilities for 3D TE constructs, especially for autologous approaches where only a relatively small number of cells can be taken from patient biopsies as start of the culture (Jakob et al., 2012; Mason and Hoare, 2007). Moreover, the principle of applying a dynamic perfusion flow rate to induce a dynamic O_2 response that holds information on the number of cells in a scaffold is in theory generically applicable to perfusion, hollow fibre and packed bed bioreactor systems having at least one O_2 sensor, and this for any type of cell carrier and cell type.

Table 7-I: Detectable number of cells reported in literature in similar setups (however not necessarily targeted with the goal of determining the lowest detectable limit).

Reference	**Strategy**	**Cell type**	**Lowest (robustly) detectable cell number reported**
(Janssen et al., 2006a; Janssen et al., 2006b)	Difference in dissolved O_2 between 2 sensors	Goat bone marrow stromal cells	± $20x10^6$ cells seeded
(Santoro et al., 2012)	Difference in dissolved O_2 between 2 sensors	Human chondrocytes	± 500,000 cells
Current study	DBM modelling of 1 sensor in dynamic perfusion conditions	Human periosteum derived stem cells	± 100,000 cells

The design of the dynamic perfusion flow condition is critical and will have to be adapted to the specific needs for every bioreactor setup, for example depending on the O_2 consumption rate of the cells, scaffold design or the expected number of cells (Cioffi et al., 2008; Maes et al., 2009; McCoy et al., 2012). The high flow rate in the step design is fairly unimportant regarding the measurements and will most conveniently be the functional flow rate that

is used for the cell culture system. The selection of the low flow rate is more crucial, since it is subject to a trade-off between the non-destructiveness and the precision of the measurement. When the low flow rate is too low, O_2 concentrations within the TE construct might drop excessively, causing adverse effects on the TE construct quality due to O_2 depletion and the development of hypoxic regions (Das et al., 2010; Malda et al., 2007; Radisic et al., 2006; Volkmer et al., 2008). On the other hand, the flow rate has to be low enough for the O_2 sensor to be able to perceive the drop in O_2 concentration (constraint related to the sensor resolution). By making use of the cell specific oxygen consumption rate obtained from the Figure 7.7 ($1.09x10^{-17}$mol/cell.s^{-1}, corresponding with O_2 consumptions rates as found in literature for comparable cell types (Cochran et al., 2006; Lewis et al., 2005)) and Equation 6, an operating window for selecting suitable perfusion conditions for a range of cell numbers can be constructed as shown in Table 7-II. The change in perfusion rate for a given number of cells that results in O_2 concentration drops from a green to a yellow zone in the table will be sufficient for the sensor and the data-based model to be picked up, while larger drops towards the red zone might result in a decreased TE construct quality.

Table 7-II: Application specific operating window of the resulting drop in O_2 concentration ($\%O_2$) for the dynamic perfusion rates.
Changes in flow rate that result in drops in O_2 concentration that go from a green to yellow zone are deemed optimal concerning the trade-off between measurement precision and the biologic quality of the TE construct. This operating window is derived from the model described in Equation 6 for an hPDC oxygen consumption rate of $1.09x10^{-17}$ mol/(cell*s) derived from the mechanistic model fit in Figure 7.7.

Perfusion rate (ml/min) \ Number of cells	5E+04	1E+05	2E+05	5E+05	1E+06	5E+06	1E+07
0.03	0.10%	0.21%	0.42%	1.05%	2.09%	10.46%	20.91%
0.1	0.03%	0.06%	0.13%	0.31%	0.63%	3.14%	6.27%
0.2	0.02%	0.03%	0.06%	0.16%	0.31%	1.57%	3.14%
0.5	0.01%	0.01%	0.03%	0.06%	0.13%	0.63%	1.25%
1	0.00%	0.01%	0.01%	0.03%	0.06%	0.31%	0.63%
2	0.00%	0.00%	0.01%	0.02%	0.03%	0.16%	0.31%

By choosing the appropriate step change perfusion conditions, or by changing them over time during culture, the hypoxia risk can be mitigated and large ranges of cell numbers can be quantified. However, changes in flow regime itself have been seen to influence the cell state (Grayson et al., 2011; Jaasma et al., 2008; Kim and Ma, 2012; Sharp et al., 2009). Since there was no apparent effect of the used step change perfusion profile noticeable on the

metabolic activity and DNA content in the scaffolds in this dataset (Figure 7.3B), it is hypothesized that this influence is negligible for the low frequent dynamics used in this case compared to the pulsatile flow rates as for example described in Sharp et al. (2009). Moreover, it is important to note that for determining the cell number within the perfusion bioreactor the application of a step change perfusion condition does not strictly has to proceed through planned experimentation. In certain processes there might anyway be opportunities in normal operation mode to measure O_2 responses on step changes in perfusion rate, for example when perfusion is temporarily stopped during medium exchange or sample taking.

This use of DBM modelling of O_2 data in step change perfusion conditions has the potential to follow up 3D bioreactor cell cultures over time. However, temporal changes in the TE construct developmental phase (e.g. due to stem cell differentiation) could alter the metabolic activity of the cells (Quinn et al., 2012; Ward et al., 2013), and therefore the O_2 consumption rates of the cells (Zhao et al., 2005). In that case, it is expected that the linear relation between the SSG parameter, metabolic activity and cell number as seen in Figure 7.6 will not be valid over the whole culture time. This may be accounted for by previously determining a reference curve for the evolution of the SSG parameter over time in relation to DNA measurements, or by implementing other sensing techniques that can provide information on the developmental phase of the cells in the TE construct (for example by the use of lactate measurements as described by (Zagari et al., 2013)). It should also be noted that the SSG reflects the dynamics caused by the oxygen consumption of *all* the cells in the system, either attached to the scaffold or growing on the perfusion chamber. Care should be taken during long-time culture that the cell number is not overestimated due to cells that might grow close to the scaffold while not being part of the final construct.

Although more frequently used in other scientific domains, such as modelling and controlling heart rate responses of athletes (Lefever et al., 2012), energy transfer in buildings (Price et al., 1999), precision life stock farming (Silva et al., 2009), and other environmental and economic phenomena (Haredasht et al., 2011; Young, 1998), the DBM modelling technique is, as far as known by the author, unexplored in the context of bioprocess control for TE bioreactors. Nevertheless this data-based approach holds promise for the TE domain since high quality bioprocess data is often available from the bioreactor system and purely mechanistic models for complicated biological processes are often non-existent or have a significant cost of development (Koutinas et al., 2012). In addition, since the DBM approach results in low order, parametrically efficient models that describe only the dominant behaviour of the system, it

forms an ideal basis for controlling processes (Pedregal et al., 2007; Taylor et al., 2007).

7.7. Conclusion

The data-based mechanistic modelling approach combined with step changes in the perfusion flow rate allows to accurately quantify a broad range of cell numbers within a scaffold in 3D perfusion bioreactors in an online and non-destructive way. By making use of a single O_2 sensor, this approach combines accuracy with cost-effectiveness, providing quantitative information on an important TE construct quality attribute. In addition to the non-invasiveness and relative simplicity of the setup, the approach used here is generically applicable for different culture applications, bioreactor designs, cell carriers and cell types, making it an interesting quality control tool for regulatory compliant clinical TE construct production.

Chapter 8. Overall discussion, future perspectives, and conclusions

8.1. Summary

The development of controlled and cost-effective stem cell bioprocesses is imperative for the successful clinical translation and commercialization of cell-based therapies. In this doctoral thesis the large-scale expansion of mesenchymal stem cells was explored in support of an autologous cell-based ATMP that is currently under development at Prometheus (KU Leuven). In parallel, tools were developed would allow informed decision-making on critical process steps by making efficient use of process data in combination with data-based modelling techniques.

In Chapter 3 a set of process metrics (expansion factor, final cell yield, concentration of protein supplement, cell density at harvest, etc) and an interactive tool for the comparison of cell expansion processes was provided based on an analysis of 73 different cell expansion processes on 7 different cell types in 5 different culture vessels. This tool allows the user to benchmark expansion processes against each other and assess their capability to support a certain production strategy.

In Chapter 4 the translation of Prometheus' standard flask-based production process to a large-scale bioreactor-based process was described specifically for a multiplate-type bioreactor (Xpansion by Pall Life Sciences). This chapter focused on the large-scale processes (both up- and downstream), with continuous monitoring and control of environmental variables, manual metabolite samples and image-based cell growth monitoring at discrete time steps. The growth dynamics and final cell density in the bioreactor were almost identical compared to the control flask (17 500 cells/cm^2 and 17 300 cells/cm^2 respectively) and the *in vivo* potential of the cells remained

unchanged. A detailed analysis of the cell losses during the downstream process revealed that significant gains in efficiency can be achieved by further optimising the harvest procedure.

Chapter 5 specifically focused on how the monitoring and control capability of the imaging setup (Ovizio iLine S) that was incorporated in the multiplate bioreactor could be used to optimise the harvest reaction in the bioreactor. An application for the on-line model-based prediction of the optimal time to stop the enzymatic harvest reaction was developed by means of real-time imaging and quantification of cell circularity in combination with data-based models. The tool was able to accurately estimate the inhibition time (median error of 21 seconds), thereby effectively reducing the exposure time to the harvest enzymes which are potentially influencing cell quality. Because the tool informs operators in real-time and in an objective way about the time point for the cells to be retrieved from the bioreactor vessel the reproducibility of harvest experiments in a 2D culture setting can be increased.

Chapter 6 described another approach for the translation of the Prometheus flasks-based production process to a large-scale bioreactor, this time employing a hollow fibre perfusion configuration (Terumo BCT Quantum cell expansion system). The bioreactor supported efficient growth of the cells (cell yields between 316 million and 444 million starting from 20 million cells over an 8 day culture period), mainly because the hollow fibre setup supports very low seeding densities. For these processes lactate production rates were used to objectively decide on the medium feed rate and the timing of the cell harvest for donors with different growth and metabolic rates. The bioreactor setup was modified slightly in order to monitor environmental parameters in an on-line way as was seen in Chapter 4. Additionally the comparability of the process outcome, both *in vitro* and *in vivo* was evaluated for the multiple donors.

Finally, Chapter 7 provided another example on how on-line process read-outs combined with data-based models are able to provide estimates of critical quality attributes. This was aimed at perfusion bioreactors, such as the Quantum bioreactor of Chapter 6, where imaging techniques as used in Chapter 5 are generally not applicable due to the non-transparent spatial configuration of the bioreactor. On-line oxygen measurements from a single sensor in combination with controlled changes in the perfusion flow rate and a data-based model with a mechanistic interpretation allowed precise estimates of the number of cells in the bioreactor.

8.2. Overall discussion and future perspectives

The previous chapters each contain their specific discussion and conclusion section, and therefore, we will focus here on three trends that are over-arching to all the previous chapters and which are important future consideration for the development of cell-based therapies:

8.2.1. Reduction of process variability is key to assure robust *in vivo* performance

It is advisable to strive for reduced process variability, even in the very early stages of process development. This will facilitate the definition of a design space in which the process will be under control, which in turn will ensure a higher chance of producing cell batches inside the specification limits and therefore ultimately leading to more clear-cut regulatory approval of the cell-based therapeutic product.

From a raw materials perspective, process variability can be reduced by carefully selecting the process inputs. For example, switching from highly batch-dependent and poorly characterised process components such as foetal bovine serum to chemically defined culture media is despite the high cost and often lower cell yields (as concluded in Chapter 3) gaining more and more support (Heathman et al., 2015c). While efforts are made at Prometheus towards chemically defined media (Bolander et al., in press), for the large-scale experiments in this work its use was not yet considered due to the associated high costs that comes with this scale. Considering the cells themselves as a raw material in the expansion process, potentially an even larger impact could be made by switching from the more heterogeneous adult progenitor cell populations such as the hPDCs to induced Pluripotent Stem Cells (iPSC). These cells possess the advantage of being generated in the lab under standardised conditions, instead of being directly retrieved from a tissue biopsy. Additionally, iPSCs are able to differentiate into any cell type of the human body while having a phenomenal expansion capacity. This evolution will not only revolutionise the way we use cells for the treatment of diseases, but (allogeneic) iPSCs hold tremendous promise for large-scale standardised production processes (Baghbaderani et al., 2015; Rao and Atala, 2016).

Apart from the variable process input as discussed in the previous paragraph, also from a technical point of view progress can be made in order to reduce process variability. By automating the critical steps of the culture procedure and reducing the operator induced variability, the use of bioreactors will allow a more robust and reproducible process (Liu et al., 2010; Williams et al.,

2012). This could directly lead to a more uniform cell quality and subsequent less variable *in vitro* and *in vivo* performance (Santoro et al., 2010; Trainor et al., 2014). It was also shown in this work that by introducing bioreactor-based cell culture processes the variability on the process outcome can be significantly reduced. For example, in Chapter 6 it was determined that the variability on cell yield (normalised by culture surface) for the Quantum bioreactor was 2.5 times lower compared to the flask-based expansion. This significantly increases the chance of producing cell batches within the specification limits as can be seen in Figure 8.1.

However, only standardising the input materials and automating the processes will not solve the process variability issue since biological systems, in the terminology of the M3-BIORES lab, are *CITDs* or "complex, individually different, time varying in its responses, and dynamic" (Van Loon et al., 2006). The implication of a CITD system is that, especially in the context of autologous therapies, two seemingly identical biological processes might still show variability given that every individual reacts differently and in a time-variant way on a certain stimulus. In terms of bioprocess development, the CITD principle suggests that developing processes that are optimised for the average individual are still resulting in suboptimal operating conditions for a very large part of the population. Take for example the third donor in the Quantum bioreactor expansion process of Chapter 6. While the process and environmental conditions were nearly identical to the other 2 donors, the cells from the 3rd donor were not able to generate bone in the *in vivo* potency assay.

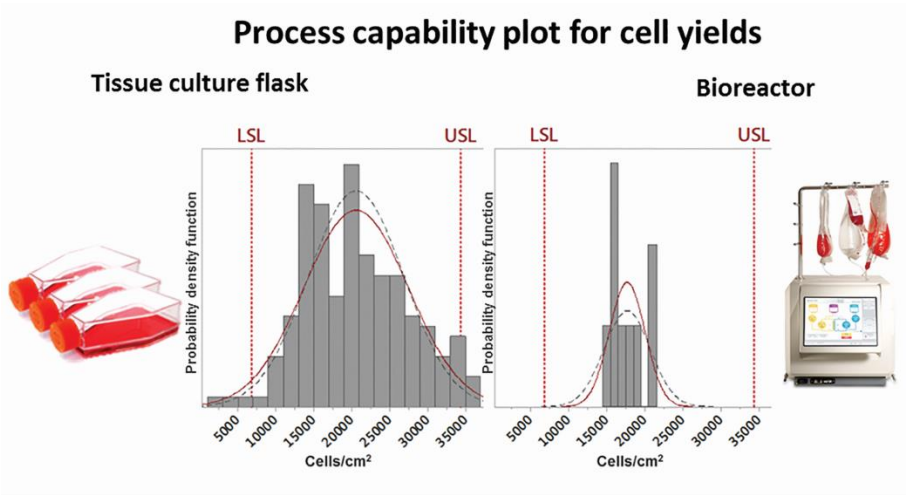

Figure 8.1 Process capability analysis based on historic harvest quantification data (cells/cm^2) from the Prometheus lab on cell expansion processes in T-flasks and the Quantum bioreactor. LSL = lower specification limit, USL = upper specification limit.

Process variability is inseparably linked to process monitoring. In the first place, process monitoring allows the detection of the (causes of) variability. Secondly, the process monitor is able to warn the operator in those case where process parameters exceed their allowable tolerance limits. In this way it can act as an early warning system able to prevent large sunken costs of processes that would otherwise only get rejected at the end of the process (end-point analysis). *On-line* process monitoring could eventually evolve towards on-line process control with self-correction, where based on the continuous process read-outs (and their link to the cell quality) continuous corrections to the process could be effectuated via the controller to better tune into the needs of each individual donor separately and in this way actively reduce the variability on the process outcome.

While on-line monitoring has a large potential to make cell culture processes more robust, finding culture parameters that can be monitored on-line and have a direct link to the critical quality attributes of the cells are difficult to find as will be discussed below.

8.2.2. Improvements in on-line monitoring techniques for critical quality attributes of cells are required to make best use of control algorithms

Based on concepts such as model-based (predictive) monitoring and control that are used in chemical plants and other process industries, automated control of dynamic systems has evolved enormously (Camacho and Bordons, 2007). An example of model-based predictive monitoring can be found in Chapter 5 where a data-based model was able to link the on-line monitored feature variable (cell circularity) to a process decision ('stop the enzymatic harvest reaction') in real-time. Even better, the on-line monitoring and data-analysis allowed to *predict* when to stop the process, while the process was still on-going (i.e. making the monitoring faster than real-time). This application is useful to quantitatively compare or optimise the incubation time for cell harvests in planar culture systems for different donors or different harvest solutions. However, similar approaches based on this on-line data-based monitoring and control strategy pose tremendous potential if one would have access to on-line readouts of biomarkers that make up a biological signature of the cellular state and therefore enable the control of *in vivo* cell potency *in vitro*.

However, the analysis of these type of biomarkers (if they are known for a specific application) require relatively complex techniques such as surface–antigen phenotyping by flow cytometry (as described and used in Chapter 4 and 6), or gene expression measurements by Real Time-PCR or microarrays. These are time consuming end-point analyses and can therefore not deliver the rate of data that is needed for active on-line control of the process quality. In other words, it is not necessarily a problem of measuring the critical quality attributes of the cells, the limiting factor for strictly controlled stem cell bioprocesses to date is the lack of non-invasive sensor systems with a measurement rate that allows on-line monitoring of the functional biomarkers. Fortunately, *on-line* does not necessarily mean that *continuous* measurements are required, but rather a measurements frequency that is faster (at minimum twice as fast) than the dynamics of the systems according to the Nyquist–Shannon sampling theorem (Jerri, 1977) as illustrated in Figure 8.2.

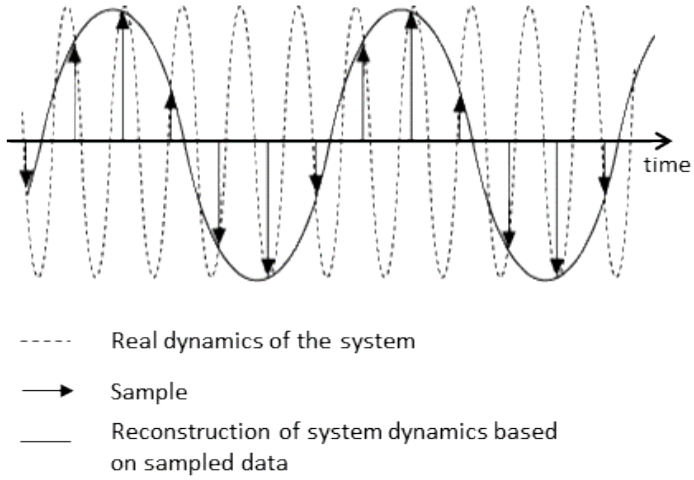

Figure 8.2: Illustration of the Nyquist–Shannon sampling theorem.
Measuring dynamic data (dotted line) with a sample frequency (arrows) that is too low could result in perceived dynamics (solid line) that are very far away from reality. Image adapted from National Instruments Corporation (http://zone.ni.com/reference/en-XX/help/370592N-01/digitizers/nyquist_theorem/).

This means that certain (off-line) sampling methods might still provide sufficient data for process control, depending on the rate of change of the feature variable. This was for example shown by the off-line threshold-level control mechanism for the determination of the harvest time of the Quantum bioreactor in Chapter 6 that was based on manual lactate samples. Also Csaszar et al. (2012) developed an automated medium dilution strategy based on off-line ELISA read-outs on spent culture medium (via a Luminex platform) that was able to increase the expansion rate of hematopoietic stem cell cultures. A more elaborate strategy (from the controller point of view) was investigated during a master's thesis project (Pauly, 2016) that was supervised by the author where off-line lactate samples were used in order to automatically refresh the medium in a perfusion bioreactor setup by controlling a pump (Figure 8.3A). To overcome the information gap caused by the off-line monitoring, a predictive data-based model was used to predict future lactate production values, based on which in turn an 'on-line' controller was able to contain the lactate concentration in the bioreactor within a certain range, ultimately providing a better controlled environment for cell growth (Figure 8.3B). A similar control strategy could be used for analytes that are currently impossible to measure on-line but that have a significant effect on the quality of the cells (e.g. expression level of a certain protein).

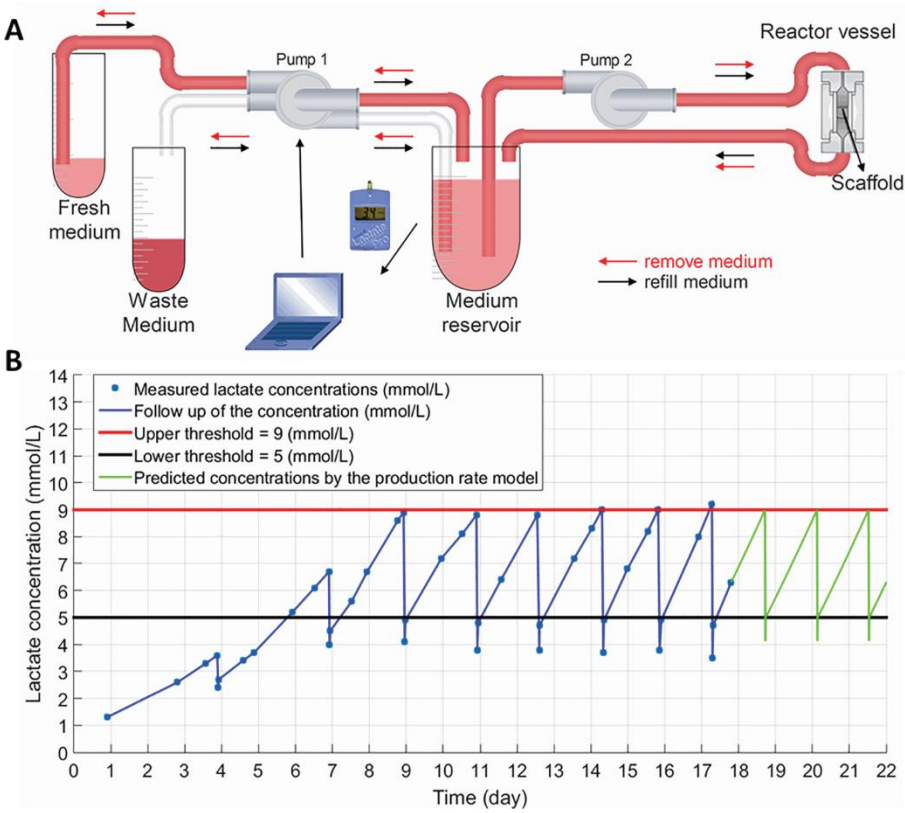

Figure 8.3: Setup and performance of lactate-based medium refreshment with a data-based model predictive control strategy.
A) Perfusion bioreactor setup with the perfusion loop on the right side (pump 2) and the lactate-based controller loop for medium refreshment on the left. B) Situation at the end of day 17 in culture where after an initial learning period for the data-based model the lactate concentration within the bioreactor circuit is automatically controlled within a certain range by optimising the medium refreshments. The green line indicates the expected evolution of the lactate concentration over the next 3 days.

Since these type of off-line measurements often still require significant manual sample preparation and time consuming handling, they are difficult to implement in cost-effective industrialised cell-based processes. However, the development of sensor hardware is continuously progressing and efforts are made to develop novel solutions for the on-line monitoring of biomarkers (Mandenius and Gustavsson, 2015; Polizzi and Kontoravdi, 2014; Zhao et al., 2015). Promising non-destructive on-line sensing approaches are the miniaturisation of ELISA or flow cytometry techniques in combination with microfluidic platforms and automated sampling (Eggeling et al., 2015), or

high-throughput use of mass spectrometry for the analysis of metabolic parameters in spent culture medium, i.e. exo-metabolomics (Kell et al., 2005).

It could be stated that having an on-line non-invasive and cost-efficient process read-out that is directly linked to the *in vivo* functionality of the cells is the holy grail in cell-based therapy manufacturing. It is not only critical in terms of optimising bioprocesses and to continuously assure the quality of the product during its life cycle (from development phase to the clinical production and potential post-approval changes), ultimately a properly controlled production system significantly facilitates regulatory approval.

8.2.3. Large-scale cell expansion and product safety

While the scientific literature is rife with reports on mouse cells that accumulate chromosomal instabilities during long term *in vitro* culture that lead to malignant transformation of these cells (Miura et al., 2006), there are conflicting reports on the spontaneous malignant transformation of human cells that are cultured *in vitro* (Bernardo et al., 2007; Røsland et al., 2009). However, since DNA damage might occur at any time, these transformations are a potential risk for any cell therapy. The risk is higher for embryonic stem cells and induced pluripotent (iPS) cells since these have a close to unlimited expansion capability and their pluripotency allows them to differentiate in any type of tissue. For the more adult multipotent mesenchymal stem cells (MSCs) or progenitor cells the risk is inherently lower since they generally undergo replicative senescence due to telomere shortening.

After the first reported (Rubio et al., 2005) human mesenchymal cells that allegedly underwent spontaneous transformation during *in vitro* culture was retracted due to cross-contamination with a cancerous cell line (followed by another similar case (Torsvik et al., 2010)), there are still a couple of studies that seem to confirm the accumulation of DNA damage during culture. For example a large scale study (4 cell therapy facilities during 2 multicentre clinical trials) on human bone marrow derived MSCs, detected certain (donor dependent) chromosomal changes that, in this case, only induced cell senescence without malignant transformation (Tarte et al., 2010). Prockop et al. (2010) claim that "clinical experience so far shows that if the cells [MSCs] are harvested for therapy well before the cultures reach senescence, there is a very low probability of malignant transformation and tumour formation in patients". This claim seems to be confirmed by Casiraghi et al. (2013) who reviewed the reported side effects (including the development of hematopoietic or solid tumours) after MSC administration in more than 700 patients in clinical studies.

Disregarding the low chance of occurrence, in any case it has to be considered whether the very high number of population doublings are really beneficial for a certain therapy and whether it is the best strategy to push the cell senescence further and further. On the other hand, spontaneous malignant transformation of MSCs might naturally occur in the human body (Houghton et al., 2004) and this raises the question whether current detection assays are sensitive enough to detect transformations in culture above the natural baseline of transformations (especially if the effect of immunosuppressive treatment, as used in allogeneic cell therapies, on cancer is taken into consideration (Grulich et al., 2007)). With more sensitive detection assays it might be possible that new effects of extensive *in vitro* culture of cells becomes apparent. For example, only very recently an age related accumulation of mitochondrial genome mutations was found in *in vitro* expanded IPS cells that influenced the cell metabolism (Kang et al., 2016). While the risk of transformations is low for human MSCs (Prockop, 2010) and the benefits of most cell-based treatments far outweigh this risk, it is advisable to remain vigilant for unwanted cell transformations until more sensitive screening technology is able to provide a definitive proof of the absence of very small numbers of potentially malignant cells.

8.2.4. Reduction of Cost Of Goods remains crucial for widespread clinical translation of cell-based therapies

Prochymal, the mesenchymal stem cell based treatment for Graft-versus-Host disease as used for the introduced in Chapter 1 costs around $200K for a course of therapy in a paediatric setting (SCSI, 2013). This would roughly compare to the price of an allogeneic bone marrow transplant (including costs of care) (Majhail et al., 2013). Although expensive, an even more mind-boggling price is the $1 million treatment with Glybera, a gene therapy developed by UniQure that uses insect cell-based manufacturing of the vector for the treatment of a rare disease called lipoprotein lipase deficiency, and which is approved by the EMA for clinical use in Europe. While such high prices are currently the exception, the challenging production processes and regulatory requirements for cell-based products lead to significant price raises compared to more standard treatments. Therefore, for every product that is being developed, the question is raised whether its costs are justifiable compared to the clinical added value for the patient. Especially for non-life threatening diseases, the cost-effectiveness of a cell-based product compared to a generally much cheaper standard treatment should be carefully examined. While trying to avoid the discussion on setting a price on a person's life, or on the quality thereof, it is clear that with some of these prices widespread clinical translation of cell therapies is difficult to support, especially in the

current economic environment where large pressure is exerted to reduce healthcare costs.

Particularly for autologous therapies, where the production and quality control costs cannot be spread over a large number of patients/clients, a significant reduction of the COGS (cost of goods sold) is of primary importance before a commercially viable therapy will be able to gain widespread clinical application. There are quite some examples for autologous cell-based therapies that struggle to translate the positive clinical results to the company's bottom line (e.g. Dendreon's Provenge). This motivates manufacturers of cell-based products to focus on reduction of production costs by introducing novel production technologies for process optimisation and automation for stand-alone point-of-care production of cell-based therapies (Rathore and Singh, 2015). A thorough evaluation of potential strategies for scale-up of autologous cell expansion early on in the development phase, as done here in Chapter 4 and 6, is a first step towards cost-efficiency. Since recently, strategies able to increase the cell potency are explored (Stegen et al., 2016), for example by cell priming steps or cell pre-selection by magnetic-activated cell sorting (MACS) or fluorescence-activated cell sorting (FACS). While these strategies are still expensive and currently still in the exploratory phase, these efforts might later lead to significantly more potent cells for autologous therapies, therefore requiring lower number of cells, and subsequently reducing the overall cost of the therapy.

For allogeneic therapies the economies of scale should be exploited to a maximum in order to drive down the production costs. Here the challenge is to manufacture reproducible, clinical-grade stem cells in mass quantities for a reasonable cost. Process harmonisation and standardisation will eventually become important considerations. Again here the allogeneic use of IPSC technology, under the form of a master cell bank with cell lines that are able to differentiate to multiple cell types guided by standardised protocols, hold great potential (Rao and Atala, 2016), and is since recently commercially exploited by companies such as Cynata therapeutics (cynata.com) and an initiative of Lonza and the National Institutes for Health (National Institutes of Health, 2016).

8.3. Overall conclusion

In the introductory chapter, two challenges were identified that hamper the translation of promising lab-scale strategies for cell-based treatments to

commercial cell therapies. First, for large-scale cultures, the gold standard flask-based cell expansion process should be translated to a more integrated bioprocess design that is able to produce cells for therapeutic products in a cost-effective and robust way. Secondly, novel monitoring strategies are needed that allow to control these bioprocesses in order to reduce process variability and improve *in vivo* potential of the cells.

This work attempted to contribute to this scientific challenge by pursuing three different but closely related aims (see Figure 8.4 below for an overview):

The first objective was to provide a framework for benchmarking cell expansion processes, so that during the development of integrated bioprocess designs an objective measure could be used when comparing different expansion processes. In Chapter 3 an interactive tool and metrics for such process comparison were presented that increases insight in process development.

The second objective was to translate the standard flask-based expansion process for the autologous Prometheus ATMP to an automated and controlled bioreactor-based process. In this way the manual manipulations required for the standard flask-based culture, which are associated with an expensive labour force and potential introduction of operator errors and contamination, can be reduced. Both Chapter 4 and Chapter 6 introduce a comprehensive bioreactor-based cell expansion strategy for which the quality of the resulting cells complied with a basic reference quality profile consisting of both *in vivo* and *in vitro* read-outs.

The third objective was to incorporate cost-effective data-based monitoring and control strategies in the large-scale production processes in order to deliver cells with a more robust quality profile and assure process comparability. Given the inherent biological variability of cell-based processes it is critical to be able to keep track of the critical quality attributes of the cells during culture in order to assure the compliance to the reference quality profile. The data-based approach used here, in which data from regular process read-outs were used to infer knowledge on the critical attributes, is compelling as often there are no on-line measurements available on these parameters. Additionally the on-line model-based control approach is able to take into account the time-varying donor specific cell characteristics, thus potentially offering a tool to deal with donor-to-donor variability. Chapter 4, 5, 6 and 7 provide monitoring tools for cell number determination, cell

detachment during harvest and donor-induced variability that allow to make informed process decisions, while Chapter 5 and Chapter 6 provide exploratory examples of how on-line control can ultimately result in a cell-based products of higher quality.

It is clear that the development of monitored and controlled cell expansion processes for cell-based therapies requires innovative insights from multiple disciplines. It involves a challenging mixture of fundamental biology, unique production technologies and the appropriate data analytics that all need to converge into one efficient process. While there are still hurdles remaining, significant progress is being made to enable the wide-spread clinical use of cell-based therapies.

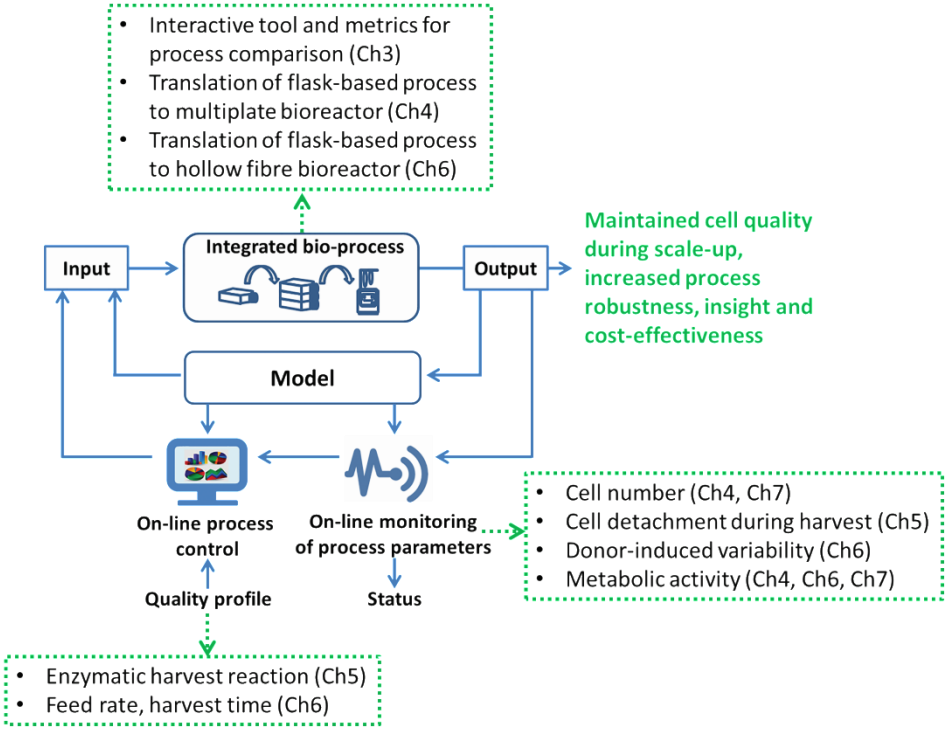

Figure 8.4: Schematic overview of the different aspects that were addressed and the obtained results during this PhD project.

Bibliography

Aehle M, Bork K, Schaepe S, Kuprijanov A, Horstkorte R, Simutis R, Lubbert A. 2012. Increasing batch-to-batch reproducibility of CHO-cell cultures using a model predictive control approach. *Cytotechnology* **64**:623–634.

Ali R, Gooding M, Szilágyi T, Vojnovic B, Christlieb M, Brady M. 2012a. Automatic segmentation of adherent biological cell boundaries and nuclei from brightfield microscopy images. JOUR. *Mach. Vis. Appl.* **23**:607–621.

Ali R, Gooding M, Szilágyi T, Vojnovic B, Christlieb M, Brady M. 2012b. Automatic segmentation of adherent biological cell boundaries and nuclei from brightfield microscopy images. *Mach. Vis. Appl.* **23**:607–621.

Archibald PRT, Chandra A, Thomas D, Morley G, Lekishvili T, Devonshire A, Williams DJ. 2015. Comparability of scalable, automated hMSC culture using manual and automated process steps. *Biochem. Eng. J.*:1–15.

de Assis AJ, Filho RM. 2000. Soft sensors development for on-line bioreactor state estimation. *Comput. Chem. Eng.* **24**:1099–1103.

Van Bael S, Kerckhofs G, Moesen M, Pyka G, Schrooten J, Kruth JP. 2011. Micro-CT-based improvement of geometrical and mechanical controllability of selective laser melted Ti6Al4V porous structures. *Mater. Sci. Eng. A* **528**:7423–7431.

Baghbaderani BA, Tian X, Neo BH, Burkall A, Dimezzo T, Sierra G, Zeng X, Warren K, Kovarcik DP, Fellner T, Rao MS. 2015. CGMP-manufactured human induced pluripotent stem cells are available for pre-clinical and clinical applications. *Stem Cell Reports* **5**:647–659.

Baksh D, Yao R, Tuan RS. 2007. Comparison of proliferative and multilineage differentiation potential of human mesenchymal stem cells derived from umbilical cord and bone marrow. *Stem Cells* **25**:1384–1392.

Balint R, Richardson SM, Cartmell SH. 2015. Low-density subculture: a technical note on the importance of avoiding cell-to-cell contact during mesenchymal stromal cell expansion. JOUR. *J. Tissue Eng. Regen. Med.* **9**:1200–1203.

Bara JJ, Richards RG, Alini M, Stoddart MJ. 2014. Concise review: bone marrow-derived mesenchymal stem cells change phenotype following in vitro culture: implications for basic research and the clinic. *Stem Cells* **32**:1713–23.

De Bari C, Dell'Accio F, Luyten FP. 2001a. Human periosteum-derived cells maintain phenotypic stability and chondrogenic potential throughout expansion regardless of donor age. *Arthritis Rheum.* **44**:85–95.

De Bari C, Dell'Accio F, Tylzanowski P, Luyten FP. 2001b. Multipotent mesenchymal stem cells from adult human synovial membrane. JOUR. *Arthritis Rheum.* **44**:1928–1942.

De Bari C, Dell'Accio F, Vanlauwe J, Eyckmans J, Khan IM, Archer CW, Jones E a, McGonagle D, Mitsiadis T a, Pitzalis C, Luyten FP. 2006. Mesenchymal multipotency of adult human periosteal cells demonstrated by single-cell lineage analysis. *Arthritis Rheum.* **54**:1209–21.

Bartunek J, Behfar A, Dolatabadi D, Vanderheyden M, Ostojic M, Dens J, El Nakadi B, Banovic M, Beleslin B, Vrolix M, Legrand V, Vrints C, Vanoverschelde JL, Crespo-Diaz R, Homsy C, Tendera M, Waldman S, Wijns W, Terzic A. 2013. Cardiopoietic Stem Cell Therapy in Heart Failure. *J. Am.*

Coll. Cardiol. **61**:2329–2338.

Beitzel K, McCarthy MBR, Cote MP, Durant TJS, Chowaniec DM, Solovyova O, Russell RP, Arciero RA, Mazzocca AD. 2013. Comparison of Mesenchymal Stem Cells (Osteoprogenitors) Harvested From Proximal Humerus and Distal Femur During Arthroscopic Surgery. *Arthrosc. J. Arthrosc. Relat. Surg.* **29**:301–308.

Berckmans. 2008. Precision livestock farming (PLF) - Preface. *Comput. Electron. Agric.* **62**:1–1.

Bernardo ME, Zaffaroni N, Novara F, Cometa AM, Avanzini MA, Moretta A, Montagna D, Maccario R, Villa R, Daidone MG, Zuffardi O, Locatelli F. 2007. Human bone marrow-derived mesenchymal stem cells do not undergo transformation after long-term in vitro culture and do not exhibit telomere maintenance mechanisms. *Cancer Res.* **67**:9142–9149.

Bianco P, Cao X, Frenette PS, Mao JJ, Robey PG, Simmons PJ, Wang C-Y. 2014. The meaning, the sense and the significance: Translating the science of mesenchymal stem cells into medicine. *Nat Med.* **19**:35–42.

Bianco P, Robey PG, Simmons PJ. 2008. Mesenchymal Stem Cells: Revisiting History, Concepts, and Assays. JOUR. *Cell Stem Cell* **2**:313–319.

Bluma A, Höpfner T, Prediger A, Glindkamp A, Beutel S, Scheper T. 2011. Process analytical sensors and image-based techniques for single-use bioreactors. *Eng. Life Sci.* **11**:550–553.

Bovy T, Fairbank A, Farid SS. 2015. Designing the Most Cost-Effective Manufacturing Strategy for Allogeneic Cell-Based Strategies. *Bioprocess Int.* **13**:36–43.

Braccini A, Wendt D, Jaquiery C, Jakob M, Heberer M, Kenins L, Wodnar-Filipowicz A, Quarto R, Martin I. 2005. Three-Dimensional Perfusion Culture of Human Bone Marrow Cells and Generation of Osteoinductive Grafts. *Stem Cells* **23**:1066–1072.

Brandenberger R, Burger S, Campbell A, Fong T, Lapinska E, Rowley J a. 2011. Cell therapy bioprocessing. *Bioprocess Int* **9**:30–37.

Bravery C a., Carmen J, Fong T, Oprea W, Hoogendoorn KH, Woda J, Burger SR, Rowley JA, Bonyhadi ML, Van'T Hof W. 2013. Potency assay development for cellular therapy products: An ISCT review of the requirements and experiences in the industry. JOUR. *Cytotherapy* **15**:9–19.

Bravery CA, French A. 2014. Reference materials for cellular therapeutics. JOUR. *Cytotherapy* **16**:1187–1196.

Brindley DA, Davie NL, Sahlman WA, Bonfiglio GA, Culme-Seymour EJ, Reeve BC, Mason C. 2012. Promising growth and investment in the cell therapy industry during the first quarter of 2012. *Cell Stem Cell* **10**:492–6.

Brosilow C, Joseph B. 2002. Techniques of Model-Based Control. *Prentice-Hall Int. Ser. Phys. Chem. Eng. Sci.* Prentice Hall xxi, 680 p.

Camacho EF, Bordons C. 2007. Introduction to Model Predictive Control. Inbook. In: . *Model Predict. Control*. London: Springer London, pp. 1–11.

Carvalho PP, Wu X, Yu G, Dietrich M, Dias IR, Gomes ME, Reis RL, Gimble JM. 2011. Use of animal protein-free products for passaging adherent human adipose-derived stromal/stem cells. JOUR. *Cytotherapy* **13**:594–597.

Casiraghi F, Remuzzi G, Abbate M, Perico N. 2013. Multipotent Mesenchymal Stromal Cell Therapy and Risk of Malignancies. *Stem Cell Rev. Reports* **9**:65–79.

Castillo J, Egloff M, Collignon F, Goffinet J, Drugmand J. 2013. Transfer of hepatic progenitor stem cell culture process from multiple tray stacks to the xpansion multiplate bioreactor. *Cytotherapy* **15**:S20.

CAT (Committee for Advanced Therapies). 2010. Challenges with advanced therapy medicinal products and how to meet them. *Nat Rev Drug Discov* **9**:195–201.

Chai YC, Kerckhofs G, Roberts SJ, Van Bael S, Schepers E, Vleugels J, Luyten FP, Schrooten J. 2012a. Ectopic bone formation by 3D porous calcium phosphate-Ti6Al4V hybrids produced by perfusion electrodeposition. *Biomaterials* **33**:4044–58.

Chai YC, Roberts SJ, Desmet E, Kerckhofs G, van Gastel N, Geris L, Carmeliet G, Schrooten J, Luyten FP. 2012b. Mechanisms of ectopic bone formation by human osteoprogenitor cells on CaP biomaterial carriers. *Biomaterials* **33**:3127–42.

Chatfield C. 2004. The analysis of time series. Chapman & Hall.

Chen AK-L, Chen X, Choo ABH, Reuveny S, Oh SKW. 2011. Critical microcarrier properties affecting the expansion of undifferentiated human embryonic stem cells. Article. *Stem Cell Res.* **7**:97–111.

Chen Y, Sonnaert M, Roberts SJ, Luyten FP, Schrooten J. 2012. Validation of a PicoGreen-Based DNA Quantification Integrated in an RNA Extraction Method for Two-Dimensional and Three-Dimensional Cell Cultures. *Tissue Eng Part C* **18**:444–452.

Cierpka K, Elseberg CL, Niss K, Kassem M, Salzig D, Czermak P. 2013. hMSC Production in Disposable

Bioreactors with Regards to GMP and PAT. *Chemie Ing. Tech.* **85**:67–75.
Cioffi M, Kuffer J, Strobel S, Dubini G, Martin I, Wendt D. 2008. Computational evaluation of oxygen and shear stress distributions in 3D perfusion culture systems: macro-scale and micro-structured models. Journal Article. *J Biomech* **41**:2918–2925.
Cochran DM, Fukumura D, Ancukiewicz M, Carmeliet P, Jain RK. 2006. Evolution of oxygen and glucose concentration profiles in a tissue-mimetic culture system of embryonic stem cells. *Ann. Biomed. Eng.* **34**:1247–58.
Croughan MS, Konstantinov KB, Cooney C. 2015. The future of industrial bioprocessing: Batch or continuous? *Biotechnol. Bioeng.* **9999**:n/a-n/a.
Csaszar E, Chen K, Caldwell J, Chan W, Zandstra PW. 2013. Real-time monitoring and control of soluble signaling factors enables enhanced progenitor cell outputs from human cord blood stem cell cultures. *Biotechnol. Bioeng.* **9999**:1–7.
Csaszar E, Kirouac DC, Yu M, Wang W, Qiao W, Cooke MP, Boitano AE, Ito C, Zandstra PW. 2012. Rapid expansion of human hematopoietic stem cells by automated control of inhibitory feedback signaling. *Cell Stem Cell* **10**:218–29.
Culme-Seymour EJ, Edwards-Parton S, Carmen J, Folkerts W, Smith D, Mason C. 2013. A new cell therapy sector arising from the convergence of cell and gene therapy. JOUR. *Cytotherapy* **15**:S52.
Culme-Seymour EJ, Davie NL, Brindley D a, Edwards-Parton S, Mason C. 2012. A decade of cell therapy clinical trials (2000–2010). *Regen. Med.* **7**:455–462.
Culme-Seymour EJ, Davies JL, Hitchcock J, Mason J, Carpenter MK, Mason C. 2015. Cell Therapy Regulatory Toolkit : an online regulatory resource. JOUR. *Regen. Med.* **10**:531–534.
Cunha BB, Aguiar T, Silva MM, Silva RJS, Sousa MFQQ, Pineda E, Peixoto C, Carrondo MJTT, Serra M, Alves PM. 2015a. Exploring continuous and integrated strategies for the up- and downstream processing of human mesenchymal stem cells. JOUR. *J. Biotechnol.* **213**:1–12.
Cunha B, Peixoto C, Silva MM, Carrondo MJT, Serra M, Alves PM. 2015b. Filtration methodologies for the clarification and concentration of human mesenchymal stem cells. *J. Memb. Sci.* **478**:117–129.
Cunha B, Silva RJS, Aguiar T, Serra M, Daicic J, Maloisel J, Clachan J, Åkerblom A, Carrondo MJT, Peixoto C, Alves PM. 2016. Improving washing strategies of human mesenchymal stem cells using negative mode expanded bed chromatography. JOUR. *J. Chromatogr. A* **1429**:292–303.
Curran KJ, Brentjens RJ, Sloan M, Cancer K, York N. 2015. Chimeric Antigen Receptor T Cells for Cancer Immunotherapy.
Das RHJ, van Osch GJVM, Kreukniet M, Oostra J, Weinans H, Jahr H. 2010. Effects of individual control of pH and hypoxia in chondrocyte culture. *J. Orthop. Res.* **28**:537–45.
Davie NL, Brindley D a, Culme-seymour EJ, Mason C. 2012. Streamlining Cell Therapy Manufacture. *Bioprocess Int.* **10**:24–49.
Deans R. 2015. Towards the creation of a standard MSC line as a calibration tool. JOUR. *Cytotherapy* **17**:1167–1168.
DeFrancesco L. 2012. Adult stem cell therapies walk the line. *Nat. Biotechnol.* **30**:739–41.
Delahaye M, Lawrence K, Ward S, Hoare M. 2014. An ultra scale-down analysis of the recovery by dead-end centrifugation of human cells for therapy. *Biotechnol. Bioeng.*:n/a-n/a.
Diogo MM, da Silva CL, Cabral JMS. 2012. Separation technologies for stem cell bioprocessing. JOUR. *Biotechnol. Bioeng.* **109**:2699–2709.
Dolgin E. 2014. Better standards sought for range of stem cells entering the clinic. JOUR. *Nat. Med.* **20**:797–798.
Dominici M, Le Blanc K, Mueller I, Slaper-Cortenbach I, Marini F, Krause D, Deans R, Keating a, Prockop D, Horwitz E. 2006. Minimal criteria for defining multipotent mesenchymal stromal cells. The International Society for Cellular Therapy position statement. JOUR. *Cytotherapy* **8**:315–7.
Dorresteijn RC, Numan KH, de Gooijer CD, Tramper J, Beuvery EC. 1996. On-line estimation of the biomass activity during animal-cell cultivations. *Biotechnol. Bioeng.* **51**:206–14.
Eggeling L, Bott M, Marienhagen J. 2015. Novel screening methods-biosensors. *Curr. Opin. Biotechnol.* **35**:30–36.
Egloff M, Castillo J. 2012. Scaling up stem cells. *Bioprocess Int.* **10**:62–64.
EMA. 2014. Guideline on process validation for finished products - information and data to be provided in regulatory submissions 1-15 p.
European Comission. 2012. PHARMACEUTICAL COMMITTEE 22 October 2012. *Eur. Comm.* 1-14 p.
Eyckmans J, Roberts SJ, Schrooten J, Luyten FP. 2010. A clinically relevant model of osteoinduction: a process requiring calcium phosphate and BMP/Wnt signalling. *J. Cell. Mol. Med.* **14**:1845–56.
Eyckmans J, Luyten FP. 2006. Species Specificity of Ectopic Bone Formation Using Periosteum-Derived

Mesenchymal Progenitor Cells. JOUR. *Tissue Eng* **12**:2203–13.

FDA. 2011. Guidance for Industry Process Validation : General Principles and Practices.

Fennema EME, Renard AJSA, Leusink A, van Blitterswijk CA, de Boer J. 2009. The effect of bone marrow aspiration strategy on the yield and quality of human mesenchymal stem cells. JOUR. *Acta Orthop.* **80**:618–21.

Foley L, Whitaker M. 2012. Concise Review: Cell Therapies: The Route to Widespread Adoption. *Stem Cells Transl. Med.* **1**:438–447.

Friel JJ. 2000. Practical Guide to Image Analysis. JOUR. ASM International.

Galipeau J. 2013. The mesenchymal stromal cells dilemma-does a negative phase III trial of random donor mesenchymal stromal cells in steroid-resistant graft-versus-host disease represent a death knell or a bump in the road? *Cytotherapy* **15**:2–8.

Glassey J, Gernaey K V, Clemens C, Schulz TW, Oliveira R, Striedner G, Mandenius C-F. 2011. Process analytical technology (PAT) for biopharmaceuticals. *Biotechnol. J.* **6**:369–77.

Gottipamula S, Muttigi MS, Kolkundkar U, Al. E. 2013. Serum-free media for the production of human mesenchymal stromal cells: a review. JOUR. *Cell Prolif* **46**:608–627.

Grayson WL, Marolt D, Bhumiratana S, Fröhlich M, Guo XE, Vunjak-Novakovic G. 2011. Optimizing the medium perfusion rate in bone tissue engineering bioreactors. *Biotechnol. Bioeng.* **108**:1159–70.

Grulich AE, van Leeuwen MT, Falster MO, Vajdic CM. 2007. Incidence of cancers in people with HIV / AIDS compared with immunosuppressed transplant recipients: a meta-analysis. *Lancet* **370**:59–67.

Hanley PJ, Mei Z, Durett AG, Cabreira-harrison MDAG, Klis M, Li WEI, Zhao Y, Yang B, Parsha K, Mir O, Vahidy F, Bloom D, Rice RB, Hematti P, Savitz SI, Gee AP, da Graca Cabreira-Harrison M, Klis M, Li WEI, Zhao Y, Yang B, Parsha K, Mir O, Vahidy F, Bloom D, Rice RB, Hematti P, Savitz SI, Gee AP. 2014. Efficient manufacturing of therapeutic mesenchymal stromal cells with the use of the Quantum Cell Expansion System. JOUR. *Cytotherapy* **16**:1449.

Haredasht SA, Barrios JM, Maes P, Verstraeten WW, Clement J, Ducoffre G, Lagrou K, Ranst M Van, Coppin P, Berckmans D, Aerts J-M. 2011. A dynamic data-based model describing nephropathia epidemica in Belgium. *Biosyst. Eng.* **109**:77–89.

van Harmelen V, Röhrig K, Hauner H. 2004. Comparison of proliferation and differentiation capacity of human adipocyte precursor cells from the omental and subcutaneous adipose tissue depot of obese subjects. Article. *Metabolism* **53**:632–637.

Harris D, Rogers I. 2007. Umbilical Cord Blood: A Unique Source of Pluripotent Stem Cells for Regenerative Medicine. Journal. *Curr. Stem Cell Res. Ther.*

Hassan S, Simaria AS, Varadaraju H, Siddharth G, Warren K, Farid SS, Gupta S, Warren K, Farid SS. 2015. Allogeneic cell therapy bioprocess economics and optimization: downstream processing decisions. JOUR. *Regen. Med.* **10**:591–609.

Heathman TRJ, Nienow W, Mccall MJ, Coopman K, Kara B, Hewitt CJ. 2015a. The translation of cell-based therapies : clinical landscape and manufacturing challenges. *Regen. Med.* **10**:49–64.

Heathman TRJ, Rafiq Q a., Chan AKC, Coopman K, Nienow AW, Kara B, Hewitt CJ. 2015b. Characterisation of human mesenchymal stem cells from multiple donors and the implications for large scale bioprocess development. *Biochem. Eng. J.*

Heathman TRJ, Stolzing A, Fabian C, Rafiq QA, Coopman K, Nienow AW, Kara B, Hewitt CJ. 2015c. Serum-free process development: improving the yield and consistency of human mesenchymal stromal cell production. *Cytotherapy* **17**:1524–1535.

Heathman TRJ, Glyn VAM, Picken A, Rafiq QA, Coopman K, Nienow AW, Kara B, Hewitt CJ. 2015d. Expansion, harvest and cryopreservation of human mesenchymal stem cells in a serum-free microcarrier process. JOUR. *Biotechnol. Bioeng.* **112**:1696–1707.

Herzenberg L a, Tung J, Moore W a, Herzenberg L a, Parks DR. 2006. Interpreting flow cytometry data: a guide for the perplexed. *Nat. Immunol.* **7**:681–685.

Higuera G, Sc M, Schop D, Janssen F, Dijkhuizen-radersma R Van, Ph D, Boxtel T Van, Blitterswijk CA Van, van Dijkhuizen-Radersma R, van Boxtel T, van Blitterswijk C a. 2009. Quantifying in vitro growth and metabolism kinetics of human mesenchymal stem cells using a mathematical model. *Tissue Eng. Part A* **15**:2653–63.

Houghton J, Stoicov C, Nomura S, Rogers AB, Carlson J, Li H, Cai X, Fox JG, Goldenring JR, Wang TC. 2004. Gastric Cancer Originating from Bone Marrow-Derived Cells. JOUR. *Science (80-.).* **306**:1568–1571.

Hourd P, Chandra A, Medcalf N, Williams DJ. 2008. Regulatory challenges for the manufacture and scale-out of autologous cell therapies. *StemBook*:1–13.

Hourd P, Ginty P, Chandra A, Williams DJ. 2014. Manufacturing models permitting roll out/scale out of

clinically led autologous cell therapies: Regulatory and scientific challenges for comparability. *Cytotherapy* **16**:1033–1047.

Hulspas R. 2010. Titration of fluorochrome-conjugated antibodies for labeling cell surface markers on live cells. *Curr. Protoc. Cytom.*:1–9.

ICH. 2009. Q8(R2) Pharmaceutical Development. *Ich* **8**:1–29.

ICH Expert Working Group. 2000. Good Manufacturing Practice Guide for Active Pharmaceutical Ingredients Q7. *ICH Harmon. Tripart. Guidel.*:49.

Impens S, Chen Y, Mullens S, Luyten F, Schrooten J. 2010. Controlled Cell-Seeding Methodologies : A First Step Toward Clinically Relevant Bone Tissue Engineering Strategies. *Tissue Eng Part C* **16**:1575–83.

Jaasma MJ, Plunkett NA, O'Brien FJ. 2008. Design and validation of a dynamic flow perfusion bioreactor for use with compliant tissue engineering scaffolds. JOUR. *J. Biotechnol.* **133**:490–496.

Jaccard N, Griffin LD, Keser A, Macown RJ, Super A, Veraitch FS, Szita N. 2014. Automated method for the rapid and precise estimation of adherent cell culture characteristics from phase contrast microscopy images. *Biotechnol. Bioeng.* **111**:504–17.

Jacquemart R, Chavane N, Durocher Y, Hoemann C, De Crescenzo G, Jolicoeur M. 2008. At-line monitoring of bioreactor protein production by surface plasmon resonance. Article. *Biotechnol. Bioeng.* **100**:184–188.

Jakob M, Saxer F, Scotti C, Schreiner S, Studer P, Scherberich A, Heberer M, Martin I. 2012. Perspective on the evolution of cell-based bone tissue engineering strategies. Journal Article. *Eur Surg Res* **49**:1–7.

Janssen FW, Hofland I, van Oorschot A, Oostra J, Peters H, van Blitterswijk CA. 2006. Online measurement of oxygen consumption by goat bone marrow stromal cells in a combined cell-seeding and proliferation perfusion bioreactor. Journal Article. *J Biomed Mater Res A* **79**:338–348.

Jenkins MJ, Farid SS. 2015. Human pluripotent stem cell-derived products: Advances towards robust, scalable and cost-effective manufacturing strategies. JOUR. *Biotechnol. J.* **10**:83–95.

Jerri AJ. 1977. The Shannon Sampling Theorem - Its Various Extensions and Applications. *Proc. IEEE* **65**:1565–1596.

Jin H, Bae Y, Kim M, Kwon S-J, Jeon H, Choi S, Kim S, Yang Y, Oh W, Chang J. 2013. Comparative Analysis of Human Mesenchymal Stem Cells from Bone Marrow, Adipose Tissue, and Umbilical Cord Blood as Sources of Cell Therapy. *Int. J. Mol. Sci.* **14**:17986–18001.

Jing D, Punreddy S, Sunil N, Aysola M, Murrel J, Niss K. 2013. Characterization of Human Mesenchymal Stem Cells: Expansion in a 3-L, Single-Use, Stirred-Tank Bioreactor. *Bioprocess Int.* **11**:30–36.

Jung S, Panchalingam KM, Wuerth RD, Rosenberg L, Behie L a. 2012. Large-scale production of human mesenchymal stem cells for clinical applications. *Biotechnol. Appl. Biochem.* **59**:106–20.

Junker BH, Wang HY. 2006. Bioprocess Monitoring and Computer Control: Key Roots of the Current PAT Initiative. *Biotechnol. Bioeng.* **95**:226–261.

Kadlec P, Gabrys B, Strandt S. 2009. Data-driven Soft Sensors in the process industry. *Comput. Chem. Eng.* **33**:795–814.

Kaiser AD, Assenmacher M, Schröder B, Meyer M, Orentas R, Bethke U, Dropulic B. 2015. Towards a commercial process for the manufacture of genetically modified T cells for therapy. *Cancer Gene Ther.* **22**:72–78.

Kalman RE. 1960. Approach to Linear Filtering and Prediction Problems. JOUR. *J. Fluids Eng.* **82**:35–45.

Kalos M, Levine BL, Porter DL, Katz S, Grupp SA, Bagg A, June CH. 2011. T Cells with Chimeric Antigen Receptors Have Potent Antitumor Effects and Can Establish Memory in Patients with Advanced Leukemia. JOUR. *Sci. Transl. Med.* **3**:95ra73-95ra73.

Kang E, Wang X, Tippner-Hedges R, Ma H, Folmes CDL, Gutierrez NM, Lee Y, Van Dyken C, Ahmed R, Li Y, Koski A, Hayama T, Luo S, Harding CO, Amato P, Jensen J, Battaglia D, Lee D, Wu D, Terzic A, Wolf DP, Huang T, Mitalipov S. 2016. Age-related accumulation of somatic mitochondrial DNA mutations in adult-derived human ipscs. *Cell Stem Cell* **18**:625–636.

Kasper C, Griensven M van, Pörtner R. 2010. Bioreactor Systems for Tissue Engineering II: Strategies for the Expansion and Directed Differentiation of Stem Cells vol 2. Springer Science & Business Media 154-5 p.

Kell DB, Brown M, Davey HM, Dunn WB, Spasic I, Oliver SG. 2005. Metabolic footprinting and systems biology: the medium is the message. *Nat. Rev. Microbiol.* **3**:557–65.

Ker DFE, Weiss LE, Junkers SN, Chen M, Yin Z, Sandbothe MF, Huh S, Eom S, Bise R, Osuna-Highley E, Kanade T, Campbell PG. 2011. An engineered approach to stem cell culture: automating the decision process for real-time adaptive subculture of stem cells. JOUR. *PLoS One* **6**:e27672.

Kim J, Ma T. 2012. Perfusion regulation of hMSC microenvironment and osteogenic differentiation in 3D scaffold. *Biotechnol. Bioeng.* **109**:252–61.

King JA, Miller WM. 2008. Bioreactor Development for Stem Cell Expansion and Controlled Differentiation. *Curr Opin Chem Biol* **11**:394–398.

Kinzebach S, Bieback K. 2013. Expansion of Mesenchymal Stem/Stromal Cells under Xenogenic-Free Culture Conditions. JOUR. *Adv. Biochem. Eng. Biotechnol.* **129**:33–57.

Kirouac DC, Zandstra PW. 2008. The systematic production of cells for cell therapies. *Cell Stem Cell* **3**:369–81.

Kiviharju K, Salonen K, Moilanen U, Meskanen E, Leisola M, Eerikäinen T. 2007. On-line biomass measurements in bioreactor cultivations: comparison study of two on-line probes. *J Ind Microbiol Biotechnol* **34**:561–6.

Koc ON, Gerson SL, Cooper BW, Dyhouse SM, Haynesworth SE, Caplan AI, Lazarus HM. 2000. Rapid hematopoietic recovery after coinfusion of autologous-blood stem cells and culture-expanded marrow mesenchymal stem cells in advanced breast cancer patients receiving high-dose chemotherapy. JOUR. *J. Clin. Oncol.* **18**:307–316.

Kourti T. 2006. The Process Analytical Technology initiative and multivariate process analysis, monitoring and control. *Anal. Bioanal. Chem.* **384**:1043–8.

Koutinas M, Kiparissides A, Pistikopoulos EN, Mantalaris A. 2012. Bioprocess systems engineering: transferring traditional process engineering principles to industrial biotechnology. *Comput. Struct. Biotechnol. J.* **3**:1–9.

Kovarova-Kovar K, Gehlen S, Kunze A, Keller T, Von Daniken R, Kolb M, Van Loon APGM. 2000. Application of model-predictive control based on artificial neural networks to optimize the fed-batch process for riboflavin production. *J. Biotechnol.* **79**:39–52.

Kumar A, Starly B. 2015. Large scale industrialized cell expansion: producing the critical raw material for biofabrication processes. JOUR. *Biofabrication* **7**:44103.

Lambrechts T, Papantoniou I, Sonnaert M, Schrooten J, Aerts JM. 2014. Model-based cell number quantification using online single-oxygen sensor data for tissue engineering perfusion bioreactors. JOUR. *Biotechnol. Bioeng.* **111**:1982–1992.

Lambrechts T, Papantoniou I, Viazzi S, Bovy T, Schrooten J, Luyten FPP, Aerts J-MM. 2016a. Evaluation of a monitored multiplate bioreactor for large-scale expansion of human periosteum derived stem cells for bone tissue engineering applications. JOUR. *Biochem. Eng. J.* **108**:58–68.

Lambrechts T, Papantoniou I, Rice B, Schrooten J, Luyten FP, Aerts J-M. 2016b. Large-scale progenitor cell expansion for multiple donors in a monitored hollow fibre bioreactor. *Cytotherapy*.

Lammens J, Laumen A, Delport H, Vanlauwe J. 2012. The Pentaconcept in skeletal tissue engineering A combined approach for the repair of bone defects. *Acta Orthop. Belg.* **78**:569–573.

Larson BL, Ylostalo J, Lee RH, Gregory C, Prockop DJ. 2010. Sox11 is expressed in early progenitor human multipotent stromal cells and decreases with extensive expansion of the cells. JOUR. *Tissue Eng. Part A* **16**:3385–3394.

Ławryńczuk M. 2008. Modelling and nonlinear predictive control of a yeast fermentation biochemical reactor using neural networks. *Chem. Eng. J.* **145**:290–307.

Lechanteur C, Baila S, Janssens ME, Giet O, Briquet A, Baudoux E, Beguin Y. 2014. Large-Scale Clinical Expansion of Mesenchymal Stem Cells in the GMP-Compliant, Closed Automated Quantum® Cell Expansion System: Comparison with Expansion in Traditional T-Flasks. JOUR. *J. Stem Cell Res. Ther.* **4**:1–11.

Lefever J, Berckmans D, Aerts J-M. 2012. Time-variant modelling of heart rate responses to exercise intensity during road cycling. *Eur. J. Sport Sci.* **14**:1–7.

Leijten J, Chai YC, Papantoniou I, Geris L, Schrooten J, Luyten FP. 2015. Cell based advanced therapeutic medicinal products for bone repair: Keep it simple? JOUR. *Adv. Drug Deliv. Rev.* **84**:30–44.

Lewis MC, Macarthur BD, Malda J, Pettet G, Please CP. 2005. Heterogeneous proliferation within engineered cartilaginous tissue: the role of oxygen tension. *Biotechnol. Bioeng.* **91**:607–15.

Liu JKH. 2014. The history of monoclonal antibody development - Progress, remaining challenges and future innovations. *Ann. Med. Surg.* **3**:113–116.

Liu Y, Hourd P, Chandra A, Williams DJ. 2010. Human cell culture process capability: a comparison of manual and automated production. JOUR. *J. Tissue Eng. Regen. Med.* **4**:45–57.

Ljung L. 1999. System Identification: Theory for the User (2nd Edition): Hall Information and System Science Series. BOOK.

Van Loon K, Aerts J-M, Meyfroidt G, den Berghe G, Berckmans D. 2006. The Use of Multivariate Autoregressive Modelling for Analyzing Dynamical Physiological Responses of Individual

Critically Ill Patients. Inbook. In: Maglaveras, N, Chouvarda, I, Koutkias, V, Brause, R, editors. *Biol. Med. Data Anal. 7th Int. Symp. ISBMDA 2006, Thessaloniki, Greece, December 7-8, 2006. Proc.* Berlin, Heidelberg: Springer Berlin Heidelberg, pp. 285–297.

Ma T, Tsai AC, Liu Y. 2015. Biomanufacturing of human mesenchymal stem cells in cell therapy: Influence of microenvironment on scalable expansion in bioreactors. *Biochem. Eng. J.*

Maes F, Van Ransbeeck P, Van Oosterwyck H, Verdonck P. 2009. Modeling fluid flow through irregular scaffolds for perfusion bioreactors. *Biotechnol. Bioeng.* **103**:621–30.

Majhail NS, Mau LW, Denzen EM, Arneson TJ. 2013. Costs of autologous and allogeneic hematopoietic cell transplantation in the United States: a study using a large national private claims database. *Bone Marrow Transplant.* **48**:294–300.

Malda J, Klein TJ, Upton Z. 2007. The roles of hypoxia in the in vitro engineering of tissues. Journal Article. *Tissue Eng* **13**:2153–2162.

Mandenius CF, Gustavsson R. 2015. Mini-review: Soft sensors as means for PAT in the manufacture of bio-therapeutics. *J. Chem. Technol. Biotechnol.* **90**:215–227.

Mandenius C-F. 2016. Challenges for Bioreactor Design and Operation. CHAP. In: Mandenius, C-F, editor. *Bioreact. Des. Oper. Nov. Appl.* Wiley-VCH Verlag GmbH & Co. KGaA, pp. 1–34.

Marketsandmarkets. 2015. Antibody Production Market by Product, Type, Technology & by End-User - Analysis & Global Forecast to 2019 Title.

Martin I, Smith T, Wendt D. 2009. Bioreactor-based roadmap for the translation of tissue engineering strategies into clinical products. Journal Article. *Trends Biotechnol* **27**:495–502.

Martin I, Wendt D, Heberer M. 2004. The role of bioreactors in tissue engineering. Journal Article. *Trends Biotechnol* **22**:80–86.

Martin I, Mastrogiacomo M. 2002. Fluorescence microscopy imaging of bone for automated histomorphometry. *Tissue* **8**:847–52.

Martin PJ, Uberti JP, Soiffer RJ, Klingemann H, Waller EK, Daly AS, Herrmann RP, Kebriaei P. 2010. Prochymal Improves Response Rates In Patients With Steroid-Refractory Acute Graft Versus Host Disease (SR-GVHD) Involving The Liver And Gut: Results Of A Randomized, Placebo-Controlled, Multicenter Phase III Trial In GVHD. *Biol. Blood Marrow Transplant.* **16**:S169–S170.

Martino M, Mochizuki M, Rothenfluh DA, Rempel SA, Hubbell JA, Barker TH. 2009. Biomaterials Controlling integrin specificity and stem cell differentiation in 2D and 3D environments through regulation of fibronectin domain stability **30**:1089–1097.

Mason C, Dunnill P. 2008. A brief definition of regenerative medicine. *Regen. Med.* **3**:1–5.

Mason C, Dunnill P. 2009. Assessing the value of autologous and allogeneic cells for regenerative medicine. *Regen. Med.* **4**:835–853.

Mason C, Hoare M. 2007. Regenerative medicine bioprocessing: building a conceptual framework based on early studies. *Tissue Eng* **13**:301–11.

Mason C, Manzotti E. 2010. Regenerative medicine cell therapies: numbers of units manufactured and patients treated between 1988 and 2010. *Regen. Med.* **5**:307–13.

Masters JR, Stacey GN. 2007. Changing medium and passaging cell lines. JOUR. *Nat. Protoc.* **2**:2276–2284.

Mastri M, Shah Z, McLaughlin T, Greene CJ, Baum L, Suzuki G, Lee T. 2012. Activation of Toll-like receptor 3 (TLR3) amplifies mesenchymal stem cell trophic factors and enhances therapeutic potency. *AJP Cell Physiol.* **303**:1–21.

Matsuoka F, Takeuchi I, Agata H, Kagami H, Shiono H, Kiyota Y, Honda H, Kato R. 2013. Morphology-based prediction of osteogenic differentiation potential of human mesenchymal stem cells. JOUR. *PLoS One* **8**:e55082.

Maus M V, Grupp S a, Porter DL, June CH. 2014. Antibody-modified T cells: CARs take the front seat for hematologic malignancies. *Blood* **123**:2625–2635.

McCoy RJ, Jungreuthmayer C, O'Brien FJ. 2012. Influence of flow rate and scaffold pore size on cell behavior during mechanical stimulation in a flow perfusion bioreactor. *Biotechnol. Bioeng.* **109**:1583–94.

McKenna D, Matthay MA, Pati S. 2014. Correspondence to: soliciting strategies for developing cell-based reference materials to advance mesenchymal stem/stromal cell research and clinical translation. *Stem Cells Dev* **23**:1717–1718.

Meijering E. 2012. Cell Segmentation: 50 Years Down the Road. JOUR. *IEEE Signal Process. Mag.* **29**:140–145.

Mendicino M, Bailey AM, Wonnacott K, Puri RK, Bauer SR. 2014. MSC-based product characterization for clinical trials: An FDA perspective. JOUR. *Cell Stem Cell* **14**:141–145.

Meuwly F, Papp F, Ruffieux PA, Bernard AR, Kadouri A, von Stockar U. 2006. Use of glucose consumption rate (GCR) as a tool to monitor and control animal cell production processes in packed-bed bioreactors. Journal Article. *J Biotechnol* **122**:122–129.

Miura M, Miura Y, Padilla-Nash HM, Molinolo AA, Fu B, Patel V, Seo B-M, Sonoyama W, Zheng JJ, Baker CC, Chen W, Ried T, Shi S. 2006. Accumulated chromosomal instability in murine bone marrow mesenchymal stem cells leads to malignant transformation. *Stem Cells* **24**:1095–1103.

Mordor Intelligence. 2016. Global Stem Cell Market Growth, Trends and Forecasts (2015-2020).

Nash JE, Sutcliffe J V. 1970. River flow forecasting through conceptual models part I — A discussion of principles. BOOK. Vol. 10 282-290p.

National Institutes of Health. 2016. Manufactured stem cells to advance clinical research. https://www.nih.gov/news-events/manufactured-stem-cells-advance-clinical-research.

Nauta AJ, Fibbe WE. 2007. Immunomodulatory properties of mesenchymal stromal cells. JOUR. *Blood* **110**:3499–3506.

Nienow AW, Rafiq Q a., Coopman K, Hewitt CJ. 2014. A potentially scalable method for the harvesting of hMSCs from microcarriers. JOUR. *Biochem. Eng. J.* **85**:79–88.

Nienow AW, Hewitt CJ, Heathman TRJ, Glyn VAM, Fonte GN, Hanga MP, Coopman K, Rafiq QA. 2016. Agitation conditions for the culture and detachment of hMSCs from microcarriers in multiple bioreactor platforms. JOUR. *Biochem. Eng. J.* **108**:24–29.

Nold P, Brendel C, Neubauer A, Bein G, Hackstein H. 2013. Good manufacturing practice-compliant animal-free expansion of human bone marrow derived mesenchymal stroma cells in a closed hollow-fiber-based bioreactor. JOUR. *Biochem. Biophys. Res. Commun.* **430**:325–30.

Oedayrajsingh-Varma MJ, van Ham SM, Knippenberg M, Helder MN, Klein-Nulend J, Schouten TE, Ritt MJPF, van Milligen FJ. 2006. Adipose tissue-derived mesenchymal stem cell yield and growth characteristics are affected by the tissue-harvesting procedure. JOUR. *Cytotherapy* **8**:166–177.

Ogura F, Wakao S, Kuroda Y, Tsuchiyama K, Bagheri M, Heneidi S, Chazenbalk G, Aiba S, Dezawa M. 2014. Human adipose tissue possesses a unique population of pluripotent stem cells with nontumorigenic and low telomerase activities: potential implications in regenerative medicine. JOUR. *Stem Cells Dev.* **23**:717–28.

Ogura N, Kawada M, Chang W, Zhang Q, Lee S, Kondoh T, Abiko Y. 2004. Differentiation of the human mesenchymal stem cells derived from bone marrow and enhancement of cell attachment by fibronectin. *J. Oral Sci.* **46**:207–213.

Oliveira P, Silva C, Cabral J. 2014. Concise Review: Genomic Instability in Human Stem Cells: Current Status and Future Challenges. *Stem Cells* **32**:2824–2832.

Papantoniou I, Chai Y, Luyten FP, Schrooten J. 2013. Process Quality Engineering for Bioreactor-Driven Manufacturing of Tissue-Engineered Constructs for Bone Regeneration. *Tissue Eng Part C* **19**:1–14.

Papantoniou I, Mantalaris A, Sonnaert M, Lambrechts T, Aerts J-M, Geris L, Schrooten J. 2014. Chapter 21 – Product and Process Design: Toward Industrial TE Manufacturing. In: . *Tissue Eng.*, pp. 747–781.

Papas KK, Pisania A, Wu H, Weir GC, Colton CK. 2007. A Stirred Microchamber for Oxygen Consumption Rate Measurements With Pancreatic Islets. *Biotechnol. Bioeng.* **98**:1071–1082.

Pattappa G, Heywood HK, de Bruijn JD, Lee D a. 2011. The metabolism of human mesenchymal stem cells during proliferation and differentiation. *J. Cell. Physiol.* **226**:2562–2570.

Paull D, Sevilla A, Zhou H, Hahn AK, Kim H, Napolitano C, Tsankov A, Shang L, Krumholz K, Jagadeesan P, Woodard CM, Sun B, Vilboux T, Zimmer M, Forero E, Moroziewicz DN, Martinez H, Malicdan MC V, Weiss KA, Vensand LB, Dusenberry CR, Polus H, Sy KTL, Kahler DJ, Gahl WA, Solomon SL, Chang S, Meissner A, Eggan K, Noggle SA. 2015. Automated, high-throughput derivation, characterization and differentiation of induced pluripotent stem cells. *Nat. Methods* **12**:885–892.

Pauly L. 2016. Development of an automated media feed-rate strategy in bioreactors for stem cell production; KU Leuven.

Pedregal D, Taylor C, Young PC. 2007. System Identification, Time Series Analysis and Forecasting. *Capt. Toolbox Handb. v2.0*.

Peters R, Vang B, Brecheisen M, Startz T, Jones M, Varella-Garcia M, Skokan M, Bryce S, Schowinsky J, Peters R, Vang B, Brecheisen M, Startz T, Frank N, Nankervis B. 2013. Genetic stability of bone marrow-derived human mesenchymal stromal cells in the Quantum System. JOUR. *Cytotherapy* **15**:1323–39.

Placzek MR, Chung I-M, Macedo HM, Ismail S, Mortera Blanco T, Lim M, Cha JM, Fauzi I, Kang Y, Yeo

DCL, Ma CYJ, Polak JM, Panoskaltsis N, Mantalaris A. 2009. Stem cell bioprocessing: fundamentals and principles. *J. R. Soc. Interface* **6**:209–32.

Polizzi KM, Kontoravdi C. 2014. Genetically-encoded biosensors for monitoring cellular stress in bioprocessing. *Curr. Opin. Biotechnol.* **31C**:50–56.

Price L, Young P, Berckmans D, Janssens K, Taylor J. 1999. Data-based mechanistic modelling (DBM) and control of mass and energy transfer in agricultural buildings. *Annu. Rev. Control* **23**:71–82.

Prockop DJ. 2010. Defining the probability that a cell therapy will produce a malignancy. *Mol. Ther.* **18**:1249–50.

Prockop DJ, Brenner M, Fibbe WE, Horwitz E, Le Blanc K, Phinney DG, Simmons PJ, Sensebe L, Keating A. 2010. Defining the risks of mesenchymal stromal cell therapy. *Cytotherapy* **12**:576–8.

Quinn KP, Bellas E, Fourligas N, Lee K, Kaplan DL, Georgakoudi I. 2012. Characterization of metabolic changes associated with the functional development of 3D engineered tissues by non-invasive, dynamic measurement of individual cell redox ratios. *Biomaterials* **33**:5341–8.

Radisic M, Malda J, Epping E, Geng W, Langer R, Vunjak-Novakovic G. 2006. Oxygen gradients correlate with cell density and cell viability in engineered cardiac tissue. *Biotechnol. Bioeng.* **93**:332–43.

Ramaswamy S, Cutright TJ, Qammar HK. 2005. Control of a continuous bioreactor using model predictive control. *Process Biochem.* **40**:2763–2770.

Rao MS, Atala A. 2016. Developing Induced Pluripotent Stem Cell-Based Therapy for the Masses. *Stem Cells Transl. Med.* **5**:129–131.

Rathore AS, Singh SK. 2015. Use of Multivariate Data Analysis in Bioprocessing. *BioPharm Int.* **28**:1–5.

Read EK, Shah RB, Riley BS, Park JT, Brorson K a, Rathore a S, Shah RB, Riley BS, Brorson K a, Rathore a S. 2010. Process analytical technology (PAT) for biopharmaceutical products: Part I. concepts and applications. *Biotechnol. Bioeng.* **105**:276–84.

Roberts SJ, van Gastel N, Carmeliet G, Luyten FP. 2014. Uncovering the periosteum for skeletal regeneration: The stem cell that lies beneath. *Bone* **70**:10–18.

Roberts SJ, Geris L, Kerckhofs G, Desmet E, Schrooten J, Luyten FP. 2011. The combined bone forming capacity of human periosteal derived cells and calcium phosphates. *Biomaterials* **32**:4393–405.

Rodrigues C, Fernandes T, Diogo M, da Silva C, Cabral J. 2011. Stem cell cultivation in bioreactors. *Biotechnol. Adv.* **29**:815–29.

Rojewski MT, Fekete N, Baila S, Nguyen K, Fürst D, Antwiler D, Dausend J, Kreja L, Ignatius A, Sensebé L, Schrezenmeier H, F??rst D, Antwiler D, Dausend J, Kreja L, Ignatius A, Senseb?? L, Schrezenmeier H. 2013. GMP-compliant isolation and expansion of bone marrow-derived MSCs in the closed, automated device quantum cell expansion system. JOUR. *Cell Transplant.* **22**:1981–2000.

Rolfe P. 2006. Sensing in tissue bioreactors. *Meas. Sci. Technol* **17**:578–583.

Røsland GV, Svendsen A, Torsvik A, Sobala E, McCormack E, Immervoll H, Mysliwietz J, Tonn JC, Goldbrunner R, Lønning PE, Bjerkvig R, Schichor C. 2009. Long-term cultures of bone marrow-derived human mesenchymal stem cells frequently undergo spontaneous malignant transformation. *Cancer Res.* **69**:5331–5339.

Rowley J, Abraham E, Campbell A, Brandwein H, Oh S. 2012. Meeting lot-size challenges of manufacturing adherent cells for therapy. *Bioprocess Int.* **10**:16–22.

Rubio D, Garcia-Castro J, Martín MC, de la Fuente R, Cigudosa JC, Lloyd AC, Bernad A. 2005. Spontaneous Human Adult Stem Cell Transformation. JOUR. *Cancer Res.* **65**:3035 LP-3039.

Sagmeister P, Wechselberger P, Jazini M, Meitz A, Langemann T, Herwig C. 2013. Soft sensor assisted dynamic bioprocess control: Efficient tools for bioprocess development. *Chem. Eng. Sci.* **96**:190–198.

Salmikangas P, Menezes-Ferreira M, Reischl I, Tsiftsoglou A, Kyselovic J, Borg JJ, Ruiz S, Flory E, Trouvin J-H, Celis P, Ancans J, Timon M, Pante G, Sladowski D, Lipnik-Stangelj M, Schneider CK. 2015. Manufacturing, characterization and control of cell-based medicinal products: challenging paradigms toward commercial use. JOUR. *Regen. Med.* **10**:65–78.

Salter E, Goh B, Hung B, Hutton D, Ghone N, Grayson WL. 2012. Bone tissue engineering bioreactors: a role in the clinic? Journal Article. *Tissue Eng Part B* **18**:62–75.

Santoro R, Braissant O, Müller B, Wirz D, Daniels a U, Martin I, Wendt D. 2011. Real-time measurements of human chondrocyte heat production during in vitro proliferation. *Biotechnol. Bioeng.* **108**:3019–24.

Santoro R, Krause C, Martin I, Wendt D. 2012. On-line monitoring of oxygen as a non-destructive method to quantify cells in engineered 3D tissue constructs. Journal Article. *J Tissue Eng Regen Med* **6**:696–701.

Santoro R, Olivares AL, Brans G, Wirz D, Longinotti C, Lacroix D, Martin I, Wendt D. 2010. Bioreactor based engineering of large-scale human cartilage grafts for joint resurfacing. *Biomaterials* **31**:8946–52.

Dos Santos F, Campbell A, Fernandes-Platzgummer A, Andrade PZ, Gimble JM, Wen Y, Boucher S, Vemuri MC, Da Silva CL, Cabral JMS. 2014. A xenogeneic-free bioreactor system for the clinical-scale expansion of human mesenchymal stem/stromal cells. JOUR. *Biotechnol. Bioeng.* **111**:1116–1127.

Dos Santos FF, Andrade PZ, da Silva CL, Cabral JMS. 2013. Bioreactor design for clinical-grade expansion of stem cells. *Biotechnol. J.* **8**:1–11.

Sart S, Agathos SN, Li Y. 2013. Engineering stem cell fate with biochemical and biomechanical properties of microcarriers. *Biotechnol. Prog.* **29**:1354–1366.

Sart S, Agathos SN, Li Y. 2014. Process engineering of stem cell metabolism for large scale expansion and differentiation in bioreactors. *Biochem. Eng. J.* **84**:74–82.

Schop D, Sc M, Janssen FW, Rijn LDS Van, Sc B, Fernandes H, Bloem RM, Ph D, Bruijn JD De, Dijkhuizen-radersma R Van. 2009. Growth, Metabolism, and Growth Inhibitors of Mesenchymal Stem Cells. *Tissue Eng Part A* **15**:1877–86.

SCSI. 2013. The Next Stem Cell Controversy: Pricing. http://busaconsultingllc.com/scsi/organelles/the_next_stem_cell_controversy.php.

Sepúlveda J, Tomé M. 2014. Cell senescence abrogates the therapeutic potential of human mesenchymal stem cells in the lethal endotoxemia model. *Stem Cells* **32**:1865–1877.

Sharma RRRR, Pollock K, Hubel A, McKenna D. 2014. Mesenchymal stem or stromal cells: A review of clinical applications and manufacturing practices. JOUR. *Transfusion* **54**:1418–1437.

Sharma S, Raju R, Sui S, Hu W-S. 2011. Stem cell culture engineering - process scale up and beyond. *Biotechnol. J.* **6**:1317–29.

Sharp LA, Lee YW, Goldstein AS. 2009. Effect of low-frequency pulsatile flow on expression of osteoblastic genes by bone marrow stromal cells. *Ann. Biomed. Eng.* **37**:445–53.

Sherman J, Morrison WJ. 1950. Adjustment of an Inverse Matrix Corresponding to a Change in One Element of a Given Matrix. JOUR. *Ann. Math. Stat.* **21**:124–127.

Siddappa R, Licht R, van Blitterswijk C, Boer J de. 2007. Donor Variation and Loss of Multipotency during In Vitro Expansion of Human Mesenchymal Stem Cells for Bone Tissue Engineering. *J. Orthop. Res.*:1029–1041.

Silva M, Exadaktylos V, Ferrari S, Guarino M, Aerts J-M, Berckmans D. 2009. The influence of respiratory disease on the energy envelope dynamics of pig cough sounds. Article. *Comput. Electron. Agric.* **69**:80–85.

Simaria AS, Hassan S, Varadaraju H, Rowley J, Warren K, Vanek P, Farid SS. 2014a. Allogeneic cell therapy bioprocess economics and optimization: Single-use cell expansion technologies. *Biotechnol. Bioeng.* **111**:69–83.

Simaria AS, Hassan S, Varadaraju H, Rowley J, Warren K, Vanek P, Farid SS. 2014b. Allogeneic cell therapy bioprocess economics and optimization: Single-use cell expansion technologies. *Biotechnol. Bioeng.* **111**:69–83.

Singh P, Schwarzbauer JE. 2012. Fibronectin and stem cell differentiation - lessons from chondrogenesis. *J. Cell Sci.* **125**:3703–3712.

De Smedt A, Steemans M, De Boeck M, Peters AK, van der Leede B, Van Goethem F, Lampo A, Vanparys P. 2008. Optimisation of the cell cultivation methods in the embryonic stem cell test results in an increased differentiation potential of the cells into strong beating myocard cells. JOUR. *Toxicol. Vitr.* **22**:1789–1796.

Sonnaert M, Luyten FP, Schrooten J, Papantoniou I. 2015a. Bioreactor-based online recovery of human progenitor cells with uncompromised regenerative potential: A bone tissue engineering perspective. JOUR. *PLoS One* **10**:e0136875.

Sonnaert M, Papantoniou I, Bloemen V, Kerckhofs G, Luyten FP, Schrooten J. 2014. Human periosteal-derived cell expansion in a perfusion bioreactor system: proliferation, differentiation and extracellular matrix formation. *J. Tissue Eng. Regen. Med.* **1**:1–12.

Sonnaert M, Papantoniou I, Luyten FP, Schrooten J. 2015b. Quantitative Validation of the Presto Blue™ Metabolic Assay for Online Monitoring of Cell Proliferation in a 3D Perfusion Bioreactor System. *Tissue Eng. Part C. Methods* **21**:519–529.

Sotiropoulou P a, Perez S a, Salagianni M, Baxevanis CN, Papamichail M. 2006. Characterization of the optimal culture conditions for clinical scale production of human mesenchymal stem cells. JOUR. *Stem Cells* **24**:462–71.

Squillaro T, Peluso G, Galderisi U. 2015. Clinical Trials with Mesenchymal Stem Cells: An Update. *Cell Transplant.*:1–53.

Stankiewicz AI, Moulijn JA. 2000. Process intensification: Transforming chemical engineering. *Chem. Eng. Prog.* **96**:22–33.

Starly B, Choubey A. 2008. Enabling sensor technologies for the quantitative evaluation of engineered tissue. *Ann. Biomed. Eng.* **36**:30–40.

Stegen S, Van Gastel N, Eelen G, Ghesquière B, D'Anna F, Thienpont B, Goveia J, Torrekens S, Van Looveren R, Luyten FP, Maxwell PH, Wielockx B, Lambrechts D, Fendt SM, Carmeliet P, Carmeliet G. 2016. HIF-1α promotes glutamine-mediated redox homeostasis and glycogen-dependent bioenergetics to support postimplantation bone cell survival. *Cell Metab.* **23**:265–279.

von Stosch M, Davy S, Francois K, Galvanauskas V, Hamelink JM, Luebbert A, Mayer M, Oliveira R, O'Kennedy R, Rice P, Glassey J. 2014. Hybrid modeling for quality by design and PAT-benefits and challenges of applications in biopharmaceutical industry. *Biotechnol. J.* **9**:719–726.

Sutlu T, Stellan B, Gilljam M, Quezada HC, Nahi H, Gahrton G, Alici E. 2010. Clinical-grade, large-scale, feeder-free expansion of highly active human natural killer cells for adoptive immunotherapy using an automated bioreactor. *Cytotherapy* **12**:1044–1055.

Sutradhar BC, Park J, Hong G, Choi SH, Kim G. 2010. Effects of Trypsinization on Viability of Equine Chondrocytes in Cell Culture. JOUR. *Pak. Vet. J.* **30**:232–238.

Takahashi K, Tanabe K, Ohnuki M, Narita M, Ichisaka T, Tomoda K, Yamanaka S. 2007. Induction of Pluripotent Stem Cells from Adult Human Fibroblasts by Defined Factors. JOUR. *Cell* **131**:861–872.

Tan KY, Reuveny S, Oh SKW. 2016. Recent advances in serum-free microcarrier expansion of mesenchymal stromal cells: Parameters to be optimized. JOUR. *Biochem. Biophys. Res. Commun.* **473**:769–773.

Tan KY, Teo KL, Lim JFYY, Chen AKLL, Reuveny S, Oh SKW. 2015. Serum-free media formulations are cell line–specific and require optimization for microcarrier culture. JOUR. *Cytotherapy* **17**:1152–1165.

Tandon N, Marolt D, Cimetta E, Vunjak-Novakovic G. 2013. Bioreactor engineering of stem cell environments. *Biotechnol. Adv.* **31**:1020–31.

Tarte K, Gaillard J, Lataillade J, Fouillard L, Becker M, Mossafa H, Tchirkov A, Gourmelon P, Gorin N, Sensebe L. 2010. Brief report Clinical-grade production of human mesenchymal stromal cells : occurrence of aneuploidy without transformation. *Blood* **115**:1549–1553.

Tay T, Mareels I, Moore JB. 1998. High Performance Control. New York: Springer Science+Business Media.

Taylor C, Pedregal D, Young P, Tych W. 2007. Environmental time series analysis and forecasting with the Captain toolbox. *Environ. Model. Softw.* **22**:797–814.

Terstegge S, Laufenberg I, Pochert J, Schenk S, Itskovitz-Eldor J, Endl E, Brustle O. 2007. Automated Maintenance of Embryonic Stem Cell Cultures. *Biotechnol. Bioeng.* **96**:1199–1210.

Thomas RJ, Hourd PC, Williams DJ. 2008. Application of process quality engineering techniques to improve the understanding of the in vitro processing of stem cells for therapeutic use. *J. Biotechnol.* **136**:148–55.

Timmins NE, Palfreyman E, Marturana F, Dietmair S, Luikenga S, Lopez G, Fung YL, Minchinton R, Nielsen LK. 2009. Clinical scale ex vivo manufacture of neutrophils from hematopoietic progenitor cells. JOUR. *Biotechnol. Bioeng.* **104**:832–840.

Torsvik A, Molven A, McCormack E, Eystein LP, Primon M. 2010. Letter to the Editor: Spontaneous Malignant Transformation of Human Mesenchymal Stem Cells Reflects Cross-Contamination : Putting the Research Field on Track. *Cancer Res.* **70**:6393–6396.

Tostões R, Dodgson J, Mason C, Veraitch F. 2015. A novel filtration device for point of care preparation of cellular therapies. JOUR. *Cytotherapy* **17**:26.

Trainor N, Pietak A, Smith T. 2014. Rethinking clinical delivery of adult stem cell therapies. *Nat. Biotechnol.* **32**:729–35.

Trounson A, Thakar R, Lomax G, Gibbons D. 2011. Clinical Trials for Stem Cell Therapies. *BMC Med* **9**:52.

Trounson A, McDonald C. 2015. Stem Cell Therapies in Clinical Trials: Progress and Challenges. *Cell Stem Cell* **17**:11–22.

Truscello S, Schrooten J, Van Oosterwyck H. 2011. A Computational Tool for the Upscaling of Regular Scaffolds During In Vitro Perfusion Culture. *Tissue Eng Part B Rev* **17**:619–30.

Viazzi S, Lambrechts T, Schrooten J, Papantoniou I, Aerts J-M. 2015. Real-time characterisation of the

harvesting process for adherent mesenchymal stem cell cultures based on on-line imaging and model-based monitoring. *Biosyst. Eng.* **138**:104–113.

Viswanathan S, Keating A, Deans R, Hematti P, Prockop D, Stroncek DF, Stacey G, Weiss DJ, Mason C, Rao MS. 2014. Soliciting strategies for developing cell-based reference materials to advance mesenchymal stromal cell research and clinical translation. JOUR. *Stem Cells Dev.* **23**:1157–1167.

Vojinović V, Cabral JMS, Fonseca LP. 2006. Real-time bioprocess monitoring. *Sensors Actuators B Chem.* **114**:1083–1091.

Volkmer E, Drosse I, Otto S, Stangelmayer A, Stengele M, Kallukalam BC, Mutschler W, Schieker M. 2008. Hypoxia in static and dynamic 3D culture systems for tissue engineering of bone. *Tissue Eng. Part A* **14**:1331–40.

Wang Y, Zhao L, Smas C, Sul HS. 2010. Pref-1 interacts with fibronectin to inhibit adipocyte differentiation. *Mol. Cell. Biol.* **30**:3480–3492.

Want AJ, Nienow AW, Hewitt CJ, Coopman K. 2012. Large-scale expansion and exploitation of pluripotent stem cells for regenerative medicine purposes: beyond the T flask. *Regen. Med.* **7**:71–84.

Ward A, Quinn KP, Bellas E, Georgakoudi I, Kaplan DL. 2013. Noninvasive metabolic imaging of engineered 3D human adipose tissue in a perfusion bioreactor. *PLoS One* **8**:e55696.

Weber E, Pinkse MWH, Bener-Aksam E, Vellekoop MJ, Verhaert PDEM. 2012. Miniaturized mass-spectrometry-based analysis system for fully automated examination of conditioned cell culture media. *Int. J. Proteomics* **2012**:1--8.

Wendt D, Jakob M, Martin I. 2005. Bioreactor-based engineering of osteochondral grafts: from model systems to tissue manufacturing. *J. Biosci. Bioeng.* **100**:489–94.

Wendt D, Riboldi SA, Cioffi M, Martin I. 2009. Bioreactors in Tissue Engineering : Scientific Challenges and Clinical Perspectives. *Adv Biochem Engin/Biotechnol* **1**:1–27.

Whitfield MJ, Lee WCJ, Van Vliet KJ. 2013. Onset of heterogeneity in culture-expanded bone marrow stromal cells. *Stem Cell Res.* **11**:1365–1377.

Wiener N. 1949. Extrapolation, Interpolation, and Smoothing of Stationary Time Series: With Engineering Applications. *J. Am. Stat. Assoc.* **47**:319.

Williams DJ, Thomas RJ, Hourd PC, Chandra a., Ratcliffe E, Liu Y, Rayment E a., Archer JR. 2012. Precision manufacturing for clinical-quality regenerative medicines. *Philos. Trans. R. Soc. A Math. Phys. Eng. Sci.* **370**:3924–3949.

Wilson K, Walker J. 2010. Principles and Techniques of Biochemistry and Molecular Biology. Cambridge University Press. 581-624 p.

Young PC. 1984. Recursive estimation and time-series analysis. Berlin: Springer-Verlag.

Young P. 1998. Data-based mechanistic modelling of environmental, ecological, economic and engineering systems. *Environ. Model. Softw.* **13**:105–122.

Young PC. 1999. Data-based mechanistic modelling, generalised sensitivity and dominant mode analysis. *Comput. Phys. Commun.* **117**:113–129.

Young PC, Garnier H, Gilson M. 2008. Refined Instrumental Variable Identification of Continuous-time Hybrid Box-Jenkins Models BT - Identification of Continuous-time Models from Sampled Data. CHAP. In: Garnier, H, Wang, L, editors. London: Springer London, pp. 91–131.

Zagari F, Jordan M, Stettler M, Broly H, Wurm FM. 2013. Lactate metabolism shift in CHO cell culture: the role of mitochondrial oxidative activity. *N. Biotechnol.* **30**:238–45.

Zhao F, Pathi P, Grayson W, Xing Q, Locke BR, Ma T. 2005. Effects of oxygen transport on 3-d human mesenchymal stem cell metabolic activity in perfusion and static cultures: experiments and mathematical model. *Biotechnol. Prog.* **21**:1269–80.

Zhao L, Fu HY, Zhou W, Hu WS. 2015. Advances in process monitoring tools for cell culture bioprocesses. *Eng. Life Sci.*:459–468.

Zhou X, Holsbeeks I, Impens S, Sonnaert M. 2013. Noninvasive Real-Time Monitoring by AlamarBlue During In Vitro Culture of Three-Dimensional Tissue-Engineered Bone Constructs. *Tissue Eng Part C* **19**:720–729.

Curriculum vitae

Personal information:

Name: Toon Lambrechts

Date of birth: April 30, 1988 (Leuven, Belgium)

Email: toon.lambrechts@kuleuven.be, toon.lambrechts@gmail.com

Telephone: +32 476 46 51 77

Education:

2013 – 2016: PhD Researcher at M3BIORES: Measure, Model & Manage Bioresponses and Prometheus, Division of Skeletal Tissue Engineering, KU Leuven

2012 : Internship at Octane, Kinston (Canada)

2011 – 2012: Master in International Business at Grenoble Graduate School of Business, Grenoble (France)

2009 – 2011: Master of Science in Bioscience Engineering: Biosystems Engineering at KU Leuven

2006 – 2009: Bachelor of Bioscience Engineering at KU Leuven

Publications:

Articles in internationally reviewed academic journals:

Lambrechts, T., Sonnaert, M., Schrooten, J., Luyten, F.P., Aerts, J.M., Papantoniou, I. (2016) Large-scale mesenchymal stem/stromal cell expansion: a visualisation tool for bioprocess comparison, Tissue Eng. Part B Rev. [Epub ahead of print] doi:10.1089/ten.TEB.2016.0111.

Lambrechts, T., Papantoniou, I., Rice, B.,Schrooten, J., Luyten, F.P., Aerts, J.M. . (2016) Large-scale autologous stem cell expansion in monitored hollow fibre bioreactors: evaluation of donor-to-donor variability, Cytotherapy. 18 (19), 1219-1233

Lambrechts, T., Papantoniou, I., Viazzi, S., Bovy, T., Schrooten, J., Luyten, F.P., Aerts, J-M. (2015) Evaluation of a monitored multiplate bioreactor for large-scale expansion of human periosteum derived stem cells for bone tissue engineering applications, Biochemical Engineering Journal. 108, 58-68.

Viazzi, S., Lambrechts, T., Papantoniou, I., Aerts, J.-M. (2015). Real-time characterization of harvesting process for adherent cell culture based on on-line imaging and model-based monitoring. Biosystems Engineering journal. 138, 104-113.

Lambrechts, T., Papantoniou, I., Sonnaert, M., Schrooten, J., Aerts, J. (2014). Model-based cell number quantification using online single-oxygen sensor data for tissue engineering perfusion bioreactors, Biotechnology and Bioengineering, 111 (10), 1982-1992.

Papantoniou, I., Sonnaert, M., Lambrechts, T., Aerts, J.M., Geris, L., Luyten, F.P, Schrooten, J. (2014). Analysis of Gene Expression Signatures for Osteogenic 3D Perfusion-Bioreactor Cell Cultures Based on a Multifactorial DoE Approach. Processes, 2, 639-657.

Book chapters:

Papantoniou, I., Mantalaris, A., Sonnaert, M., Lambrechts, T., Aerts, J., Geris, L., Schrooten, J. (2015). Product and Process Design: Toward Industrial Tissue Engineering Manufacturing. In: van Blitterswijk C. (Eds.), Tissue Engineering, Chapt. 22 Elsevier.

Conference participation (presentations):

Lambrechts, T., Sonnaert, M., Schrooten, J., Luyten, F.P., Papantoniou, I. Aerts, J.M., (2016) Process Performance Analysis for Large-Scale Cell Expansion. Belgian Symposium on Tissue Engineering, Leuven, 14-15 April 2016

Lambrechts T , Papantoniou I, Rice B, Schrooten J, Luyten FP, Aerts J-M. (2015) Clinical-scale expansion of human periosteum-derived stem cells. Belgian Symposium on Tissue Engineering, Leuven, 19-20 March 2015

Lambrechts, T., Papantoniou, I., Viazzi, S., Bovy, T., Schrooten, J., Luyten, F.P., Aerts, J-M. Xpansion bioreactor for large-scale production of MSCs for bone tissue engineering. Workshop & User Meeting: Innovation for Growing and Analyzing Cells, Liège, February 2015

Lambrechts T , Papantoniou I, Rice B, Schrooten J, Luyten FP, Aerts J-M. (2015) Clinical-Scale Expansion Of Human Periosteum-Derived Mesenchymal Stem Cells In A Hollow Fiber Bioreactor And Assessment Of Their In Vivo Bone Forming Activity. Scale-Up and Manufacturing of Cell-Based Therapies IV ECI conference, San Diego, 18-22 January 2015.

Conference participation (posters):

Lambrechts, T., Papantoniou, I., Viazzi, S., Bovy, T., Schrooten, J., Luyten, F.P., Aerts, J-M. (2015) Large-scale expansion of human progenitor cells for bone tissue engineering applications in a

monitored multiplate bioreactor. 2nd annual meeting of the Belgian Society for Stem Cell Research. Bussels, September 18 2015.

T. Lambrechts, S. Viazzi, E. Claes, V. Bloemen, I. Papantoniou, J.-M. Aerts. (2015) Automatic Detection Of Confluence In Tissue Engineering Bioreactors. 3rd Belgian Symposium on Tissue Engineering (BSTE). Leuven, 19-20 March 2015.

S. Viazzi, T. Lambrechts, I. Holsbeeks, I. Papantoniou, J.-M. Aerts, V. Bloemen. (2015) Live Cell Monitoring System (LIMSY). 3rd Belgian Symposium on Tissue Engineering (BSTE). Leuven, 19-20 March 2015.

Lambrechts, T., Papantoniou, I., Sonnaert, M., Schrooten, J., Aerts, J. (2013). Data-based Mechanistic Models for Bioprocess Monitoring in Tissue Engineering Bioreactors. 2nd Belgian Symposium on Tissue Engineering (BSTE). Leuven, 24-25 October 2013.

Lambrechts, T., Papantoniou, I., Sonnaert, M., Schrooten, J. (2013). Non-Invasive On-Line Measurement of Stem Cell Proliferation in a 3D Perfusion Bioreactor Using Data-Based Modelling. Tissue Engineering and Regenerative Medicine International Society (TERMIS-EU 2013). Istanbul, Turkey, 17-20 June 2013.

Pellens, E., Wauthlé, R., Lambrechts, T., Bourgine, P., Appeltans, I., Colsoul, B., Holsbeeks, I., Schrooten, J., Bloemen, V. (2013). Comparison of different scaffold materials and different cell types in a 2D+ bioreactor system by LiMSy, a Live cell Monitoring System. Belgian Symposium on Tissue Engineering. Leuven, 24-25 October 2013.

Tambuyzer, T., Pellens, E., Appeltans, I., Bloemen, V., Colsoul, B., Holsbeeks, I., Lambrechts, T., Schrooten, J., Aerts, J. (2013). Automated camera-based monitoring of cell populations. Belgian Symposium on Tissue Engineering. Leuven, 24-25 October 2013.

Lambrechts, T., Sonnaert, M., Impens, S., Bloemen, V., Holsbeeks, I., Schrooten, J., Aerts, J. (2012). Non-invasive on-line measurement of cell activity in a 3D perfusion bioreactor. Belgian Symposium on Tissue Engineering. Leuven, Belgium, 16-17 September 2012.